Aptamer Based Targeted Delivery System: Developing Aptamer Encapsulated Polyelectrolyte Microcapsules by the Layer-by-Layer Technique

By

Xueru Zhang

A thesis submitted to the faculty of Graduate and Postdoctoral Affairs in partial fulfillment of the requirements for the degree of

Master of Science

To

The Faculty of Graduate and Postdoctoral Affairs

Department of Chemistry

Carleton University

Ottawa, Ontario

Canada

Your file Votre référence
ISBN: 978-0-494-83197-7
Our file Notre référence
ISBN: 978-0-494-83197-7

Abstract

Polyelectrolyte microcapsules have great potential in serving as targeted carriers to deliver their contents when triggered by external stimuli. Aptamers are newly developed antibody-like biosensors. They are synthesized ssDNA or RNA which can bind with a specific target with high affinity and selectivity. In this work, polyelectrolyte microcapsules encapsulating aptamers were obtained by layer-by-layer assembly of oppositely charged polyelectrolyte films on a sacrificial template, $CaCO_3$. Aptamers were captured within the porous $CaCO_3$ particles in a coprecipitation process. Based on systematic trials, Aptamer:PSS-$(PDDA/PSS)_5$ microcapsules were successfully synthesized. These microcapsules would release the encapsulated contents upon the binding of aptamer with target. In addition, aptamer polymer was also obtained and the aptamer polymer rmicrocapsules for triggered delivery will be investigated in future work. The results of this work promise potential applications in smart fertilizers or other fields such as sensing or controlled release drug delivery.

Acknowledgments

I want to first and foremost thank my family. I would say that without my family I would not have been able to finish my Master studies. They have been a tremendous support system for me whenever I needed them, especially when my parents assisted in looking after my young daughter during my time at Carleton University, Ottawa.

I would like to extend my sincere appreciation to my Supervisor, Prof. Maria DeRosa, for having offered me this amazing opportunity of researching smart fertilizer. I highly appreciate her support, encouragement and trust when my experiments encountered difficulties. She is an incredible source of knowledge and information and all her advice was very valuable. She is a cherished friend and a mentor both in and out of the lab environment and has constantly provided hope and encouragement whenever I faced challenges.

I would like to sincerely thank Dr. Carlos Monreal and Morris Schnitzer at Agriculture and Agri-Food Canada for the strong financial support in this project. I would like extend my gratitude to Dr. Farid Bensebaa at National Research Council Canada in ICPET Institute for his kind support by allowing access to the Zetasizer equipment.

I would like to acknowledge and appreciate the constructive input from Dr. Jianqun Wang and his infinite patience during scanning electron microscope measurements. I would also thank Dr. Anatoli Ianoul for the atomic force microscope measurements and his advice on sample preparations.

In the chemistry department, I would like to thank Prof. Sundararajan, Prof. Wayne Wang and Prof. Edward Lai for sharing their knowledge and broadening my perception

of Chemistry. I would also like to extend my thanks to Dr. Robert Burk for his help and advice during my academic life at Carleton University.

Last but not least, I would like to thank all the members of the DeRosa lab. The lab has been a second home throughout the whole project. A special thanks to Yasir Sultan, who was an asset to me during confocal laser scanning microscope measurements and discussions for various challenges I faced in the project. I would also want to thank Ryan Walsh for his insight on various biological techniques and sharing his knowledge and Maureen McKeague for her help in freebase database entries. Also, I would like to thank Erin McConnell, Elyse Bernard, Amanda Giamberardino, Mike Beking and Tariq Francis for being amazing friends and great help throughout my project.

This thesis is dedicated to all my friends, my family and mentors who helped and inspired me during every step I have made in the life.

Table of contents

Page

List of Figures

Page

List of Tables

Page

List of abbreviations

AFM--- Atomic Force Microscope

BSE--- Back Scattered Electron

CLSM--- Confocal Laser Scanning Fluorescence Microscope

DI water--- Distilled water

EDS--- Energy Disperssive X-ray Analysis

EDTA--- ethylenediaminetetraacetic acid

EtBr--- Ethidium bromide

FRAP---- Fluorescence Recovery after Photobleaching

LbL--- Layer-by-Layer

NUE--- nitrogen use efficiency

PAH--- polyallylamine hydrochloride

PAGE--- polyacrylamide gel electrophoresis

PCR--- Polymerase Chain Reaction

PDDA--- polydiallyldimethylammonium chloride

PNIPAM--- poly N-isopropylacrylamide

PSS--- poly sodium-4-styrene sulfonate

RCA--- Rolling Circle Amplification

SE--- Secondary Electron

SELEX--- Systematic Evolution of Ligands by Exponential enrichment

SEM--- Scanning Electron Microscope

SRB--- sulforhodamine B

TBE--- Tris/Borate/EDTA

TMR--- Tetremethylrosamine chloride

TEMED--- N,N,N',N'-tetramethylethylenediamine

List of Publications

Xueru Zhang, Yasir Sultan, Maria DeRosa, "Fabrication of aptamer-polyelectrolyte capsules by the layer-by-layer technique". *Pacifichem 2010 congress*, Hawaii, December 15-19, 2010.

Jose Cruz-Toledo, Maureen McKeague, Xueru Zhang, Amanda Giamberardino, Erin McConnell, Tariq Francis, Maria C. DeRosa, Michel Dumontier, "Aptamer Base: A collaborative knowledge base to describe aptamers and SELEX experiments". *In progress*.

Chapter1 Introduction

The goal of this research project is to lay the groundwork for the development of a "smart fertilizer" that could allow for the synchronization of nutrient uptake by crops with the release of nutrients from fertilizers. Aptamers are - nucleic acid "antibodies"- that can bind with a wide range of targets with high affinity and selectivity, as well as change conformation upon binding with the targets. The introduction of aptamers into the field of fertilizer delivery may offer a feasible way to fabricate a "smart fertilizer". In the long term, this work could provide the basis of a new paradigm for fertilizer delivery and insights provided by this project could be applied to other areas of triggered release, such as drug delivery.

1.1 Inefficient delivery of fertilizer to crops leads to detrimental effects on economy and environment

1.1.1 The demands for increasing nitrogen use efficiency

In the last one hundred years, the world population has grown exponentially, reaching to 6.8 billion in 2010. It is estimated that in 2043, the world population will reach to 9 billion. [1] With the rapid increase in world population, the demand for food increases every year. On the other hand, the area of cultivable land has decreased dramatically in the past decades due to soil degradation, drought, flood, global warming, and industrial occupancy and so on. All this leads to the price of food increasing every year, especially from 2007 to 2008, when the price of wheat increased from $200/tonne to $400/tonne. [2] The global food crisis that occurred in 2008 impacted both poor and developed countries. All this implies that the efficiency of agricultural food output per unit of cultivable area

needs to be tremendously improved to relieve the burden of the increased demand for food in the world.

Since the "green revolution" in the late 1960's, new technologies such as pesticides, herbicides, fertilizers and new crop breeds were widely employed to greatly increase the yield and quality of global food production. Among these new technologies, artificial fertilizers play an important role to provide nutrients to crops. Nitrogen, which is the key nutrient for the growth and survival of crops unfortunately cannot be fixed by most crops themselves and this leads to the dependence on the usage of artificial fertilizers. New breeds of maize, wheat and rice developed in the green revolution have greater requirement for nitrogen than normal crops due to their high yield. For example, the usage of nitrogen fertilizers increased almost 15 times in the US and UK for maize plants in the last 40 years. [3] Every year nitrogen fertilizers provide 53 million tonnes of N in foods for human consumption. [4] However, comparing with nitrogen inputs in fertilizers, irrigation water or seeds, the nitrogen use efficiency (NUE) or agricultural output of nitrogen, is quite low. [5]

1.1.2 Nitrogen circulation in environment

Ammonium (NH_4^+) and nitrates (NO_3^-) salts are the major forms of N which can be taken up by plants. [6] Unfortunately when conventional nitrogen fertilizers composed of NH_4^+ or NO_3^- are applied to crops, almost 50-70% of nitrogen is lost due to volatilization, leaching, denitrification or mineralization processes.[7] The nitrogen circulation in environment is shown in Fig.1-1. [6] The inefficient delivery of nitrogen fertilizers to the crops leads to adverse effects on environment, economy, as well as human and animal health. The leaching of soluble nitrates into groundwater is a direct threat to fish and

marine ecosystems. The volatilization of nitrous oxides and gaseous ammonia into the atmosphere has a detrimental effect on the ecology system, climate, and our health. Nitrous oxides are very powerful greenhouse gases and ammonia may be oxidized, converted into nitric acid and then form acid rain. [8] Besides the negative effects on environment and health, it has been reported that the associated economic losses from this lost nitrogen for Canadian farmers alone reaches from $680 M to $1.13 B per year. [9]

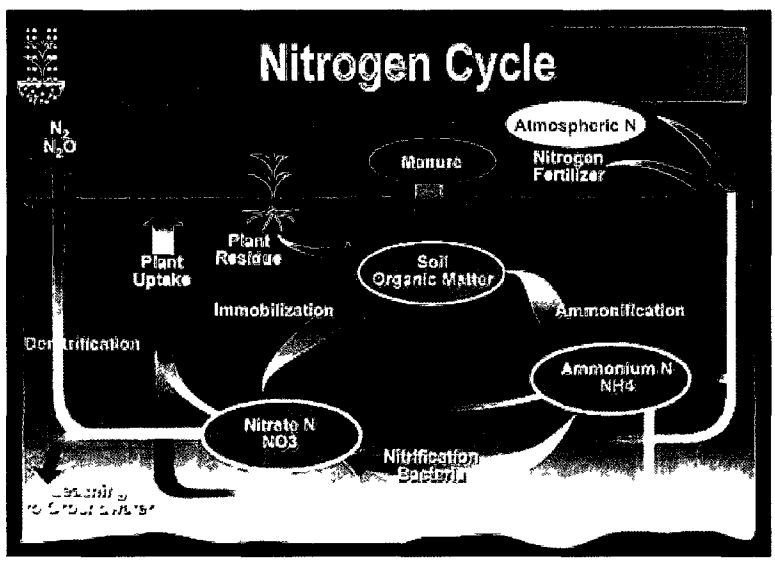

Fig.1-1 Nitrogen circulation in environment [6] (reprinted with permission of http://bioscholars2.wikispaces.com/Biogeochemical Cycles)

1.1.3 Controlled release fertilizers

New methodologies are necessary in an effort to stem fertilizer losses and mitigate environmental impact. Economic performance for farmers would improve by about $4.7 B annually if nitrogen usage efficiency increased by 20% worldwide. [9, 10] Controlled or slow release fertilizers have been developed as enhanced efficiency nitrogen fertilizer products and have begun to come into the markets. For example, Agrium Advanced Technologies, a worldwide leader in slow release fertilizers, produces "Environmentally

Smart N" (ESN). It releases nitrogen in response to increased soil temperature over the growing season. [11]

Based on preparation methods and release mechanisms, currently developed controlled or slow-release fertilizers can be generally classified into three categories.[12]

1) Organic-N low solubility fertilizers: Nitrogen compounds condensed with aldehydes form slowly released Organic-N compounds due to the low solubility of these compounds in water. Urea-formaldehyde is one of the most researched and widely used compounds in this type of fertilizer. [13]

2) Inorganic low solubility fertilizers: ammonium, phosphate or potassium salts are mixed together to make inorganic N-P or N-P-K fertilizers. Because of the low content of nitrogen and the poor controlled release property, the practical usage of inorganic low solubility fertilizers is limited. [14]

3) Fertilizers with physical barriers to control the release rate: Fertilizers are wrapped with biodegradable polymer coatings as a physical barrier to control the release of Nitrogen. Compared to the low solubility fertilizers, fertilizers with polymer coatings show better controlled release performance and have been widely investigated in recent years. The research has indicated that this kind of fertilizer releases nutrients continuously at low concentrations to feed the crops. [15]

While controlled release fertilizers are a major improvement over conventional systems, they have their own limitations. The currently developed bacterial, ionic strength, soil temperature or light controlled release fertilizers [15] reduce leaching to the air or water and elongate their presence in soil. But the main problem is that controlled release

fertilizers cannot track with the crops growth or release nitrogen synchronized with the requirements of crops. The ideal fertilizer delivery system would release fertilizer based on signals from the crops themselves which indicate the need for nitrogen, rather than from outside environmental stimuli.

1.2 Crops excrete root exudates that may serve as a signal of the crop's need for nitrogen

1.2.1 Root exudates

The plant root system, called the hidden half of a plant, serves a multitude of functions in plant growth including the anchorage, provision of nutrients or water, and production of root exudates. [16] Root exudates with growth regulatory properties are released from the root hairs or fibrous roots to the root soil interface "rhizosphere" --- the most active site within the soil matrix in response to biotic or abiotic stresses. [17] The symbiotic association between the roots of seed crops and the mycelium of a fungus as mycorrhiza are typically found in rhizosphere system. The mycorrhiza which are important components in the soil chemistry system, will improve the water and mineral absorption efficiency of the crops as mycorrhizal mycelia will provide a larger surface area to explore a greater soil volume than the crop roots. Besides this, some organic acids which are excreted from the membrane of fungi will aid in the ion displacement of the crops. Mycorrhiza is very beneficial to crops for nutrients absorption, especially in nutrient poor soils.

Root exudates include ions, oxygen, and water, but most of them are composed of carbon-containing compounds such as amino acids, sugars, organic acids, vitamins,

steroids, flavonoids, terpenoids, polyacetylenes, enzyme and nucleotides. [18] The root exudates can impact the soil microbial community in the rhizosphere and:

-act as regulators of microbial growth and function

-mediate plant to plant communication and inhibit the growth of competing plant species

-alter the chemical and physical properties of the soil to provide beneficial symbioses

-regulate plant internal metabolic process such as respiration of plant

-prompt external metabolic process such as nutrient acquisition. [19]

Root exudates are released in three different ways. Low molecular weight molecules can diffuse through the lipid bilayer of the root membrane. Some specific carboxylates can exude from ion channels. High molecular weight compounds generally exude via vesicle transport. [17, 20] Both the quantity and type of root exudates released from plants vary considerably with the species, age, cultivar and stress factors. [18a, 21] Moreover, increased release of root exudates has been observed in response to decreased nutrient availability such as nitrogen deficiency. [22]

1.2.2 The mechanism of nutrient uptake

Plant root hairs play an important role in water and nutrient uptake from the rhizosphere and soil. They contain nanometer sized pores which work as the channel for the transportation of ions and molecular species. [16a, 23] Plants can increase the capacities of ion transportation and enzyme activity in response to the limited availability of nutrients. The root architecture will also be altered to build the optimal root system and grow into nutrient rich areas.[24] (Fig.1-2) But, until now, how plants adapt to nutrient deficiency or excess and how root hairs metabolize and develop are still mysterious.[25]

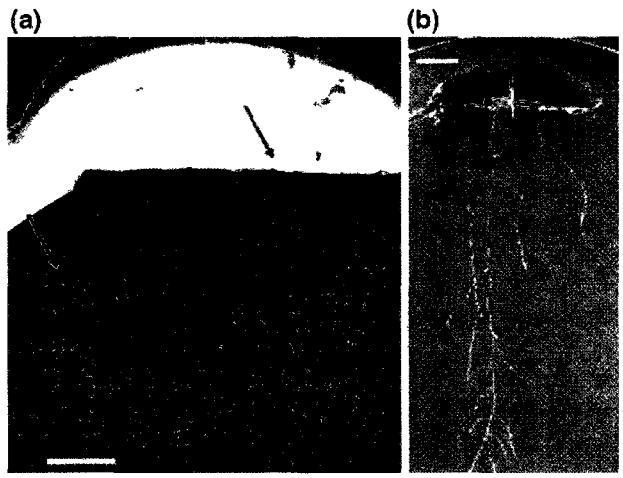

Fig.1-2 The elongation of root hairs in the response to root signals, (a) with and (b) without the addition of activated charcoal. Red arrows shown the beginning and the end of one lateral root [26] (reprinted with permission from Springer, Plant Growth Regulation)

Research into root exudates that can regulate nitrogen uptake and control root system development could help optimize nitrogen use efficiency in plants. A previous study indicated that an amino acid-lysine may be an exudate signal for crop nitrogen uptake. It may stimulate nutrient release from endogenous microbial communities to the soils. [27] Synchronizing the release of fertilizers with the detection of chemical signals and tailoring of the fertilizers to the needs of the crops could dramatically improve nitrogen use efficiency. The release of nutrients on demand will prevent the premature conversion of fertilizers into un-usable forms before they are taken up by the plants as well as reduce environmental contamination due to leaching and volatilization of fertilizers into the water or air.

1.3 Nanoscale multilayer polyelectrolyte thin films used in controlled release systems (e.g. drug delivery) and could be adapted to fertilizer release

1.3.1 LbL technique

The Layer-by-Layer (LbL) method was first introduced by Iler in 1966 and developed by Decher group in 1990s. [28] It is now widely used and has generated more and more attention due to its simplicity, versatility and potential applications in sensing and controlled release of medicines, cosmetics, or pharmaceuticals and so on. [29] This powerful technique enables precise control of thickness, structure and composition of the films on nanoscale by appropriate choice of deposition components, the number of layers, deposition order or by adjusting the deposition conditions such as component molecular weight, concentration, component charge density, deposition temperature, solution pH value and ionic strength. [30]

LbL assembly is extremely versatile, as inorganic nanoparticles, functional polymers, orientable chromophores, lipid bilayers, or biological macromolecules such as enzymes, polypeptides/proteins, polysaccharides and nucleic acids can all serve as the building blocks. [31] It is a convenient approach for the assembly of multilayered polymer films on planar substrates or three dimensional templates by alternative exposure of these charged substrates to oppositely charged polyelectrolyte solutions. [32] The deposition of multilayer polyelectrolyte films onto three dimensional templates including colloidal particles, polystyrene latexes, melamine resin particles, silica particles, biological cells and organic or inorganic crystals and subsequent removal of the core to get hollow capsules are dramatically extending the usage of the LbL technique. [33] The schematic procedure for the assembly of multilayer polyelectrolyte films onto three dimensional substrates are shown in Fig.1-3.

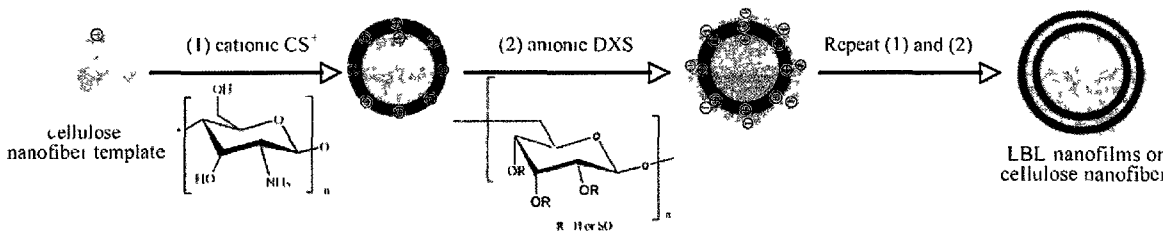

Fig.1-3 Schematic diagram illustrating LbL deposition of chitosan and dextran sulfate as bilayer assembled biofilms on cellulose nanofibers. (reprinted with permission from John Wiley and Sons, Journal of applied polymer science) [32a]

1.3.2 The mechanisms for films formation

The main driving force for the deposition of each polyelectrolyte layer is the formation of a large amount of electrostatic bonds between the oppositely charged polymers. This is an overcompensation process, each successful deposition step leads to surface charge reversal and then the zeta potential value which present the surface charge of particles alternates between positive and negative values upon the formation of films. [34] (Fig.1-4)

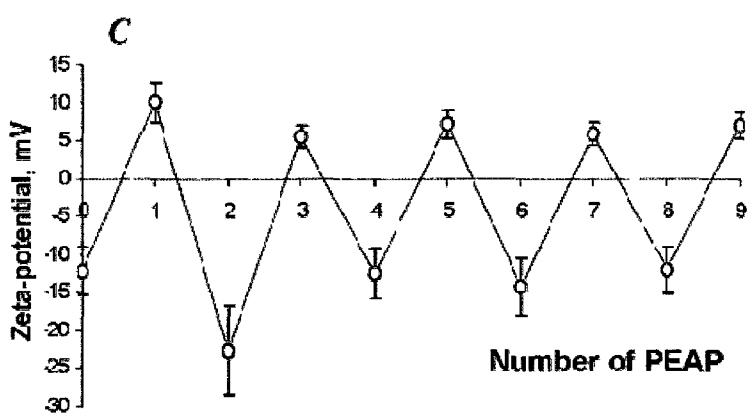

Fig.1-4 Demonstration of zeta potential as a function of polyelectrolyte adsorption procedures (PEAP) [34a] (reprinted with permission from American Chemical Society, Langmuir)

In this deposition process, the salts (ionic strength) also play an important role. The deposition of polyelectrolyte onto the surfaces includes two processes: the first process is an intrinsic adsorption process. Charged groups in the polycation and polyanion will form a large amount of ion pairs between each other in this compensation process. In the second process, the remaining partially uncomplexed charged groups will be extrinsically compensated by counter ions. [30, 31, 35] Besides working as counter ions in the extrinsic deposition process, the salts also influence the degree of interdigitation of the polymer. In the absence of salts, polyelectrolyte such as PAH (polyallylamine hydrochloride) or PSS (poly sodium-4-styrene sulfonate) will be rod-like shape; while with the salts, they will switch to coiled-shaped as the salts will partially reduce the electric repulsion between the charged groups along polyelectrolyte chains. [36]

The other main factors in the formation of the films will be the pH value of the solution and deposition temperature. For weak polyelectrolyte, which pKa or pKb are at 2~10 range, adjusting the pH value of the solution will impact the degree of ionization, which then influences the properties of the films.[37] In solutions of high salt concentration, when the electrostatic attraction between the polyelectrolyte is strongly screened, the deposition of the films depends on the temperature-influenced hydrophobic interaction between the polymers. [34a]

1.3.3 The applications of LbL technique

One of the significant uses of LbL technique is to fabricate external stimuli responsive polyelectrolyte multilayers. The wettability, adhesivity, permeability or porosity of these polyelectrolyte multilayers will be changed based on external stimuli such as the change

of pH, pressure, temperature, ionic strength, magnetic fields, lights, enzymatic degradation, or hydrolysis. [34, 38]

The degradation or disassembly properties of multilayered films upon external stimuli are attracting increased interest for application in the area of controlled release. The variation of the pH of a solution will change the degree of protonation and charge density in weak polyelectrolyte, which will affect the binding between the layers of the polyelectrolyte films and then lead to a change of porosity and permeability of the polyelectrolyte films. [39] Polymers as PNIPAM (poly N-isopropylacrylamide) which have thermo-reversible phase transition properties can be used in fabrication of thermally responsive films. [40] The shrinkage of these polymers upon an increase in temperature will induce the collapse of polymers; Polyelectrolyte containing UV absorbing groups (such as aromatic groups) will shrink dramatically upon UV irradiation and eventually rupture as the absorption of UV light can cause a change of chemical structure of these functional groups in the polymers; [41] Biocompatible and/or biodegradable polyelectrolyte formed multilayer films can be degraded by enzymes, thus controlling the concentration of enzyme will control the release rate of the contents from the multilayer films. [42]

Among these stimuli-responsive systems, biodegradable polyelectrolyte microcapsules which can be used for drug delivery have been the most attractive in recent years. Microcapsules can serve as targeted carriers and for the delivery of contents such as drugs, cosmetics, cells, catalysts, etc when triggered by external stimuli. The commonly used methods to encapsulate contents inside of the microcapsules are 1) by a coprecipitation process: the contents are simultaneously trapped inside porous templates

by the precipitation of the templates [43] 2) after the fabrication of hollow multilayered microcapsules the contents permeate into the microcapsules. [44]

Our goal is to design a system in which the dissociation of the polyelectrolyte films and concomitant release of a molecular payload (e.g. nitrogen fertilizer) occurs upon detection of a target molecule (e.g. key root exudate). This would require a sensing element or receptor specific for the target to be incorporated into these thin films.

1.4 Aptamers offer a feasible solution to the problem of inefficient fertilizer delivery

1.4.1 What is an aptamer?

In the early 1990s, synthesized nucleic acids which bind with enzymes, proteins or organic dyes with high affinity and selectivity were successfully reported by Joyce, Gold, and Szostak groups separately. [45] These "antibody-like" functional single stranded DNA and RNA molecules, generally composed of 15-60 nucleotides, were termed as "Aptamer", derived from latin aptus for "fit" and the Greek word meros for part or piece.

Aptamer can be generated by an *in vitro* process known as SELEX (Systematic Evolution of Ligands by Exponential enrichment) from a DNA/RNA pool which contains up to 10^{16} random DNA/RNA strands with high diversity. (Fig.1-5) After several repetitive selection and partitioning rounds, the unbound or low affinity DNA/RNA strands will be discarded and the potential aptamer candidates are enriched through PCR (Polymerase Chain Reaction) methods. Several methods have been developed to effectively partition between target-binding and non-binding nucleic acids strands, including affinity chromatography, capillary electrophoresis, nitrocellulose filters, flow cytometry and target-coated magnetic beads. The choice for separation methods depends

on the properties of the random RNA or DNA pool and the size, charge, or functional groups of the targets. [46] Typically, the stringency is increased after each competitive selection and partitioning round. Besides this, a counter selection is also incorporated in SELEX to remove strands with low discrimination ability to molecules which have similar chemical structure. At last, the final strands will be cloned and sequenced. [47]

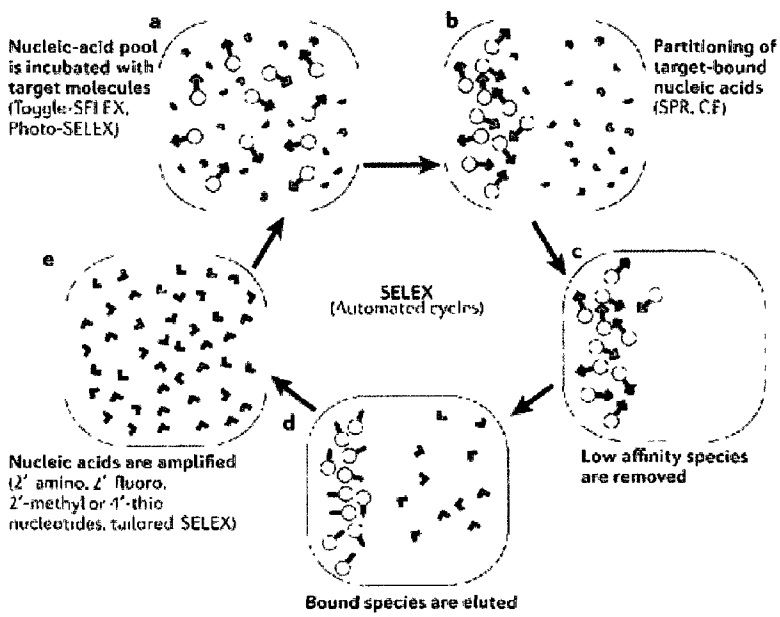

Fig.1-5 Schematic process for in vitro selection of target-specific aptamer using SELEX technology [53a] (reprinted with permission from nature publishing group, Nature Reviews Microbiology)

Aptamer will bind with targets through non-covalent interactions such as electrostatic interaction, π-π stacking of aromatic rings, hydrogen bonds or a combination of these effects. Understanding the binding mechanisms between aptamer and their targets will enhance the rational design of aptamer. Upon binding with the targets, aptamer will form into specific three-dimensional spatial conformations to fit with a wide range of targets from small molecules such as ethanolamine or acetylcholine to large protein complexes and even whole cells. [48] The secondary structure of aptamer include G-quadruplexes,

loops, bulges, hairpins, pseudoknots, triplexes or 2-way to 5-way junctions. [49] See Fig.1-6 for an example of an aptamer-target structure.

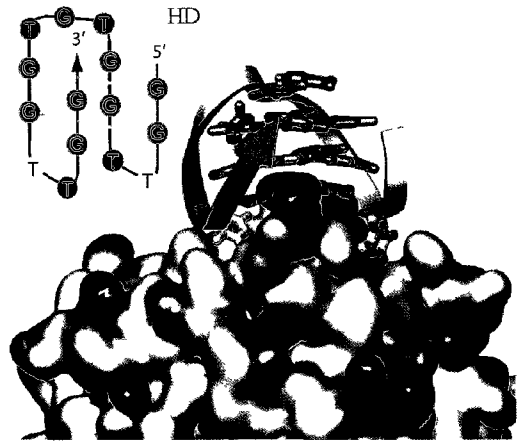

Fig.1-6 Schematic representation of the antiparallel G-quadruplex structure of the thrombin aptamer HD and aptamer bound to thrombin. Negatively charged areas of thrombin in red color and positively in blue; aptamer bound with the positive areas in thrombin. [49b] (reprinted with permission from Oxford University Press, Nucleic Acid Research)

1.4.2 The dissociation constant (Kd) of aptamers

Binding affinity is an important characteristic of an aptamer and subsequent applications of an aptamer mainly depend on its specificity and affinity. The smaller Kd (dissociation constant) value designates a higher affinity to the target. The measured Kd values for many aptamers reach in the low nanomolar to picomolar range. Several methods such as dialysis, ultrafiltration, gel electrophoresis, capillary electrophoresis, UV-Vis absorption, fluorescence, surface plasmon resonance, and fluorescence anisotropy are widely used to determine the Kd value. Each method has its application condition and Kd values from different measurement methods may show a little variation. [50] Even though the size, complexity, and quantity of targets do not determine the specificity and affinity of the aptamer, [47f] a few interesting trends can be concluded based on the previous Kd studies. For example, larger molecular targets normally have lower Kd values than small targets

due to the opportunity for more potential non-covalent (electrostatic, hydrogen bonding) interactions between the large target and aptamer. Another interesting phenomenon is that targets which contain the heterocyclic bases like cyanocobalamin, theophylline and ATP will bind better with aptamer than those without heterocyclic bases. [51]

For a simple 1:1 aptamer to target stoichiometry, assuming that aptamer either associate (Kon) or dissociate (Koff) from the target and there is no other reaction between them, this reversible reaction can be described by:

A (aptamer) + T (target) $\rightleftharpoons$ C (aptamer-target complex)

So the Kd which is defined as the equilibrium constant, will be equal to: [50]

$$K_d = \frac{[A][T]}{[C]}$$

Where the [A] is the free aptamer, [T] is the free target molecule, and the [C] is the concentration of aptamer-target complex at the equilibrium point. The Kd value is commonly measured by titration methods. Generally, the concentration of one species such as the target is kept constant, while the concentration of other species, the aptamer, is gradually increased over a range of several orders of magnitude. The fluorescent intensities, UV adsorption intensities or refractive index changes of the free and bound aptamers are monitored at each point, and then the fa (bound fraction) can be calculated. The binding curve is obtained with the X-axis as the concentration of varied species, and the Y-axis as the bound fraction. Then the Kd value will be fitted based on the following formula. [50] The Kd value can be described as the aptamer concentration at the point which 50% of the aptamer is bound to the targets.

$$f_a = \frac{[T]}{K_d + [T]}$$

1.4.3 Advantages of aptamer

Aptamer, which is innovative alternatives to antibodies used to detect, purify, or remove molecules as affinity tools, are attracting a great deal of attention. Compared to antibodies which are evolved *in vivo,* aptamer have some advantages.

1) The *in vitro* nature of SELEX allows for more precise control of binding conditions and minimizes batch to batch variation, meaning the developed aptamer has consistent structure-activity. SELEX technology is a powerful and universal tool to evolve aptamer for a wide range of targets. The targets can be well-known molecules and also can be complex mixtures with unknown structure or composition. The selected aptamer can be synthesized by a chemical process with high accuracy and reproducibility. The produced aptamer can be purified under stringent conditions to ensure the purity of products. [47]

2) Comparatively, aptamer is less immunogenic and less toxic than antibodies. Aptamer display low to no immunogenicity to humans, which is important for applications in therapeutics. Aptamer-based drugs are coming into the market in recent years. [52]

3) Modified, high-throughput SELEX methods with reduced selection rounds result in shorter times and less cost to generate aptamer than that for antibodies. The Ellington group was the first to automate the SELEX process and highly improve the efficiency of selection. The isolation time was reduced from several months to a few days. [53] Besides this a major improvement is that by using capillary electrophoresis, high affinity aptamer can be isolated in a single round. [53] Innovations to improve the partition efficiency also reduce the generation time for aptamer.

4) Moreover, laboratory-made aptamer molecules are easily modified with functional groups to optimize the aptamer for increased the stability, cellular uptake efficiency, target binding affinity or multifunctional properties. The modified aptamer have higher temperature and nuclease resistance than the natural nucleic acids. They have potential diagnostic and therapeutic applications and can be stored over a long period. [54]

Locked nucleic acids (LNAs) which contain a methylene bridge connecting the 2'-ribose oxygen with the 4'-carbon have higher nuclease resistance and target binding affinity than natural nucleic acids. [55] The substitution of 2'-OH groups of ribose with 2'-F or 2'-NH_2, or 2'-O- methyl groups will protect RNA aptamer from degradation by nucleases. 3'-end capping with amine, phosphate, polyethyleneglycol (PEG), cholesterol, fatty acids or proteins will increase the circulation half-life inside of biological systems by defending the aptamer from the exonucleases and reducing clearance.[56]

5) Denatured aptamer can be regenerated easily within a few minutes while antibodies have a limited shelf life, are sensitive to temperature and easily undergo irreversible denaturation. [57]

1.4.4 Aptamer applications

The stability, reusability, multifunctionality of aptamer, along with their high binding affinity, specificity and regulating ability, allow for promising applications in numerous fields, especially in bioanalytical and biomedical areas. [58]

Aptameric biosensors have been well-developed over the past few years. The basic principle for aptamer-based biosensors is that the capture of analytes by aptamers will be transduced into detectable signals such as electrochemical, piezoelectric, colorimetric,

refractive index or fluorescent response. [59] The typical example is aptamer beacon. In aptamer beacons, a fluorophore and a quencher are attached to the 3' and 5' ends of the aptamer respectively. In the absence of analyte, due to the inherent flexibility of aptamer, the fluorophore is far away from the quencher, so fluorescent signal is "on". After analyte binding, the aptamer may fold into a compact structure so the 3' and 5' ends of aptamer will be brought closer together. Thus, the fluorescent signal will be turned to "off". The target-induced conformational change property of aptamer has wide usage, not only in detecting contaminants in the environment, but also in diagnostic fields. [60]

The discriminatory ability of aptamer can be applied for the purification of key analyte. The analyte will bind to the aptamer under certain conditions and thus can be enriched. This method can yield high purity analyte especially for trace proteins, which can be purified in a few steps or single step. [61]

Aptamer can work as vehicles to deliver therapeutic and diagnostic reagents. [62-64] For example, aptamer can serve as both the target recognition agents and building blocks to crosslink linear polyacrylamide chains and then form a target-responsive hydrogel. The binding of aptamer with the target can facilitate the release of model drugs. In another example, DNA micelles which are composed of a hydrophilic DNA shell and hydrophobic polymer core are effective detection/delivery vehicles. The outside free aptamer can recognize and bind with the cancer cells. This system has promising applications for targeted drug delivery. In aptamer/polyacrylamide hydrogel and DNA micelles, the binding affinity of aptamer is preserved and the recognition and binding of aptamer with the targets will trigger alterations of the scaffold structure and drug release.

1.5 Objectives

The primary motivation for this project is towards the development of a "smart" fertilizer to maximize nitrogen use efficiency by releasing nitrogen in response to the need of crops during their growth cycle.

Recently, our groups reported on the successful embedding a DNA aptamer into a multilayered polyelectrolyte film. [65] We confirmed that the matrix was flexible enough to permit our aptamer to fold into its active conformation, allowing for the films to bind with the target strongly and specifically. Thus, the unique properties of aptamers, namely their affinity and specificity for a molecular target as well as the effect of their molecular conformation on target binding, can be integrated into multilayered polyelectrolyte films to yield innovative functional films for a range of applications.

Based on the results of several groups which have explored the use of template-assisted LbL assembly to prepare multilayered capsules, [43] polyelectrolyte films deposited onto sacrificial spherical template which can be removed by dissolution or degradation after film deposition, we propose to develop a new approach for smart fertilizer systems using aptamer/polyelectrolyte thin film coatings. The aims of this work are to prepare a model strategy for triggered capsule rupture. (Fig.1-7) Here, aptamer serve as a part of a scaffold for a polyelectrolyte microcapsule. Shape changes that take place in the aptamer upon target binding lead to collapse and rupture of the capsules, initiating payload release. Long polymers of aptamer sequences prepared by rolling circle amplification will also be investigated as microcapsule scaffolds.

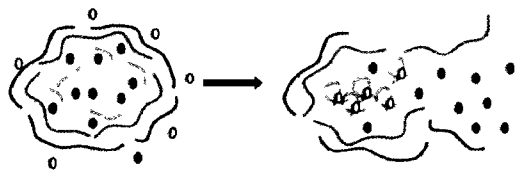

Fig.1-7 Target binding changes the shape of the aptamer leading to collapse of a capsule scaffold. Aptamer will be used in long polymer form or as unlinked sequences

Our eventual goal will be to have the fertilizer encapsulated with a smart biosensor "aptamer" into the sacrificial porous $CaCO_3$ templates in a coprecipitation process, followed by the layer-by-layer deposition of a multilayer protective polyelectrolyte film. After the dissolution of the $CaCO_3$ template, the polyelectrolyte microcapsules containing fertilizers and aptamers will be obtained. The trigger for the bursting of these microcapsules and the release of fertilizers will be root exudates excreted from the crops into the soil as a biochemical signal to stimulate the uptake of nitrogen at the required moment. The aptamer can detect this root exudate and bind to it with high affinity, and then aptamers will fold into certain structure upon the binding. The folded aptamers no longer can work as a scaffold for the microcapsules, leading to microcapsules collapse. Meanwhile, in the absence of this triggering molecule, the fertilizers will be protected and stay stable inside of the microcapsules. In this project, we will test this idea, in the absence of a fertilizer payload, with a target dye molecule as the trigger for aptamer binding and microcapsules collapse.

Chapter 2 Aptamer-based targeted delivery polyelectrolyte microcapsules

2.1 Introduction

Polyelectrolyte microcapsules have the potential to serve as targeted carriers to deliver their contents when triggered by external stimuli. [39-42] Aptamers are newly developed "antibody-like" biosensors. They are synthesized ssDNA or RNA that have high affinity and selectivity for specific targets. [45] The introduction of a "molecular recognition probe" aptamer into polyelectrolyte microcapsules could allow for controlled uptake of reactants or even aptamer-triggered release of their contents under selective conditions. These microcapsules with added functionality could be potentially used in a number of important areas such as drug delivery or "smart" fertilizers. [23, 27]

The previous studies in our group indicate that free aptamers retain their binding affinities even after being embedded within polyelectrolyte films. [65] In this project, we attempted to fabricate an aptamer-based triggered delivery system. Biodegradable polyelectrolyte microcapsules with encapsulated aptamers as a core were prepared by layer-by-layer assembly of oppositely charged polyelectrolyte films on a sacrificial template, $CaCO_3$. Aptamers were captured within the porous $CaCO_3$ microparticles in a coprecipitation process when mixed with aqueous solutions of $CaCl_2$ and $NaHCO_3$. After deposition of the polyelectrolyte films, the $CaCO_3$ template was dissolved using EDTA, leaving aptamer-loaded microcapsules. Upon the binding of aptamer with specific target molecule, the conformation of aptamer will change, and they may no longer serve as a scaffold to support the stability of microcapsules. So, the binding of the aptamer with its target will drive the collapse of microcapsules and then contents will be released. The

whole process is shown in Fig.2-1. In the following sections, the detailed information of each experiment will be provided.

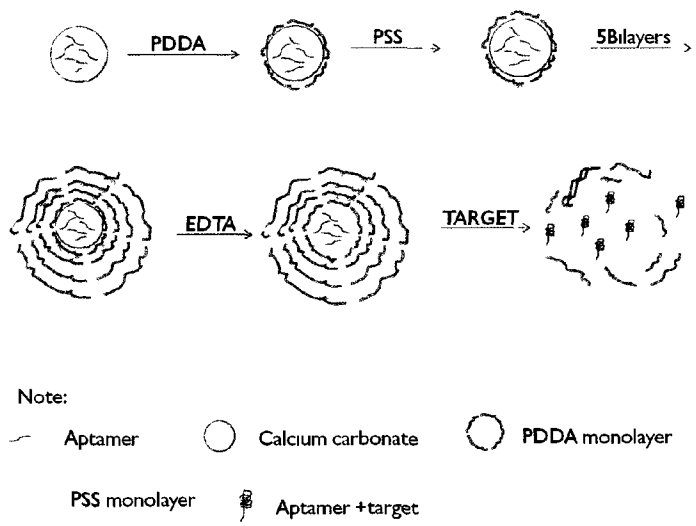

Fig.2-1 Schematic picture for project process

2.1.1 Porous $CaCO_3$ particle synthesis and mechanism

Over the past few decades, morphology-controlled synthesis of $CaCO_3$ particles has attracted considerable attention. [66] The $CaCO_3$ particles have wide applications in industry, technology, or medical fields. They are used as filler in paints and rubber, [67] as well as a biomimetic scaffolds for target drug delivery systems and tissue engineering systems. [68] In particular, spherical porous $CaCO_3$ particles are the main template choice for the preparation of polyelectrolyte microcapsules due to their structural control and the ease of dissolution. [69]

There are several methods to fabricate morphology-controlled $CaCO_3$ particles, such as Langmuir monolayer, reverse microemulsion, self-assembled monomolecular films or double hydrophilic block copolymer. [70] In these methods, an organic macromolecule serves as the template to mediate the morphology of the $CaCO_3$ particles. In this thesis, a

simple method, the crystallizations of inorganic salts (sodium bicarbonate and calcium chloride) from supersaturated solution, has been explored. To get the uniform and non aggregated porous $CaCO_3$ particles with homogenous sizes, reaction conditions such as the concentration of the salts, [66] temperature, [71] stirring rate of solution and reaction time [71] will be the determining factors.

Spherical porous $CaCO_3$ particles with hollow cores are formed by the aggregation of the $CaCO_3$ nanoparticles (in some papers, also called the $CaCO_3$ nucleus). [72] The mechanism of formation of the spherical porous $CaCO_3$ particles is shown in Fig.2-2. The morphology of a single $CaCO_3$ and a broken spherical $CaCO_3$ particle which can demonstrate the hollow core of $CaCO_3$ particle is shown in Fig.2-3.

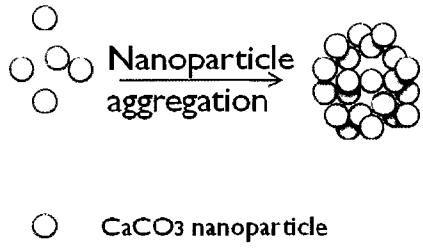

Fig.2-2 Graphical growth process of spherical porous $CaCO_3$ particle

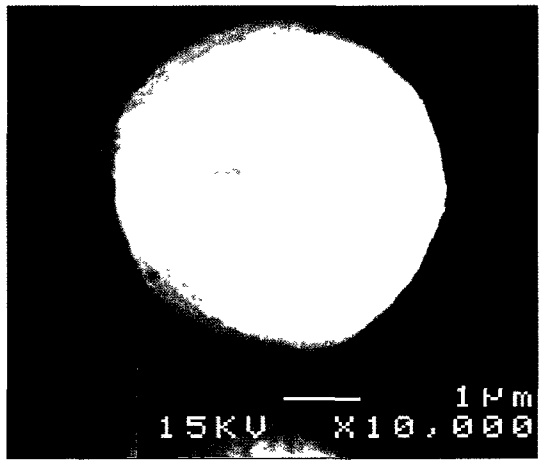

Fig.2-3 SEM image of a single spherical porous $CaCO_3$ particle, the inset is a broken one displaying the empty core

2.1.2 Methods for encapsulating biomaterials into polyelectrolyte microcapsules

Biomaterials such as proteins, DNA, enzymes and drugs can be encapsulated into microcapsules using different approaches. 1) After proteins are precipitated in high salt concentration solution, the oppositely charged polyelectrolyte can be added, which are used to wrap the protein microaggregates to get microcapsules. This is a simple method to get microcapsules but the disadvantage is that the activity of the proteins is dramatically reduced. [73] 2) The permeability of polyelectrolyte microcapsules is changed through a change in the pH value of the solution. By controlling pH value, the biomaterials are allowed to permeate into the hollow microcapsules. The advantage of this method was that the size of microcapsules was uniform but the loading efficiency was low because some biomaterials will be absorbed on the surface of microcapsules due to electrostatic intereactions. [44] 3) Biomaterials are loaded into sacrificial templates by a coprecipitation method. After the layer-by-layer polyelectrolyte film deposition process, the templates are dissolved, yielding microcapsules with biomaterials within their core. This method is currently widely used to load biomaterials into the microcapsules. [72, 43] In this thesis, the third method was adopted.

In this thesis, the biomaterial of interest is a model aptamer system, the sulforhodamine B (SRB) aptamer. Sulforhodamine B aptamer was generated by Wilson and Szostak in 1998 by in vitro SELEX method.[74] This short strand of DNA composed of 29 nucleotides will form a three-tiered G-quartet structure upon the binding with the sulforhodamine B dye at 1:1 stoichiometric ratio. The monovalent cations K^+ are required to stabilize the folding of Sulforhodamine B aptamer into their active conformation. There will be no binding between aptamer and SRB dye without K^+.[27c,74] This aptamer

binds to SRB dye with high affinity and selectivity. The Kd for free SRB dye can reach to 660nM±60nM. On the other hand, tetramethylrhosamine (TMR) dye, which has a similar chemical structure to SRB dye, has no affinity for the SRB aptamer. (SRB and TMR chemical structures are shown in Fig.2-4.) Our group's previous studies proved that SRB aptamer retained its binding selectivity and affinity with the target molecule and also that the permeability of a SRB-embedded polyelectrolyte multilayer film will be increased when incubated with the target dye. [23, 27]

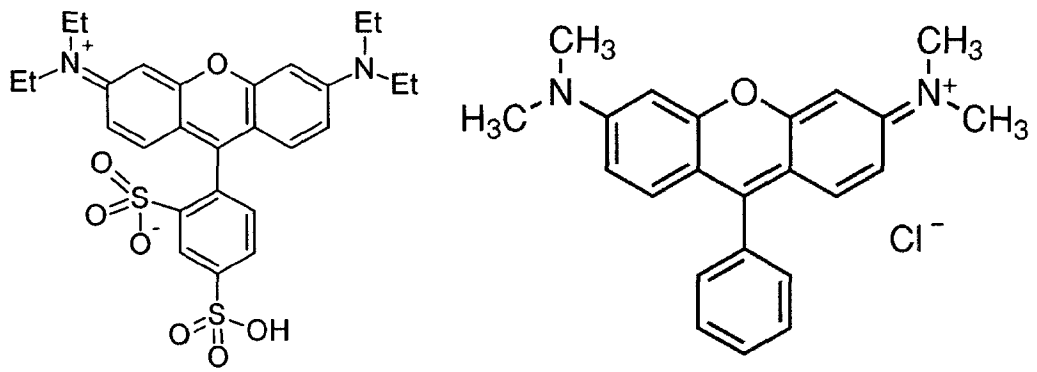

Fig.2-4 Chemical structures of Sulforhodamine B (left) and Tetramethylrosamine (right)

2.1.3 ζ potential and multilayer films formation mechanism

The ζ potential is the surface charge of a particle at the slipping plane. When particles are dispersed in the solution, these particles will absorb bilayer ions onto their surfaces; one is the condensed layer and the other one is the loose layer. These bilayer ions will move together with the particles as a single entity in the solution. The plane which contains these bilayer ions is called as the slipping plane.

The ζ potential of the particles can be measured by using Henry equation: [75]

$$V/E = \varepsilon \zeta f(ka)/6\pi\eta$$

V: the velocity of the particles

E: the strength of applied electrical field

ε: dielectric constant of the medium

ζ: zeta potential of the particle

f(ka): correction factor

η: viscosity of the medium

Electrophoretic mobilities of the particles in the solution can be converted to ζ potential by this Henry equation. The ζ potential of particles may be varied with dispersion medium, pH value, ionic strength of the solution, or the type of the salt. In this chapter, ζ potential, as well as SEM, EDS and fluorescence microscopy, will allow for the characterization of core particles and microcapsules.

2.2 Experimental

2.2.1 Synthesis of spherical porous $CaCO_3$ particles in low volume

2.2.1.1 Materials

Calcium chloride anhydrous (≥93.0%, granular), Sodium bicarbonate (Bioultra®, ≥99.5%) were purchased from Sigma-Aldrich (Oakville, ON).

2.2.1.2 Methods

A series of experiments was conducted to examine the effect of concentration, temperature and reaction time on the formation of spherical porous $CaCO_3$ particles in a

low reaction volume solution. Parametric study on the synthesis was investigated aiming at to producing a large percentage of spherical porous $CaCO_3$ particles.

Firstly, the effect of concentration on the formation of spherical porous $CaCO_3$ particles was checked. 1ml of 1M, 0.33M and 0.1M $CaCl_2$ solution were obtained by dissolving $CaCl_2$ in DI water. Then they were mixed with 1ml $NaHCO_3$ solution prepared at the same concentration under vigorous stirring condition (1000rpm) at room temperature for 20 seconds. After 20 seconds, the solutions were left unstirred for 30 minutes. All experiments were conducted on the IKA® RCT basic dry bath heat block. Then the solutions were filtered with a medium porosity DIMA GLASS® filter to collect the $CaCO_3$ particles, which were dried overnight.

After the appropriate concentration was obtained, the influence of temperature on the formation of porous $CaCO_3$ particles was compared. $CaCl_2$ solutions were mixed with $NaHCO_3$ solutions at 10°C, 15°C and 20°C respectively with all the other reaction conditions as previously described.

Lastly, the reaction time was investigated. The sitting times were set at 4 minutes, 5 minutes, 6 minutes, 7 minutes and 8 minutes at the refined reaction concentration and temperature.

The morphologies of all samples were checked by Tescan VegaII XMU SEM (Scanning Electron Microscope) with SE (Secondary Electron) Detector. The dried samples were uniformly spread onto the aluminum stubs and then sputtered with a thin layer of gold film.

2.2.2 Preparation of aptamer-$CaCO_3$ particles

2.2.2.1 Materials

$CaCl_2$ and $NaHCO_3$ were as same as described above. The four basic phosphoramidites : dA-CE phosphoramidite, dT- CE phosphoramidite, dmf-dG-CE phosphoramidite and Ac-dC-CE phosphoramidite and 5'-Fluorescein phosphoramidite which used to add fluorophore to the DNA were purchased from Glen Research (Sterling, VA) in powder form. The diluent anhydrous acetonitrile was also purchased from Glen Research. Activator, deblock, capping and oxidizer solution for DNA synthesis were purchased from BioAutomation (Irving, TX). MerMade 1000 Å CPG 1μmol support column were used for synthesizing DNA strands. Note that the first nucleotide at the 3' end of the DNA is already attached to the controlled pore glass beads in these support columns.

2.2.2.2 Methods

Synthesis of sulforhodamine B (SRB) *aptamer*: SRB aptamer *5'-CCG GCC TAG GGT GGG AGG GAG GGG GCC GG-3'* was prepared on a MerMade 6® DNA synthesizer by standard phosphoramidites. The fluorescein modified SRB aptamer was used to check aptamer status in particles and non modified SRB aptamer was synthesized for particles morphology measurements. After DNA synthesis, the columns were immersed in 1ml 28% concentrated NH_4OH solution overnight to cleave the DNA strands from the columns and dried in a Thermo Savant® DNA 120 SpeedVac Concentrator to evaporate the NH_4OH. Then DNA strands were purified with DI water to get rid of the remained organic solvent and dried to store SRB aptamers.

Fabrication of aptamer-$CaCO_3$ particles: A series of experiments was conducted to compare the loading efficiencies in which the weight ratio between SRB aptamers and $CaCO_3$ particles were at 1:6.6, 1:22.0, and 1:47.2, respectively. The appropriate amount of SRB aptamers was dissolved in 0.33M $NaHCO_3$ solution, and then mixed with 0.33M $CaCl_2$ solution under vigorous stirring condition at 1000 rpm at 10°C for 20 seconds. After the 20 seconds reaction time, the solution was left unstirred for 6 minutes. The solution was filtered and dried overnight.

Measurements: Zeiss LSM510® (5% laser intensity) Confocal Laser Scanning Fluorescence Microscope (CLSM) with a Plan-Acochromat 63x/1.4 Oil Dic objective and LP950 filter was used to characterize SRB aptamer the loading within the $CaCO_3$ particles. The exciting wavelength for fluorescein is at 492nm and emission wavelength is at 520 nm. Aptamer-$CaCO_3$ particles were dispersed into DI water, put onto the glass slides, and dried overnight to prepare the samples.

The morphology of Aptamer-$CaCO_3$ particles was measured by a Tescan VegaII XMU SEM with a thin layer gold coating to check whether the particles remained spherical.

2.2.3 Multilayer film formation and scrutiny

2.2.3.1 Materials

The positive charged polymer PAH (polyallylamine hydrochloride), average Mw~56,000 and the negative charged polymer PSS (poly sodium-4-styrene sulfonate), average Mw~70,000, were purchased from Sigma-Aldrich Company. The Bis-tris buffer: 2, 2-Bis (hydroxyl methyl) -2, 2', 2''-nitrilotriethanol, (Mw at 209.24 g), used to adjust the pH value of the solution, was purchased from Alfa-Aesar. Sodium Chloride,

biotechnology performance certified, using for adjust the ionic strength of the solution, was from Sigma Company.

2.2.3.2 Methods

Parameter validation of the ionic strength: The ionic strength was adjusted by two different NaCl solutions; one at 0.2M, another one at 0.5M. PAH was dissolved in these two different NaCl solutions. The amount of PAH was increased from 5μg/ml to 40μg/ml, each time increasing 5μg/ml to make two series PAH-NaCl solutions. (0.2M NaCl + varying [PAH], and 0.5M NaCl + varying [PAH]). Then 1mg Aptamer-$CaCO_3$ particles were incubated into 1ml these series PAH-NaCl solution respectively in a Labnet® mini incubator at room temperature for 30 minutes. After incubation, the particles were centrifuged at 6000g for 2 minutes and the supernatant was removed. The particles were then dried under vacuum.

ζ potentials of these PAH-coated Aptamer-$CaCO_3$ particles were measured on a Malvern Zetasizer 3000HS instrument at 25°C in DI water. The samples were dispersed into 10 ml DI water, and after 5 minutes of sonication the colloidal solution was used for the measurements. The pH values of the dispersion solutions were measured by inserting pH probe. The recorded ζ potentials values will have small variations due to a slight drift in pH value of the dispersed solutions, so each sample were measured 5 times and the average value was used to compare the data.

Parameter validation of the pH of deposition: The Aptamer-$CaCO_3$ particles were incubated in 1) 2mg/ml PAH solution with the Bis-tris buffer to adjust the pH value to 6.55 (no added NaCl); 2) 2mg/ml PAH with 0.5M NaCl optimal ionic strength solution (no added bis-tris buffer); 3) 2mg/ml PAH in 0.5M NaCl solution and with Bis-tris

buffer, pH=6.55 respectively in mini incubator for 30 minutes. Then, the particles were washed with DI water and centrifuged three times to get rid of the suspension. Malvern Zetasizer 3000HS instrument were used to measure the ζ potentials of these particles.

Parameter validation of the concentration of polyelectrolytes: The 1mg Aptamer-$CaCO_3$ particles were incubated in 2mg/ml PAH-0.5M NaCl solution and 3mg/ml PAH-0.5M NaCl solution respectively, in the mini incubator for 30 minutes to coat the particles with the first positively charged layer. Then, the particles were washed with DI water and centrifuged three times to remove the supernatant which contained excess PAH. Then particles were then dried under vacuum.

Then particles coated with the first positive layer were incubated in PSS-0.5M NaCl solution in mini incubator for 30 minutes to add the first negatively charged layer. Aptamer-$CaCO_3$ particles incubated in lower PAH concentration solution were incubated in 2mg/ml PSS-0.5 M NaCl solution, while particles coated in higher PAH concentration solution were incubated in 3mg/ml PSS-0.5M NaCl solution. Centrifugation and washing were used to remove the excess PSS. At this point, the particles were now coated with one bilayer of polyelectrolyte.

ζ potentials of these coated Aptamer-$CaCO_3$ particles were measured by Malvern Zetasizer 3000HS instrument at same condition as described previously. The morphologies of the particles were checked by SEM.

2.2.4 Fabrication of Aptamer - $(PAH/PSS)_x$ microcapsules

2.2.4.1 Materials

Sulforhodamine B aptamer, PAH, PSS and NaCl were the same as previous described. EDTA (ethylenediaminetetraacetic acid), biotechnology grade was purchased from Bioshop Company. The cell culture tested dye Sulforhodamine B powder was purchased from Aldrich Company.

2.2.4.2 Methods

The Aptamer-$CaCO_3$ particles were incubated in polyelectrolyte, alternating between 3mg/ml PAH or 3mg/ml PSS in 0.5M NaCl solution in the mini incubator for 30 minutes repeatedly with intervening centrifugation and washing steps (3 times) to constitute a range of different films such as 5 bilayer (PAH/PSS) or three layer PAH/PSS/PAH films onto the particles. Each time, before incubation in the polymer solution, the particles were mildly shaken on a vortex for 5 minutes to avoid the agglomeration of the particles and the sticking of the charged particles to centrifuge tube walls. The microcapsules were obtained after dissolution of the sacrificial $CaCO_3$ template with 0.5M EDTA, pH= 6.97 with overnight sitting. This high concentration of EDTA was crucial to completely remove all the calcium carbonate. The extra EDTA was washed away with DI water before any measurements.

The morphologies of the coated Aptamer-$CaCO_3$ particles after deposition of 5 bilayer or three layer polyelectrolyte films and microcapsules (after dissolution of $CaCO_3$ template) were checked by SEM. The fluorescein labeled SRB aptamer was used to check the state of aptamers in Aptamer-$(PAH/PSS)_5$ microcapsules by confocal microscope.

2.2.5 Fabrication of Aptamer:PSS - $(PAH/PSS)_x$ microcapsules

2.2.5.1 Materials

Sulforhodamine B aptamer, PAH, PSS, NaCl and EDTA were the same as previous described.

2.2.5.2 Methods

Both PSS and aptamer (weight ratio 1:5) were encapsulated inside of the porous $CaCO_3$ particles in coprecipitation process as described before. The Aptamer:PSS-$CaCO_3$ particles were incubated in 1ml 3mg/ml PAH or 3mg/ml PSS in 0.5M NaCl solution alternatively, for 30 minutes with intermediate washing steps (3 times DI water) to constitute a single bilayer (PAH/PSS) film on the particles to check the feasibility of the introduction of PSS into the core of the microcapsules.

The deposition steps were monitored by a Malvern Zetasizer and SEM as in previous studies.

2.2.6 Fabrication of Aptamer: PSS - $(PDDA/PSS)_5$ microcapsules

2.2.6.1 Materials

Sulforhodamine B aptamer, PSS, NaCl and EDTA were the same as previous described. Medium Molecular weight (Mw~200,000) PDDA (20% aqueous solution) was purchased from Aldrich Company.

2.2.6.2 Methods

Aptamer:PSS-$CaCO_3$ particles were fabricated in the same process as described above.

The Aptamer: PSS-$CaCO_3$ particles were incubated into 3mg/ml PDDA or 3mg/ml PSS in 0.5M NaCl solution, alternatively, for 30 minutes with intermediate centrifugation and washing steps (3 times) to construct a 5 bilayer (PDDA/PSS) film on the particles. 0.5 M EDTA solution was used to dissolve the template to get the microcapsules.

The deposition steps were monitored on a Malvern Zetasizer and SEM. The elemental analysis was conducted on an Oxford EDS® (Energy Dispersive X-ray Analysis) instrument, with INCAx-act® Detector and INCA Energy software was used to analysis the components. The samples were spread evenly on Al studs and the elemental analysis measurements were conducted in Nitrogen environment.

2.2.7 Triggered release properties of Aptamer:PSS-$(PDDA/PSS)_5$ microcapsules

2.2.7.1 Materials

Aptamer:PSS-$(PDDA/PSS)_5$ microcapsules were fabricated following the steps as described before. Sulforhodamine B dye was purchased from Aldrich Company. Tetremethylrosamine chloride (TMR) (378.90g/mol) was purchased from Invitrogen Company.

2.2.7.2 Methods

Aptamer:PSS-$(PDDA/PSS)_5$ microcapsules were incubated with Sulforhodamine B (SRB) dye at different concentrations and incubation times to achieve suitable parameters for the triggered release. Besides this, the microcapsules were also incubated with non target molecule-Tetramethylrosamine (TMR) dye to check the selectivity of microcapsules. After incubations all samples were washed three times with DI water and stored at -80°C freezer before measurements.

$(PDDA/PSS)_5$ coated Aptamer:PSS-$CaCO_3$ particles and Aptamer :PSS-$(PDDA/PSS)_5$ microcapsules were also spread onto the Al studs immediately after sample fabrication and stored at -80°C for using as control samples.

The SEM images were conducted on Cryo Stages. After leaving samples at -20°C for a few minutes to allow the water solvent to evaporate, all the measurements were operated at -30°C in Low Vacuum Environment SEM by using BSE (Back Scattered Electron) Detector under 10 Pascal Nitrogen pressure condition.

2.2.7.3 The calculation for aptamer molarity in each microcapsule

Before designing experiments to unravel the required parameters for triggered release in Aptamer:PSS-$(PDDA/PSS)_5$ microcapsules, the molarity of aptamers in the each microcapsules needed to be calculated.

There were 3.3×10^{-4} moles $CaCl_2$ in 1ml 0.33M $CaCl_2$ solution, and 3.3×10^{-4} moles $NaHCO_3$ in 1ml of 0.33M $NaHCO_3$ solution. Assuming 100% porous spherical $CaCO_3$ particles were produced (no cubic $CaCO_3$), then the mass of porous $CaCO_3$ will be 0.0330g.

The density of porous $CaCO_3$ particles $\rho=1.6g/cm^3$ [76], $m_{CaCO3} = 0.0330g$,

Then the total volume of the $CaCO_3$ particles: $V_{CaCO3} = m/\rho=0.0206cm^3 =2.06\times10^{-8}m^3$.

Based on SEM images measurements, the average radius of particles r is at 2.4μm, so the volume of each individual particle is equal to: $V=4/3\pi r^3= 5.6\times10^{-17} m^3$.

Then, the number of porous $CaCO_3$ particles in total will be: $N=2.06\times10^{-8} m^3 / 5.6\times10^{-17}m^3 =3.69\times10^8$

In each reaction, 0.64mg of aptamer was loaded into these $CaCO_3$ particles, so in each porous $CaCO_3$ particle, it contains $0.64\times10^{-3}/3.69\times10^{8}=1.74\times10^{-12}$ g Aptamer.

The molecular weight for sulforhodamine B Aptamer is 9146.9g, [77] so in each $CaCO_3$ particle contains $1.74\times10^{-12}/9146.9=1.90\times10^{-16}$ moles Aptamer.

Based on CLSM measurements, the average radius for the core of porous $CaCO_3$ is 1.6μm, the volume of Aptamer in each $CaCO_3$ particle is equal to $V'= 4/3\pi r^3 = 1.715\times10^{-17}m^3=1.715\times10^{-14}L$.

Assuming all aptamers were loaded inside of $CaCO_3$ particles and none was left in DI water solvent and also that aptamers distributed in each particle evenly, then the volume of aptamers in each particle will be equal to the volume of $CaCO_3$ hollow core. So maximum molarities for Aptamers in each particles will be $1.90\times10^{-16}/1.715\times10^{-14}=1.11\times10^{-2}M$.

2.2.7.4 Parametric study of triggered release conditions

SRB dye concentration: If the incubated SRB dye concentration equals 10μM, [dye] × [Aptamer] $=10\times10^{-6}\times1.11\times10^{-2}=1.11\times10^{-7}$ < Kd (660nM=6.6×10^{-7} M), which means that only a low proportion of aptamer-dye complex will form in this sample. If the SRB dye concentration is increased to 1mM, [dye] × [Aptamer] = $1\times10^{-3}\times1.11\times10^{-2}=1.11\times10^{-5}$ > Kd, then more than 50% aptamer-dye complex will form. (Equation for Kd was given in introduction)

Time: 16 hours, 1 day and 6 days were chosen to check the release status of microcapsules.

Then a systematic experiment was designed as follows:

1) Microcapsules incubated in 1mM SRB dye for 16 hours, 1 day and 6 days; 2) Microcapsules incubated in 10μM SRB dye for 1 day and 6 days to compare the microcapsules status. All SRB dyes were dissolved in 0.1M KCl solution. All samples were imaged under frozen conditions on cryo stages by SEM and EDS.

2.3 Results and discussions

2.3.1 Effect of concentration, temperature and reaction time on the synthesis of $CaCO_3$ particles

In this project, spherical porous $CaCO_3$ served as the template for the formation of polyelectrolyte microcapsules. While spherical $CaCO_3$ particles can be obtained from low reactant concentrations, (0.1M $CaCl_2$ and 0.1M $NaHCO_3$), the yield of spherical $CaCO_3$ is too low to continue the experiments. (Fig.2-5a). Under high reactant concentrations (1M of salts) all particles are cubic. (Fig.2-5b) In the intermediate case (0.33M salts), more spherical $CaCO_3$ particles were formed than in 0.1M and 1M solution but some $CaCO_3$ particles still were cubic. (Fig.2-5c) Comparing all three SEM images, the 0.33M concentration was studied for further parameter determination.

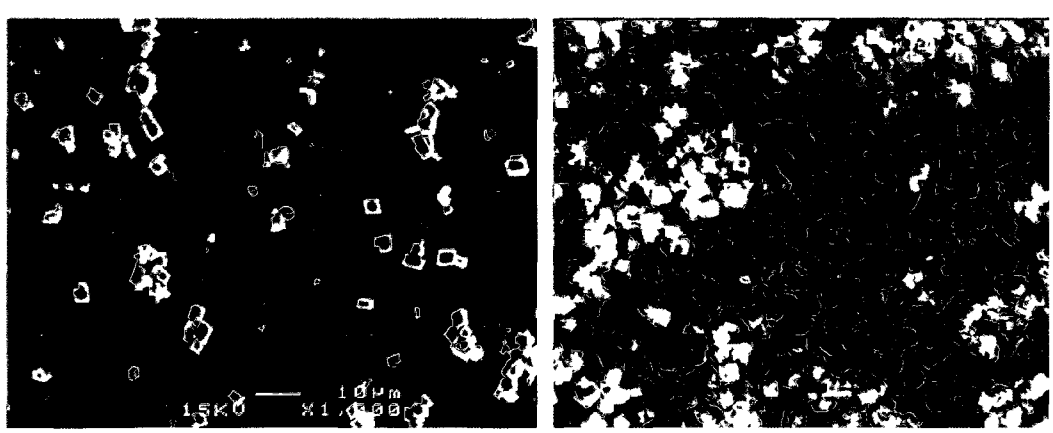

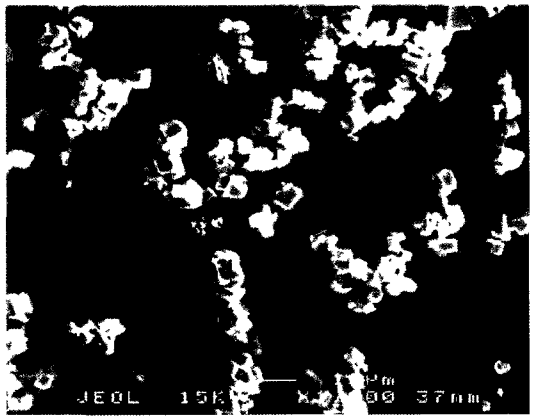

Fig.2-5 SEM images of $CaCO_3$ particles from different salt concentrations reacted at room temperature and left to sit for 30 minutes: a) 0.1 M, b) 1M, c) 0.33M

The effect of temperature was next examined. When the sample was reacted at 10°C, the percentage of spherical particles increased compared with which reacted at room temperature (both at 0.33M concentration). The SEM image is shown in Fig.2-6a. At higher reaction temperature (15 °C or 20°C), almost all particles were cubic. The SEM images are shown in Fig.2-6b and Fig.2-6c respectively.

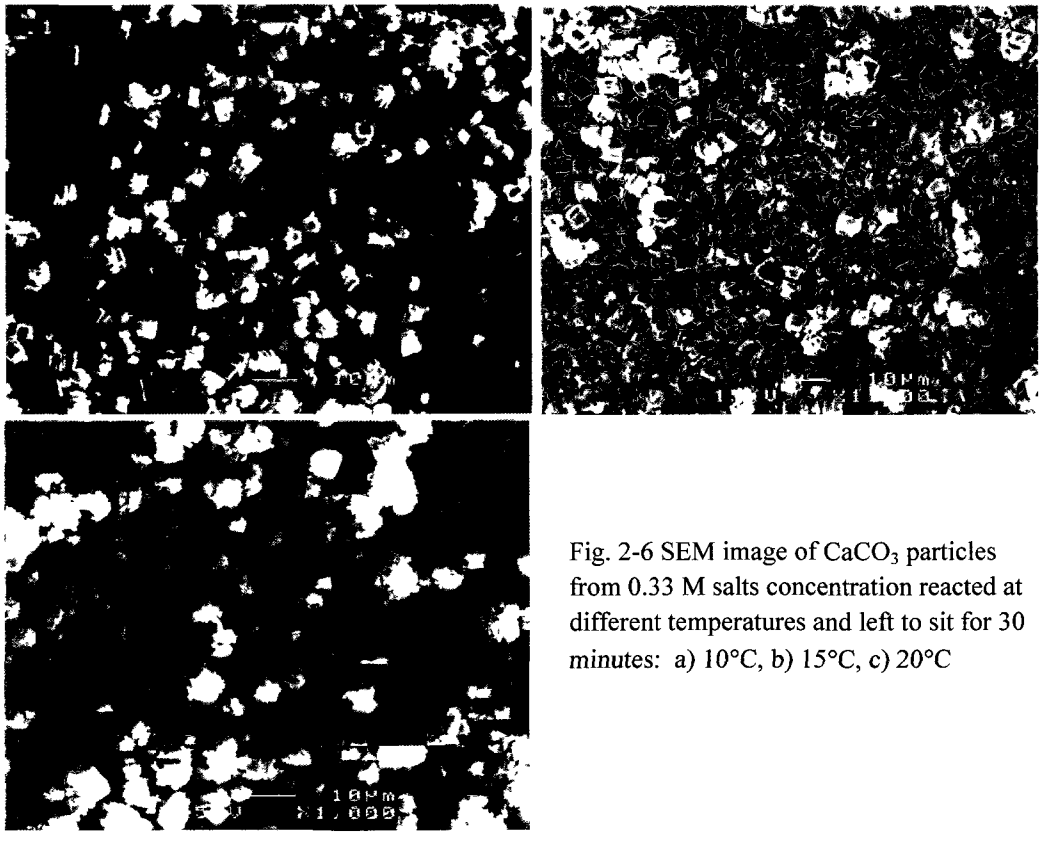

Fig. 2-6 SEM image of $CaCO_3$ particles from 0.33 M salts concentration reacted at different temperatures and left to sit for 30 minutes: a) 10°C, b) 15°C, c) 20°C

The possibility of forming spherical $CaCO_3$ particles at different reaction times was investigated in detail. As shown in Fig.2-7a, when left to sit for 4 minutes, spherical $CaCO_3$ particles can be obtained, but the percentage is low. When the reaction time is elongated to 5 minutes (Fig.2-7b) and 6 minutes (Fig.2-7c), the percentage of spherical $CaCO_3$ particles increased with 6 minutes showing the highest percentage. But when the reaction time was increased further to 7 minutes and 8 minutes, (Fig.2-7d and Fig.2-7e) most particles went back to cubic structure.

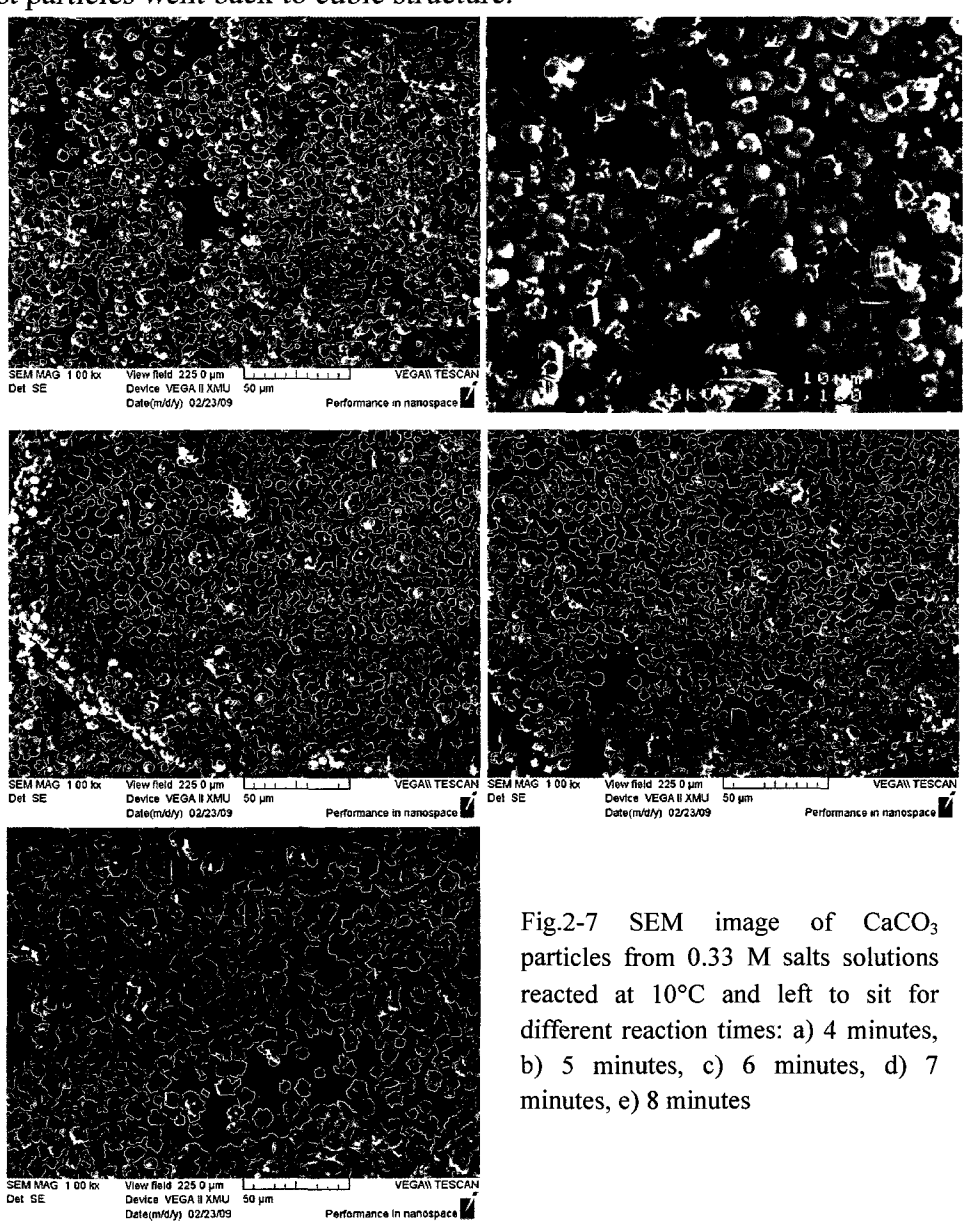

Fig.2-7 SEM image of $CaCO_3$ particles from 0.33 M salts solutions reacted at 10°C and left to sit for different reaction times: a) 4 minutes, b) 5 minutes, c) 6 minutes, d) 7 minutes, e) 8 minutes

Comparing the morphologies of $CaCO_3$ particles in all the SEM images, 0.33M of salt concentration, reacted at 10°C and left to sit for 6 minutes, as shown in Fig.2-7c were the refined parameters for fabricating a large percentage of spherical $CaCO_3$ particles (Biomaterials such as aptamer can be loaded inside) in low reaction volume. Based on the size measurements of the spherical $CaCO_3$ particles in these SEM images, the size of the spherical porous $CaCO_3$ was from 4-6μm, which is also the same size range as described in the literature. [72]

2.3.2 Synthesis of aptamer-$CaCO_3$ particles

Aptamer-embedded $CaCO_3$ particles were prepared by a coprecipitation process with varying aptamer to $CaCO_3$ ratios. Confocal imaging was used to characterize these particles as the used aptamer was tagged with fluorescein. Fig.2-8a shows the fluorescent image from the confocal microscope for the samples prepared at a ratio of 1:6.6. This image clearly presented that in some areas the fluorescent intensity was stronger than the background. The Fig.2-8b shows the light image for the same sample. This image shows that there are some particles on the glass slide and the sizes of these particles were in 4-6μm ranges which were in the range for the porous $CaCO_3$ particles. The Fig.2-8c is the overlay of these two images. The Fig.2-8 proved that the higher fluorescent areas were coming from the porous $CaCO_3$ particles. The results indicated that coprecipitation method was suited for the fabrication of Aptamer-$CaCO_3$ particles. But these CLSM images also showed that there were lots of free aptamer left outside of the porous $CaCO_3$ particles. These free aptamer were spread on the glass slide and presented as the small green spots on the background. The results show that not all the aptamer was included in the coprecipitation process. Even after three DI water washing steps, there were still too

much unwrapped aptamer left outside. Reducing the added amount of aptamer was then investigated.

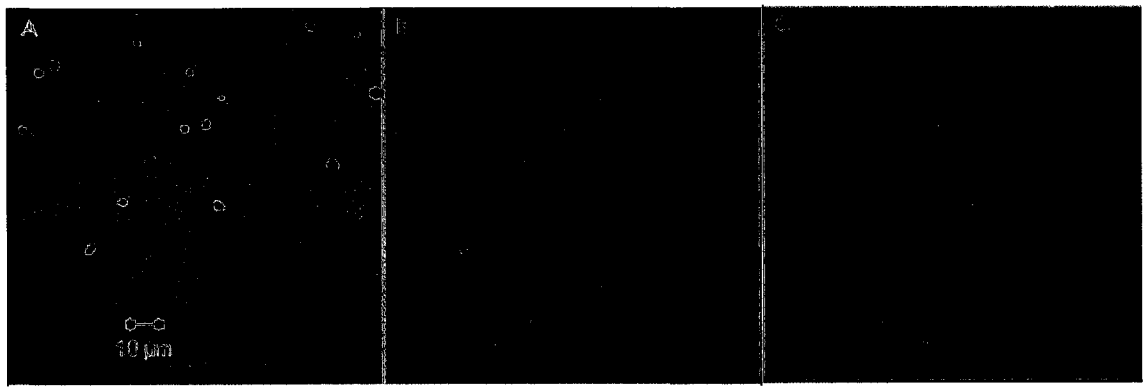

Fig.2-8 Confocal images of Aptamer-$CaCO_3$ particles from aptamer: $CaCO_3$ weight ratio at 1:6.6. A) fluorescent image, B) light image, C) overlay of A and B.

Changing the aptamer to $CaCO_3$ ratio to 1:22.0 (Fig.2-9) led to a reduction in the background green spots. However the enlarged inset in Fig.2-9c clearly presented that several Aptamer-$CaCO_3$ particles were aggregated together, perhaps due to extra aptamer on the surface of the $CaCO_3$ particles linking the separated $CaCO_3$ particles together.

Fig.2-9 Confocal images of Aptamer-$CaCO_3$ particles from aptamer: $CaCO_3$ weight ratio at 1:22.0. A) fluorescent image, B) light image, C) overlay of A and B. Inset image is enlarged image.

Changing the ratio further to 1:47.2, all fluorescent signals were coming from the Aptamer-$CaCO_3$ particles and no particles were found that were aggregated together, suggesting that no free aptamer was left outside of the particles (Fig.2-10). The status of

the aptamers in these $CaCO_3$ particles was checked by high magnification images. The previous studies showed that pure $CaCO_3$ will be evident as non fluorescent particles and fluorescein-tagged aptamers will be evident as a green fluorescent. In Fig.2-10c, the green colour is only present inside of the hollow cores of porous $CaCO_3$ particles and was uniformly distributed throughout the whole core of the particles. There were no fluorescent signals from the walls of the Aptamer-$CaCO_3$ particles suggesting that no aptamer is bound to the outside of the particles. Based on the measurements of different individual Aptamer-$CaCO_3$ particles, the width of the porous $CaCO_3$ wall were in the 1.5-2μm range. The average radius of the cores of these particles was 1.6μm. If aptamers were distributed evenly inside of these particles, then aptamers in each particle occupy the same volume as the Aptamer-$CaCO_3$ core.

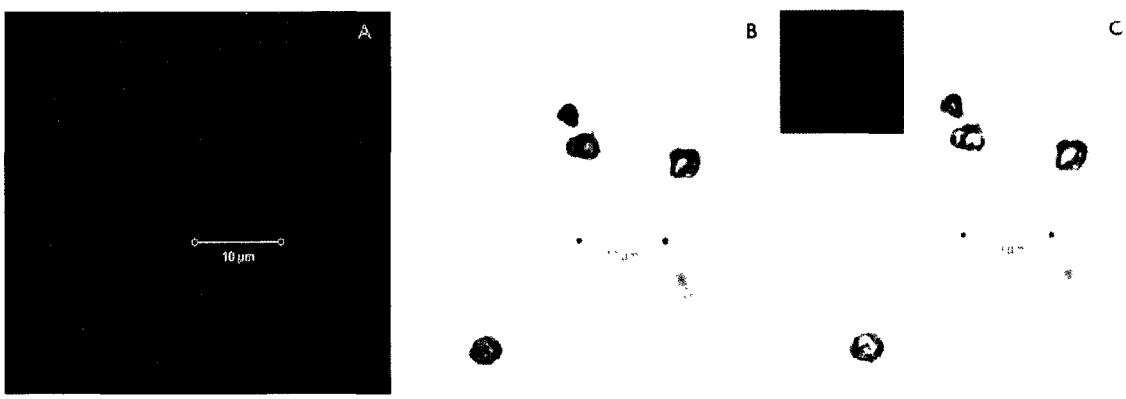

Fig.2-10 Confocal images of aptamer-$CaCO_3$ particles from aptamer: $CaCO_3$ weight ratio at 1:47.2, A) fluorescent image, B) light image, C) overlay of A and B. Inset is enlarged particles.

The morphology of these Aptamer-$CaCO_3$ particles from the 1:47.2 weight ratio syntheses was checked by SEM. After loading the aptamers inside the $CaCO_3$ particles, the particles still remain in a spherical structure as shown in Fig.2-11. The surfaces of the particles were as smooth as those without embedded aptamers. The encapsulation of the DNA aptamers did not change the morphologies of these particles.

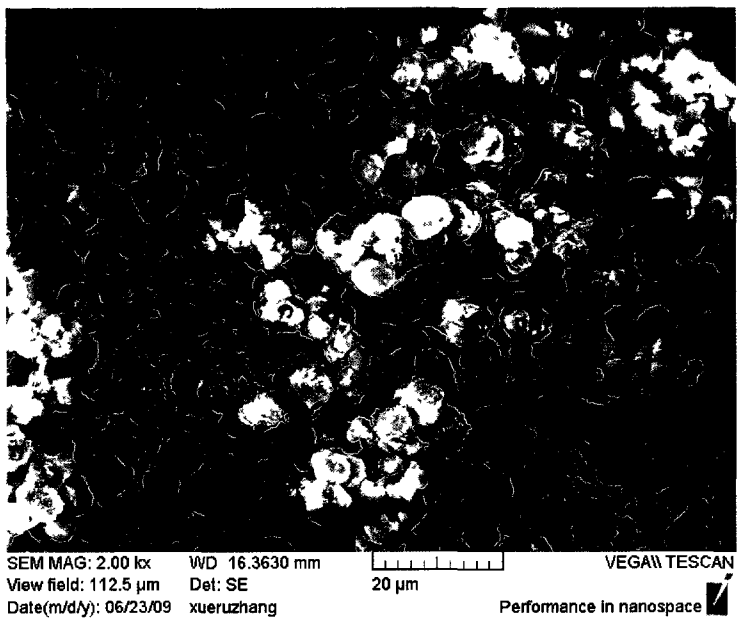

Fig.2-11 SEM image of Aptamer-$CaCO_3$ particles

Thus, the Aptamer-$CaCO_3$ particles were successfully fabricated by a coprecipitation method and the aptamers were uniformly distributed inside of the core of the porous $CaCO_3$ particles at a weight ratio of aptamer to $CaCO_3$ was at 1:47.2. After aptamer loading into the $CaCO_3$ particles, the morphology of the particles remained as spherical structures.

2.3.3 Parametric study of multilayer film formation

As discussed in the introduction, oppositely charged polyelectrolytes will form a large amount of ion pairs between each other or with the charged substrates to form films. This is an overcompensation electrostatic interaction process. The equilibrium adsorption will be obtained until the polyelectrolytes are electrostatically repelled from each other. [34] In this process, the concentration of the polyelectrolyte, the ionic strength (including the type of the salts) and the pH value of solution will determine the properties of the films. [34-37] So, we conducted a series of experiments to obtain proper synthesis parameters in

terms of the concentration of the polyelectrolyte, the ionic strength and the pH value of solution.

2.3.3.1 Effect of Ionic strength

The measured ζ potential of the pure $CaCO_3$ particles dispersed in DI water is positive at 12.5 mV. After sulforhodamine B aptamers were loaded into the core of $CaCO_3$ particles, the ζ potential of particles switched to negative at -22.3mV. This result further confirmed that the aptamers have been loaded into the $CaCO_3$ particles. (see Table 2-1).

Then, Aptamer-$CaCO_3$ particles were incubated into two series of PAH-NaCl solutions (series 1 was in 0.2M NaCl and series 2 was in 0.5M NaCl). The results suggested that in high ionic strength lower amounts of PAH was needed to reach the highest ζ potential value. (Fig.2-13) The reason for this may be that the deposition of PAH on the surface of the Aptamer-$CaCO_3$ particles includes two processes. The first process is an intrinsic absorption process. Only PAH deposits onto the particles, so ζ potential value will go to the positive direction. The second process is an extrinsic process. When the charge density of the PAH deposited on the particles surface is higher than the saturated value, the particles will absorb some oppositely charged counter ions from the solution. Then ζ potentials will go to the negative direction. [78] Comparing the two plots in Fig.2-13, at 0.5 M NaCl solution, only 15μg PAH was needed for the charge density of the PAH polymer chain to be saturated. But in 0.2M NaCl solution, 25μg PAH was required to get the saturated charge density. It was reported that with the increasing ionic strength of the solution, the polyelectrolytes will have more possibility to reorganize their structure. [79] In high salt concentration solution, polyelectrolytes will coil up together and no longer remain in a rod-like structure and this coiled structure is easier to deposit onto the

spherical particles. Beside this, with increased ionic strength, the pH value near the surface of the polyelectrolyte will decrease. While in a lower pH value solution, the degree of protonation of the weak polyelectrolyte PAH will increase and this will improve the formation of films. The influence of pH value on the degree of protonation of PAH will be further discussed in the next section 2.3.3.2.[80] As a result, 0.5M NaCl was chosen to adjust the ionic strength.

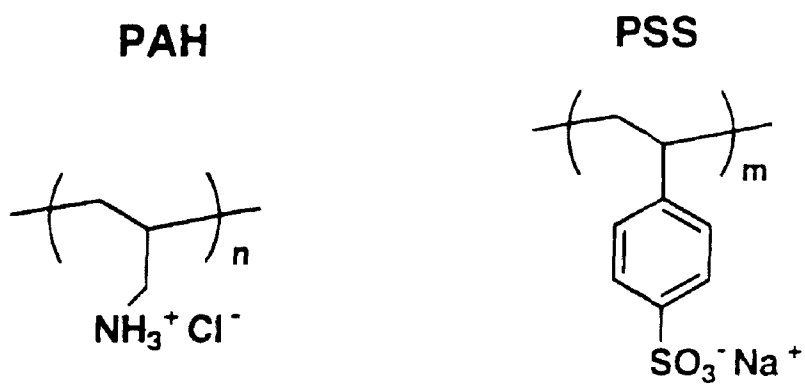

Fig.2-12 Chemical structure of PAH and PSS

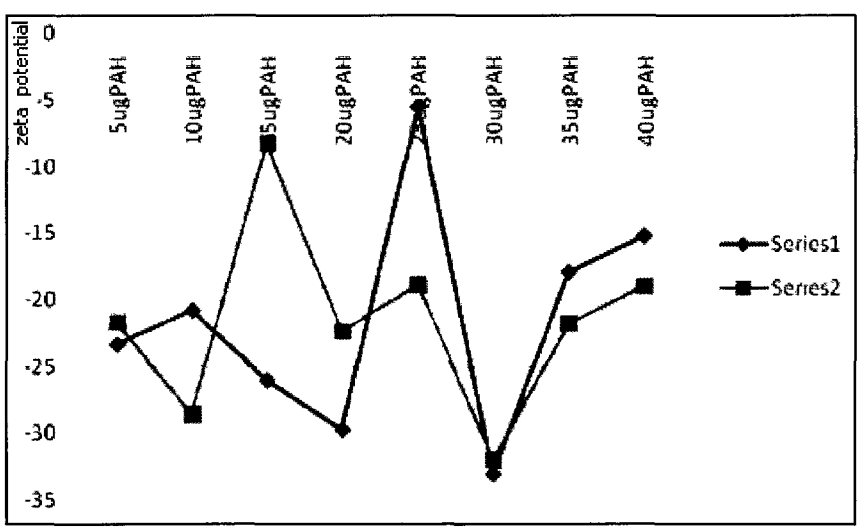

Fig. 2-13 ζ potential of aptamer-$CaCO_3$ particles as a function of amount of PAH (series 1 in 0.2M NaCl solution, series 2 in 0.5M NaCl solution)

2.3.3.2 Effect of deposition conditions

With the increasing deposition amount of PAH, the particles' ζ potential will be increased and at last they will switch to positive which has already been demonstrated for hollow porous $CaCO_3$ particles. [32b] But as seen above, none of the particles' ζ potential had became positive. The reason may be that as the PAH concentration was too low but the concentration of salts was high, these PAH polymer strands cannot effectively wrap on the whole surface of particles. For a single PAH polymer chain there may remain free functional groups which will absorb counter ions to reduce the electrostatic repulsion along the polymer chains. If the ζ potential of the particles did not switch to positive, it would be difficult to continue the LbL process. To minimize the effect of high ionic strength, the concentration of PAH was increased to supersaturation as reported in the literature. [35]

As a weak polycation, the pKa of the primary amine in free PAH in solution is about 10.5. [78] Under low and moderate pH conditions, the amine group is positively charged and the degree of ionization of PAH is high. But under high pH conditions, the dissociation of H^+ ions from PAH will lead to uncharged free amine groups. Then the degree of ionization of PAH will decrease, which will damage the formation of the films. [81] In the previous study, the pH value of DI water medium was close to neutral, which was within the suitable condition for a high degree of protonation. The question then is would the deposition efficiency be enhanced if the pH value was held at 6.55 for the whole deposition process by the addition of bis-tris buffer? To achieve appropriate the best deposition conditions, three different experiments were compared: 1) bis-tris buffer was added, 2) NaCl was added; 3) both bis-tris and NaCl were added.

The results in Tab.2-1 demonstrated that the ζ potential of Aptamer-$CaCO_3$ particles incubated with PAH/NaCl or PAH/bis-tris all switched to positive values. And in PAH/NaCl solution the highest ζ potential value was obtained. But the Aptamer-$CaCO_3$ particles incubated both with the PAH and NaCl/bis-tris buffer still remained at negative values, which perhaps means that the deposition of PAH polymer was low. The low deposition efficiency may be caused by competitive adsorption of bis-tris buffer salts with PAH. The bis-tris buffer, which contains hydroxyl functional groups, will be attracted by the Aptamer-$CaCO_3$ particles and may bind with them.[81] As a result, the formation of the film is not as ideal as without the buffer.

Besides the obviously low deposition efficiency in bis-tris buffer solution, the number of particles after incubation in buffer was reduced compared to the number of particles without buffer condition. The reason may be that by adjusting the buffer pH value will dissolve the solid $CaCO_3$ templates slowly during the incubation process. The possible reaction was shown as below.

$$2H^+ + CaCO_3\,(s) \rightleftharpoons Ca^{2+} + 2\,HCO_3^-$$

All of the results revealed that bis-tris buffer will impair the deposition of the PAH. So the idea of using buffer in film formation process was discarded.

Sample	ζ potential (mV)
$CaCO_3$ particles	12.5
Aptamer-$CaCO_3$ particles	-22.3
Aptamer-$CaCO_3$ in 2mg/ml PAH solution, pH=6.55	2.52
Aptamer-$CaCO_3$ in 2mg/ml PAH-0.5 M NaCl solution	3.98
Aptamer-$CaCO_3$in 2mg/ml PAH-0.5 M NaCl solution, pH=6.55	-5.76

Table 2-1 ζ potentials of $CaCO_3$, aptamer-$CaCO_3$ particles and coated particles under different conditions

2.3.3.3 Effect of polyelectrolyte concentration

There was not much difference in surface charge of the particles in low or in high PAH concentration- 0.5M NaCl solutions; both become positive at 3.98mV or 3.50mV. In high concentration PAH deposition solution, the ζ potential value was even a little lower. The positive surface charges indicate the successful deposition of PAH onto the surface of Aptamer-$CaCO_3$ particles. But the value is lower than that normally observed for PAH as the outermost layer in hollow microcapsules (which is typically about 40mV). [34b] This phenomenon may be caused by the loading of the negatively-charged aptamer inside of the $CaCO_3$ particles which could partially neutralize the positive charge of PAH. [82]

Then, particles were incubated in PSS/NaCl solution to continue the assembly process. At this time, the surface charges of particles obtained from the two different concentration conditions were quite different. After coating two layers of polyelectrolyte films in low concentration, surface charge was at about -0.7mV, a value too low to continue the layer-by-layer assembly process as ζ potentials of particles should alternate between positive and negative values during alternative absorption of polycation and

polyanion. [32b] When both PAH and PSS concentration was increased to 3mg/ml, the surface charge of particles after coating with the PSS film switched to -18.46mV. This value suggested that the absorption of PSS onto the surface of Aptamer-$CaCO_3$ particles was successful. (Table 2-2)

sample	ζ potential (mV)
Aptamer-$CaCO_3$ coating the first layer in 2mg/ml PAH	3.98
Aptamer-$CaCO_3$ coating the first layer in 3mg/ml PAH	3.50
Aptamer-$CaCO_3$ coating one bilayer film in 2mg/ml PAH and 2mg/ml PSS	-0.70
Aptamer-$CaCO_3$ coating one bilayer film in 3mg/ml PAH and 3mg/ml PSS	-18.46

Table 2-2 ζ potential of the aptamer-$CaCO_3$ particles after coating one layer of PAH and bilayer PAH/PSS at different concentrations. (ionic strength is 0.5 M NaCl)

SEM images will provide information about the surface morphology of the particles which will confirm the completeness of the films. [43a] As shown in Fig.2-14, even though the ζ potential value of the particles after deposition of the first layer of polyelectrolyte was similar, the morphology of the film obtained from the low concentration experiments were not as complete as that from the high concentration series. After deposition of PAH, the morphology of the particles in high concentration looks like a pine cone. (recall that without PAH, the surface of Aptamer-$CaCO_3$ particles was smooth). This difference between the film morphologies at different polyelectrolyte concentrations became more obvious when we continued the assembly process. (Fig.2-15) The lower density of the films meant lower deposition efficiency of the films and this result also further confirmed

the difference between ζ potential values obtained from the two different polyelectrolyte concentrations.

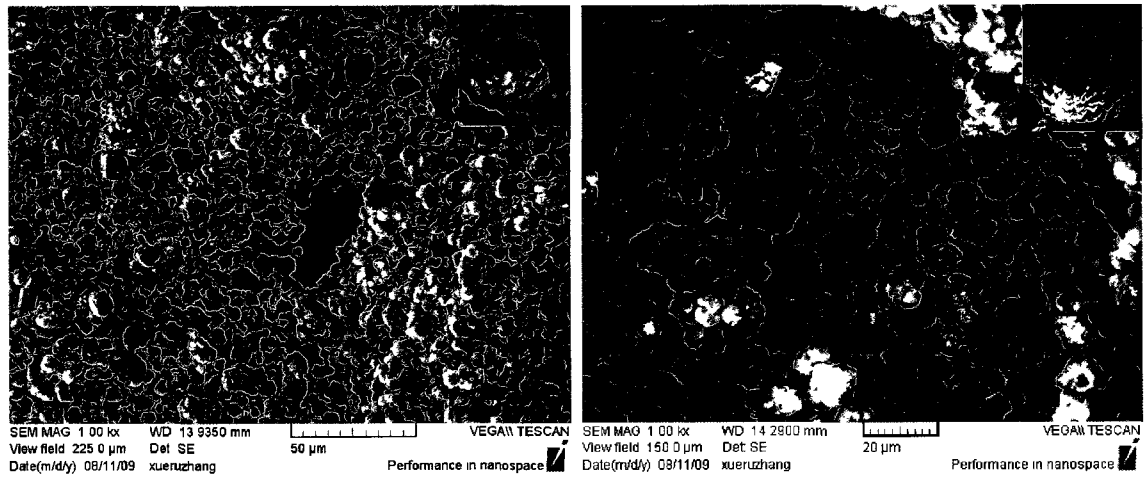

Fig.2-14 SEM images after deposition of the first layer of PAH. 2mg/ml (left), 3mg/ml (right), Insets were the enlarged particles. (ionic strength is 0.5M NaCl)

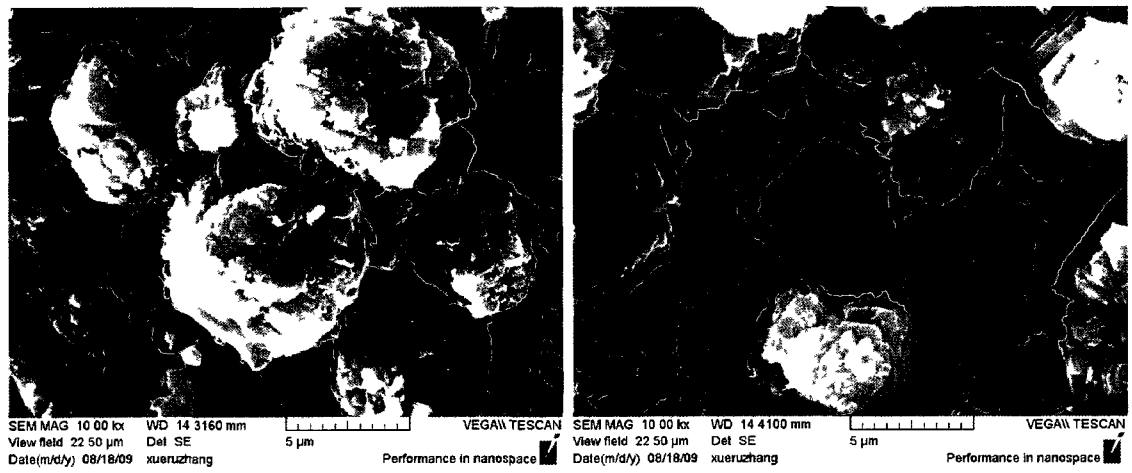

Fig.2-15 SEM images after deposition of one bilayer of PAH/PSS. 2mg/ml (left) , 3mg/ml (right). (ionic strength is 0.5M NaCl)

Overall, these parametric studies of the experiments found that no buffer was needed to adjust the pH value of solution for the deposition. High ionic strength was shown to enhance the deposition efficiency of the films, so 0.5M NaCl was chosen to adjust the

ionic strength. Furthermore, supersaturated polyelectrolyte concentration solutions at 3mg/ml provided the best performance.

2.3.4 Characterization of Aptamer-$(PAH/PSS)_5$ microcapsule

The morphology of particles after deposition of one bilayer PAH/PSS films in 3mg/ml polyelectrolyte concentration was already confirmed. But after repeating the layer-by-layer process under the same deposition conditions until a 5 bilayer polymer film was deposited, the size of most individual particles increased to 20μm, (Fig. 2-16) and film morphologies were no longer as regular and complete as what was seen after a single bilayer deposition. (Fig.2-15 right) If the polyelectrolyte films bound to the Aptamer-$CaCO_3$ particles normally, the thickness of each layer of film is about 3-5nm. [43] The average size for Aptamer-$CaCO_3$ particles is in the 4-6μm range, so after 5 bilayer deposition the size of these particles should have remained in the 4-6μm range. The reason of the formation of this irregular 5 bilayer Aptamer-$CaCO_3$ structure may be that the weak polyelectrolyte PAH may contain some degrees of the uncharged free amine groups under experimental conditions, so the electrical repulsion between the particles and polymers will be weak. [79, 80] Due to the fact that supersaturated polyelectrolyte solutions were used in the film formation process, extra polyelectrolyte PAH will be attracted by the particles, and the size of aptamer-$CaCO_3$ particles will be increased abnormally. With the increased number of layers deposited, the possibility of forming these artifacts will be increased. Besides this, the evidence of different particles linked together by the polymers was also found. (Fig. 2-16 right) So the size may be also increased by the aggregation of individual particles. [32b] In addition, with the increased layer number this aggregation phenomenon will be more obvious.

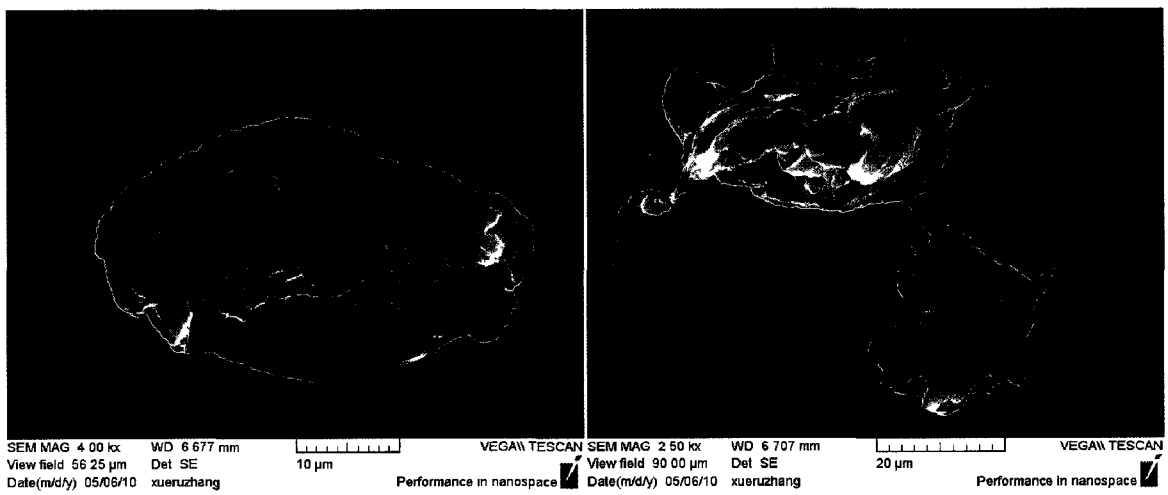

Fig.2-16 SEM images of the aptamer-$CaCO_3$ particles after coating $(PAH/PSS)_5$

After the dissolution of $CaCO_3$ template, the size of Aptamer-$(PAH/PSS)_5$ microcapsules should decrease or they should stay flat on the surface of the substrate (almost no 3-dimensional structure) under dry conditions. But most SEM images for aptamer-$(PAH/PSS)_5$ show that after dissolving the $CaCO_3$ template by EDTA, the capsules were still larger than 6µm (what would be the average size of porous $CaCO_3$ particles). (Fig.2-17) The irregular deposition of polyelectrolyte and the aggregation of aptamer-$CaCO_3$ particles will form larger than expected microcapsules. The image on the left may be individual capsules and the right image may present several capsules aggregated together. As a result, the majority of the particles seen on the SEM appeared to be agglomerates.

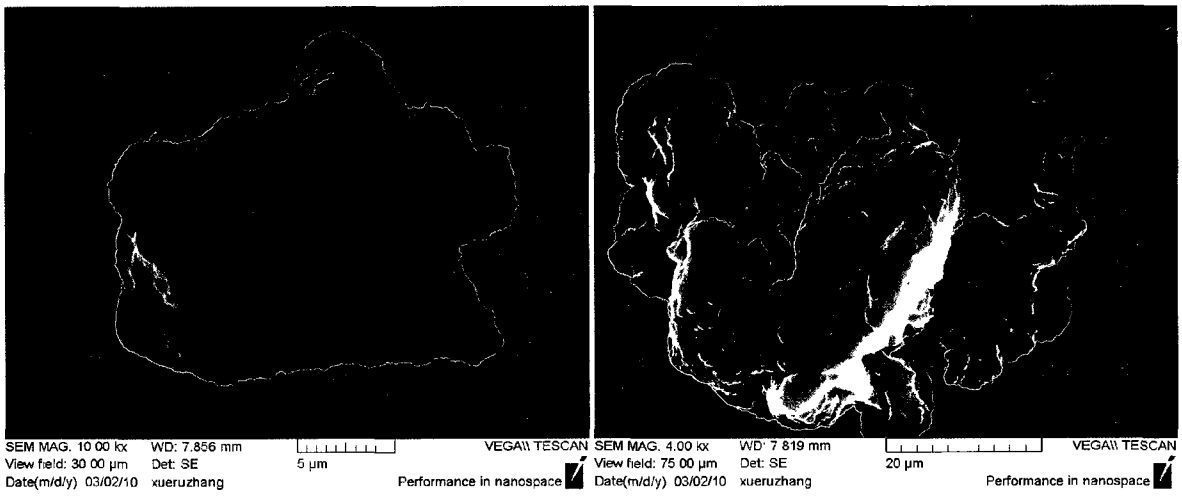

Fig.2-17 SEM images of Aptamer-$(PAH/PSS)_5$ microcapsules

While the majority of the particles seen on the SEM appeared to be agglomerates, the CLSM images showed a few samples that were in the correct size range for an individual microcapsule. Fig.2-18 shows a capsule after the template dissolution. The fluorescence from the aptamer within the capsule can still be seen, confirming that the aptamer remained within the capsule after template dissolution.

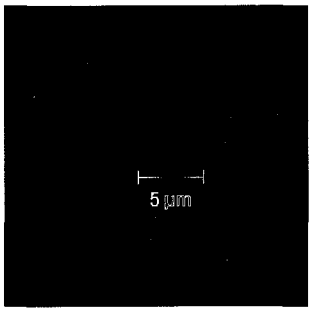

Fig.2-18 CLSM image of the aptamer-polyelectrolyte microcapsules

2.3.5 Characterizations for Aptamer-(PAH/PSS/PAH) microcapsule

Because the majority of the Aptamer-$(PAH/PSS)_5$ samples imaged did not contain individual capsules, but rather agglomerates of capsules, fewer polyelectrolyte layers were deposited to Aptamer-$CaCO_3$ particles to reduce the possibility of aggregation during the layer-by-layer fabrication process. The morphologies of Aptamer-$CaCO_3$ cores

coated with a three layer PAH/PSS/PAH film were checked by SEM. After three deposited layers, however, agglomeration of the particles was still observed. Some of the particles were linked together by the polymers and were no longer as regular as what was seen for two layers. (Fig.2-19)

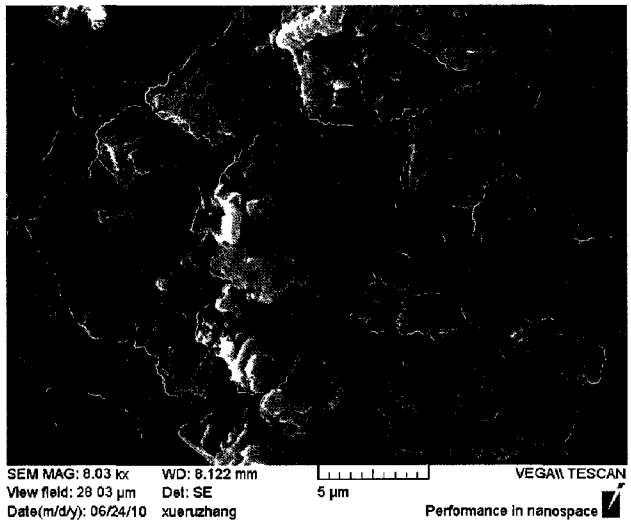

Fig.2-19 SEM image of the Aptamer-$CaCO_3$ particles after coating PAH/PSS/PAH

After dissolution of the $CaCO_3$ template, some cracks were found on the surface of microcapsules, suggesting poor stability and weak mechanical strength of these microcapsules.[83] It has been reported that unwanted leakage of the contents such as catalase enzyme from the 3 bilayer microcapsules can reach to 33% due to an unintegrated membrane.[84] The cracks found in the microcapsules will be mainly responsible for the leakage of the contents. Besides this, some microcapsules were still aggregated together, even though it was not as serious as seen with 5 bilayer microcapsules. (Fig.2-20)

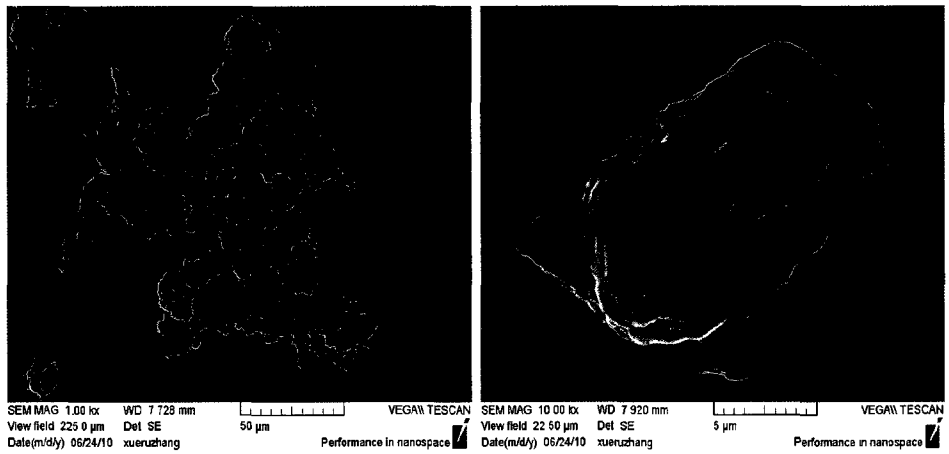

Fig.2-20 SEM images of the Aptamer- PAH/PSS/PAH microcapsules

There are two big issues to prevent the successful fabrication of Aptamer-$(PAH/PSS)_x$ microcapsules. 1) Aggregation of the Aptamer-$CaCO_3$ particles during the layer-by-layer deposition of polyelectrolyte films process is quite serious. Even when the deposition layers have been reduced to 3 layers this phenomenon still exists. 2) Besides this the stability of microcapsules with lower layer number is quite poor. The selectively increased permeability of microcapsules or the triggered release of contents properties are difficult to check.

In the next experiments, a small amount of PSS was encapsulated along with SRB aptamer inside the microcapsules. PSS doped porous $CaCO_3$ template have been shown to increase the stability of microcapsules after the dissolution of $CaCO_3$. [82, 85] PSS will bind with the opposite charged polymers which are deposited on the surface of particles instantaneously after being released from the porous $CaCO_3$ in the dissolution process, leading to the hardening of the microcapsule shell. The introduction of PSS in the $CaCO_3$ core will be a valid approach to fabricate stable microcapsules with a few layers of films. If both PSS and SRB aptamers work as the collapsible scaffold, it will not only improve the stability of the shell but also add the target selectivity function to the microcapsules.

2.3.6 Synthesis of Aptamer: PSS-$CaCO_3$ particles

The morphologies of the $CaCO_3$ particles after encapsulating with both SRB aptamer and PSS were checked by SEM. Most $CaCO_3$ particles remained as spherical structures and the surface of these particles was still quite smooth. (Fig.2-21) Compared to the Aptamer-$CaCO_3$ particles, the PSS-doped Aptamer-$CaCO_3$ sample contained a higher percentage of spherical particles. Like most organic macromolecules such as sodium dodecyl sulfate (SDS), [66] poly (acrylic acid), [70a] octadecyltrichlorosilane (OTS), [70b] and poly (alpha, beta)-DL-aspartic acid, [70d] PSS can also work as a template to mediate the morphology of the $CaCO_3$ particles. So, the yield of the spherical structures will be increased.

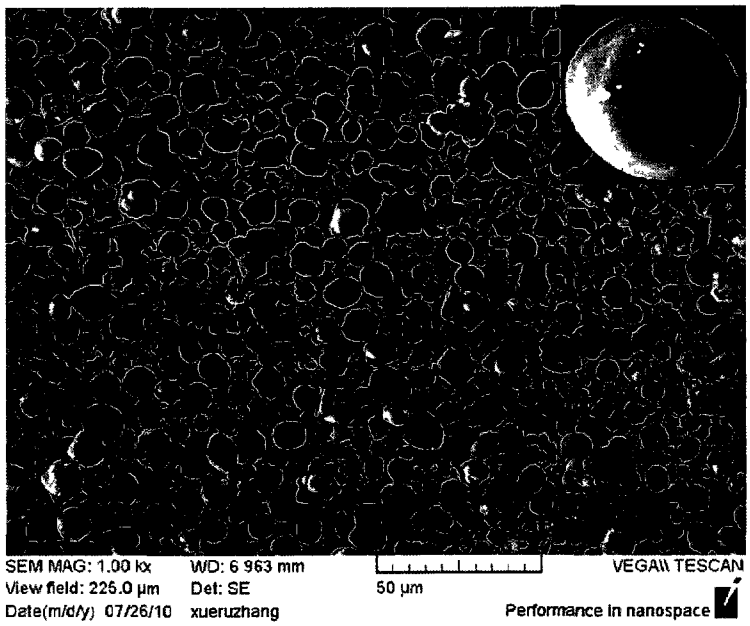

Fig.2-21 SEM images of the Aptamer: PSS $CaCO_3$ particles, inset is an enlarged one

The loading of the aptamer and PSS inside the $CaCO_3$ particles was characterized by ζ potential measurements. The ζ potential for pure $CaCO_3$ particles is at about 12.5mV, and after encapsulating the SRB aptamer, the ζ potential of Aptamer-$CaCO_3$ switched into the

negative range at -22.3mV (Table 2-1). After both the SRB aptamer and PSS were encapsulated in the $CaCO_3$ particles, the ζ potential of Aptamer: PSS-$CaCO_3$ particles turned out to be -16.7mV (Table 2-3). This value was even less negative than that of just $CaCO_3$ doped with SRB aptamer alone, the reason may be that PSS contributes less to the surface charge than aptamer by remaining more confined to the interior of the particles.

2.3.7 Characterization of Aptamer: PSS-(PAH/PSS) microcapsules

In this section, the deposition of polyelectrolyte films onto the Aptamer: PSS-$CaCO_3$ particles and the properties of Aptamer:PSS-(PAH/PSS) microcapsules are discussed mainly based on SEM measurements. The results for ζ potential measurements after coating with first layer PAH will be discussed later.

After coating one layer of PAH, the surfaces of most particles were no longer as smooth as before. Some regular, small chips like fish scales could be observed on the surfaces of the particles due to the adsorption of PAH. (Fig.2-22) After deposition of the first layer of PSS, most particles remained separated as individual particles. The results suggest that having the PSS inside the $CaCO_3$ template is helpful to increase the electrostatic repulsion between the particles and keep them separate. But evidence of aggregation by the polymer still can be found. (Fig.2-23) If the polyelectrolyte deposition process was continued to add more layer, the aggregation of the particles would likely worsen. So after deposition of just one bilayer PAH/PSS film, the particles were dissolved in an attempt to make the microcapsules. After dissolution of the $CaCO_3$ templates, the individual microcapsules flat on the surface of substrate were observed, but unfortunately, the structure of some microcapsules looked incomplete. As the polyelectrolyte wall of the microcapsules was only one bilayer thick, the mechanical

strength of the microcapsules was likely too low, even with the inner structural support of the PSS, causing unwanted breakage of microcapsules. Furthermore, most of these Aptamer: PSS-(PAH/PSS) microcapsules were still agglomerates. (Fig.2-24)

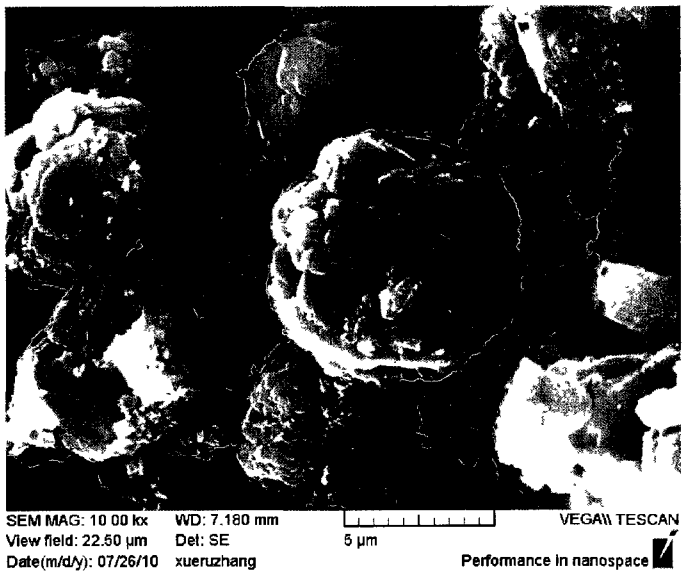

Fig.2-22 SEM image of the Aptamer: PSS-$CaCO_3$ particles after coating the first layer of PAH

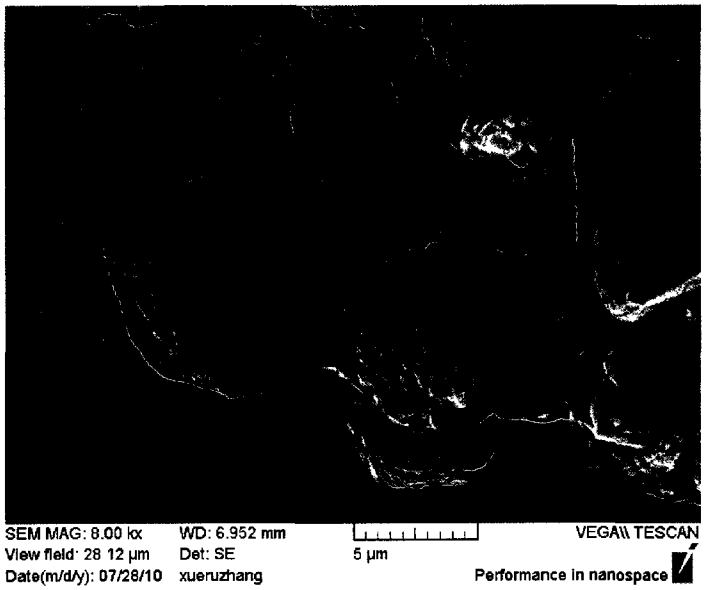

Fig.2-23 SEM image of the Aptamer: PSS-$CaCO_3$ particles after coating PAH/PSS

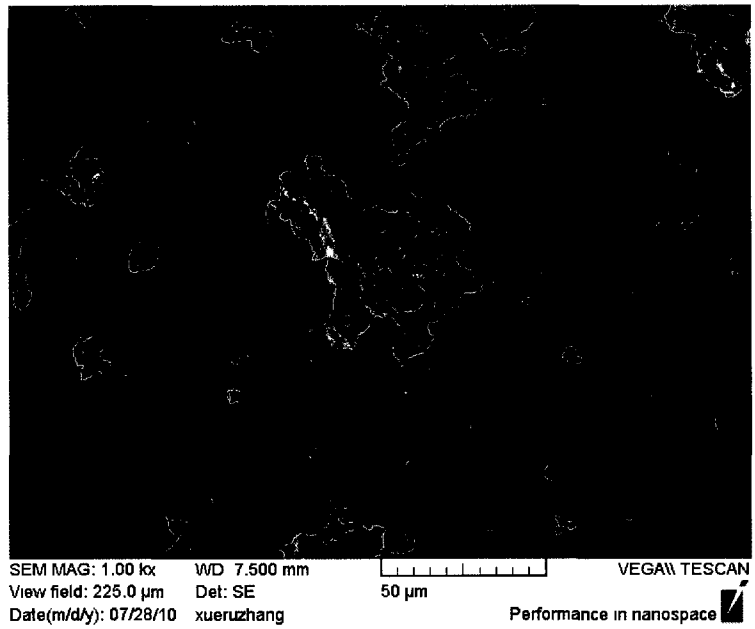

Fig.2-24 SEM image of aptamer: PSS-(PAH/PSS) microcapsules

The main advantages of doping PSS into the $CaCO_3$ cores will be that: 1) the macromolecular PSS can work as a template to provide nucleation sites for the growth of spherical $CaCO_3$ particles, leading to a higher percentage of synthesized spherical structure of $CaCO_3$ particles. 2) In the polyelectrolyte layer-by-layer deposition process, more individual particles were obtained than without the PSS doping.

Unfortunately, the aggregation phenomenon in Aptamer: PSS-(PAH/PSS) microcapsules was still observed. The electrostatic repulsion between the particles or microcapsules was perhaps too low leading to aggregation. Besides this, the broken microcapsules were observed due to low mechanical strength of these thin-walled microcapsules. So, in the following experiments, the partially charged, weak polymer PAH was replaced with the high charge density, strong polycation PDDA (polydiallyldimethylammonium chloride) and the LbL assembly process was continued until 5 bilayer films were deposited.

2.3.8 Characterization of Aptamer:PSS-(PDDA/PSS)$_5$ microcapsule

2.3.8.1 PAH vs PDDA

PAH, a weak base polyelectrolyte has pH dependent charge density along the polymeric chains. After incorporation into the polyelectrolyte multilayer film, each functional group on PAH will also be influenced by neighboring groups (they will create a potential to attract or repel protons), so the apparent dissociation constant of PAH in films will be reduced from 10.5[78] (for pure PAH) to 8.6. [86] As a result, PAH is more protonated at low pH values (pH < 4[86]) but in this pH range, the stability of the aptamer is low. [57] Even though the deposition behavior of PAH can be refined by adjusting the pH value of solution, this method still was discarded in this project.

On the other hand, PDDA has a pH-insensitive quaternary ammonium polycation that has high charge density in all pH ranges. It has been reported that the deposition behavior of PDDA was quite different than PAH. PDDA has easier access to the coiled conformation and increased contact sites with the polyanion substrates. So both the roughness and thickness of PDDA films are larger than PAH film. [87-89]

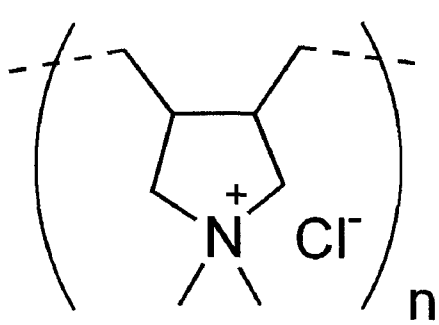

Fig.2-25 Chemical structure of PDDA

2.3.8.2 ζ potential measurements

As shown in Table 2-3, after one layer of PAH was deposited on the Aptamer:PSS $CaCO_3$ particles, the surface charge of particles switched to positive at 2.6mV. When the high charge density positive polymer PDDA was used to form the films, the surface charge of particles was at about 2.2mV, which was smaller than that of PAH. If no aptamer or PSS were doped inside of $CaCO_3$ particles, the surface charge of the outermost layer of PDDA has been reported to be higher than that of PAH. [32b, 87] In these hollow microcapsules or polyelectrolyte multilayer films, the bulky and rigid charged groups of PDDA will extend outward further than functional groups in PAH contributing more to the surface charge, so the measured ζ potential value will be higher than PAH. But in this experiment, the negatively charged PSS and aptamers were already encapsulated inside the $CaCO_3$ particles, thus the binding or electrostatic interactions between the PDDA or PAH with PSS and aptamers will greatly influence the measured surface charge. Comparing the PDDA/PSS acid-base pair with PAH/PSS pair, the charge density between the PDDA and PSS will be better matched than that between PAH and PSS (PAH is just partially charged at this experiment condition). PDDA will bind with PSS in a more condensed manner and fewer charged functional groups of PDDA can extend outside, which may be the predominant factor for the decrease in surface charge. [87]

sample	ζ potential (mV)
Aptamer : PSS- $CaCO_3$	-16.7
Coating one layer of PAH (3mg/ml, 0.5M NaCl)	2.6
Coating one layer of PDDA (3mg/ml, 0.5M NaCl)	2.2

Table 2-3 The surface charge of Aptamer: PSS-$CaCO_3$ particles and after coating one layer of PAH or PDDA

2.3.8.3 SEM and EDS analysis

The surface morphologies of particles after coating the first layer of PDDA were checked by SEM. The results showed that a condensed film was deposited onto the surface of the particles. (Fig.2-26) Unlike coating with one layer of PAH, the particles looked like a pine cone. For PDDA, the particles remained as spherical structures, but the surfaces of these particles were completed covered with condensed films with some ridges due to the roughness of the films. The morphology difference between PDDA and PAH films may be due to the fact that PDDA will bind with Aptamer:PSS-$CaCO_3$ particles more tightly compared to the binding of PAH with Aptamer:PSS-$CaCO_3$ particles. This may also further explain why the surface charge after PDDA coverage is lower than after PAH coverage.

When the deposition process was continued to add a PSS layer, the roughness of the surface on most particles became more obvious. (Fig.2-27) The morphology of the films was no longer as even as after deposition of one layer of PDDA. The reason may be that the thickness of the PDDA/PSS film increase in an exponential way, [88] the films will form bottom-ridges structure due to the interpenetration between the PDDA and PSS

polymers; While PAH/PSS bilayer films will grow in a linear way, the thickness of films will increase evenly.

The common phenomenon of particle aggregation by excess polyelectrolytes was not observed when PDDA/PSS bilayer was deposited. The separation between the particles was important to continue the layer-by-layer process.

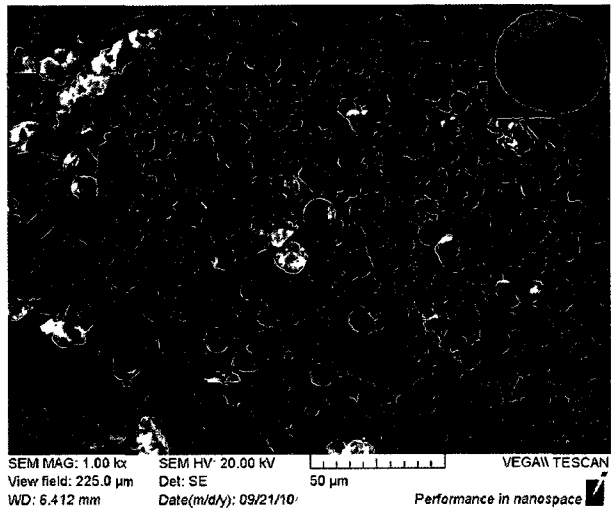

Fig.2-26 SEM images of the Aptamer:PSS $CaCO_3$ particles after coating the first layer of PDDA, inset is an enlarged one

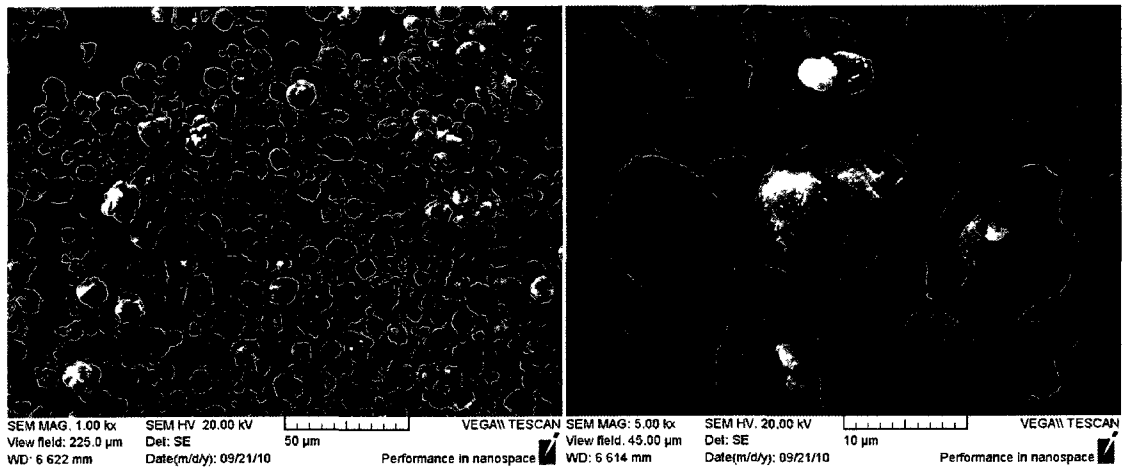

Fig.2-27 SEM images of Aptamer: PSS-$CaCO_3$ particles after coating the first PSS layer, the right one is a close-up view

A trial to check if, after dissolving the $CaCO_3$ templates, whether these microcapsules remain separate was conducted after depositing one bilayer of PDDA/PSS films. In a large area SEM image, all microcapsules were flat on the substrate surface and separate. The results indicating that charge density match between PDDA/PSS films is important to keep the microcapsules individually. (Fig.2-28 left) But after enlarging the SEM image, (Fig.2-28 right) some small holes can be clearly observed in individual microcapsules and some broken microcapsules will lead to unwanted leakage of contents from microcapsules.[84] So 5 bilayer polyelectrolyte films were deposited to fabricate ideal microcapsules.

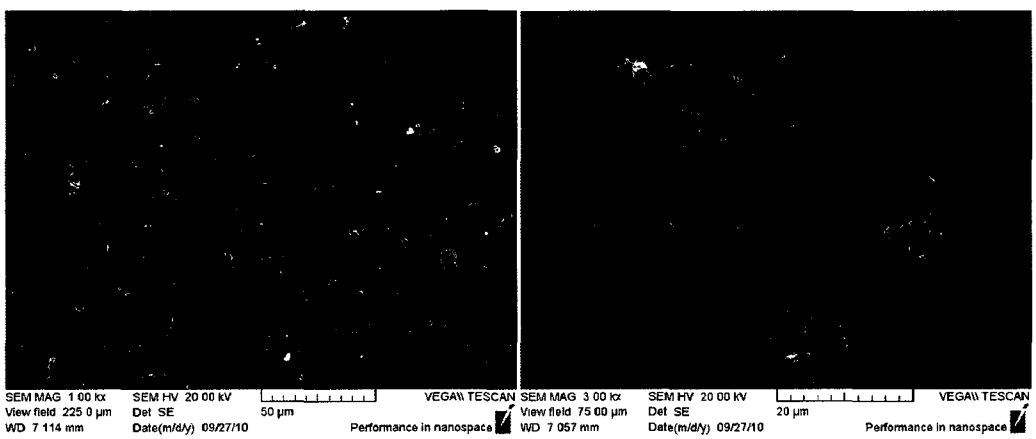

Fig.2-28 SEM images of Aptamer: PSS- (PDDA/PSS) microcapsules, the right one is a close-up view

After deposition of 5 bilayer PDDA/PSS films onto the Aptamer:PSS-$CaCO_3$ particles, the morphology of the separated particles turned to a flower-like structure due to the exponential growth model of PDDA/PSS films and the interpenetration between them.[88] (Fig.2-29) Whether aptamers still remained inside of these particles was checked by EDS. Before the EDS measurements for 5 bilayer wrapped Aptamer:PSS-$CaCO_3$ particles, the background element analysis was conducted on the clean Al stud. The morphology of clean Al studs was not as smooth as they looked by naked eye; there are some scratches

and holes on it. (Fig.2-30) The main component of the studs, as expected, was Al with a small amount of impurities such as Mg or Cu and trace amounts of C and O. (Spe.2-1) There were some new elements in the 5 bilayer (PDDA/PSS) wrapped Aptamer:PSS-$CaCO_3$ particles compared with the Al stud background: Ca was coming from the $CaCO_3$ template, S was from the PSS polymers, and most importantly P, which was only contained in aptamer, was also found in this sample. (Spe.2-2) So, after the layer-by-layer films assembly process, aptamers still remained inside of the $CaCO_3$ templates.

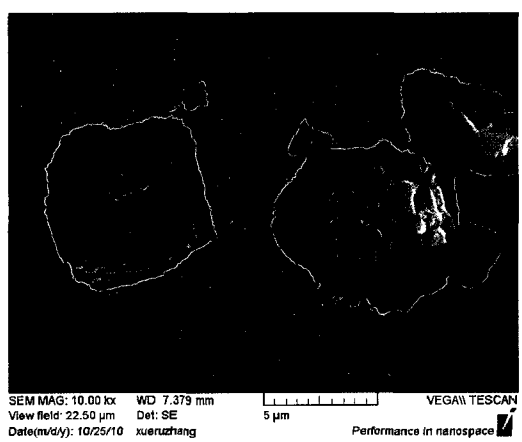

Fig.2-29 SEM image of Aptamer:PSS-$CaCO_3$ particles after deposition of $(PDDA/PSS)_5$

Element	Weight%	Atomic%
C	28.20	44.50
O	20.53	24.33
Al	31.21	21.93
P	0.17	0.10
S	0.30	0.18
Ca	17.85	8.44
Cu	1.74	0.52
Totals	100.00	

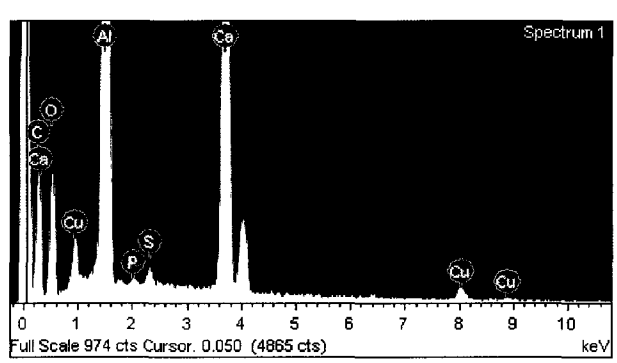

Spe.2-2 EDS Spectrum and compositions of Aptamer:PSS-$CaCO_3$ particles coated with $(PDDA/PSS)_5$

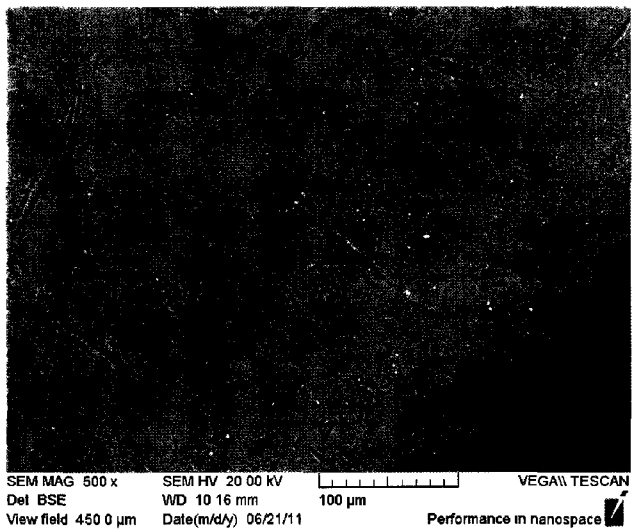

Fig.2-30 Al stud SEM image

Element	Weight%	Atomic%
C	12 13	22 72
O	6 48	9 11
Mg	3 18	2 94
Al	78 22	65 23
Totals	100 00	

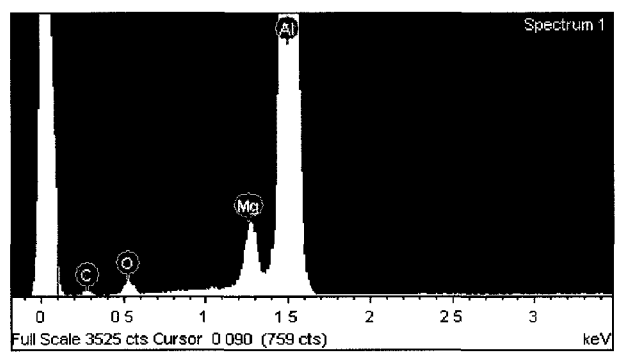

Spe.2-1 Al stud EDS spectrum and composition

After dissolution of the $CaCO_3$ templates, Aptamer:PSS-(PDDA/PSS)$_5$ microcapsules were found to be flat on the substrate when imaged under dry conditions. (Fig.2-31) The average size of the individual microcapsules was still in 4-6µm range, which proved that no aggregation took place in the PDDA/PSS films deposition process. The element Ca can no longer be detected in these microcapsules by EDS, which means that all the $CaCO_3$ was dissolved by the EDTA solution. After dissolution of Ca, the main component in the sample became C, from the backbone of the PDDA and PSS polyelectrolyte as well as the aptamer. Similarly as before, S also came from PSS. P

from the aptamers was also detected in the sample. Thus, after the dissolution process, the aptamer was still present.

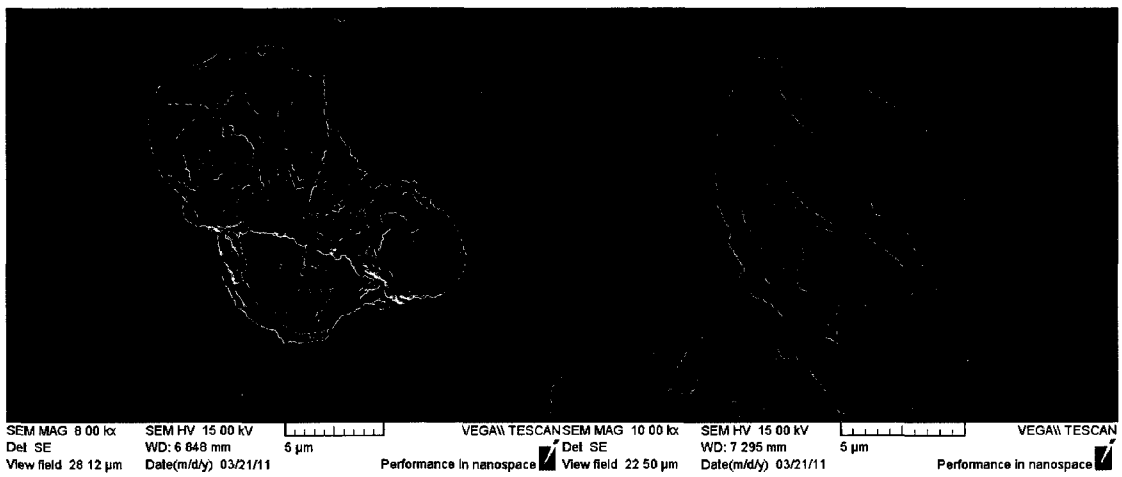

Fig.2-31 SEM image of dried aptamer:PSS-$(PDDA/PSS)_5$ microcapsules

Element	Weight%	Atomic%
C	55.64	71.90
O	8.96	8.69
Na	0.41	0.28
Al	27.94	16.07
P	0.11	0.05
S	5.48	2.65
Cu	1.46	0.36
Totals	100.00	

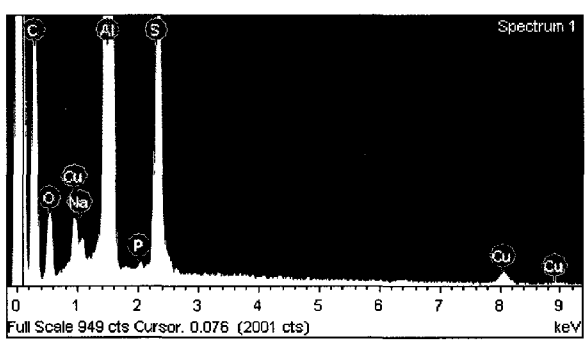

Spe.2-3 Dried Aptamer:PSS-$(PDDA/PSS)_5$ microcapsules EDS spectrum and their compositions

$(PDDA/PSS)_5$ microcapsules encapsulating aptamers and PSS were successfully fabricated, likely because the charge density match between PDDA and PSS was better than that in PAH and PSS pair under these experimental conditions. There was no aggregation between particles and microcapsules after the dissolution of the template, and the size of them were all in the expected range. The encapsulated aptamers, which will

work as the biosensors to detect the target molecule, remained inside of both the particles and microcapsules, so in the following section the triggered release properties of these microcapsules were investigated.

2.3.9 Characterization of triggered release property

2.3.9.1 $(PDDA/PSS)_5$ coated Aptamer:PSS-$CaCO_3$ particles in frozen condition

SEM with a cryo stage was used to examine the hydrated sample. In this experiment, the complete microcapsules will absorb water and turn into swollen spherical structure. [90] While the broken microcapsules present as collapsed or rupture structure. The measurements were done of microcapsules in a frozen condition allowing for observation of the status of microcapsules after incubation in target or non-target molecular solution. The SEM images of $(PDDA/PSS)_5$ coated Aptamer:PSS-$CaCO_3$ particles under frozen condition (Fig.2-32) did not show any difference compared with these particles imaged under dry conditions (Fig.2-29). All particles still looked like "flowers" without any structural rearrangements and none of these particles aggregated during the frozen storage period. As these SEM images were obtained in low vacuum nitrogen environment, they were not as clear as those obtained with the thin gold coating.

The presence of Ca in the EDS spectrum means that the $CaCO_3$ templates still exist under frozen condition. The detected S from PSS polyelectrolyte was also in agreement with previous results. P, which represents the DNA aptamers, could still be found under frozen condition; however the peak is quite small. (Spe.2-4) All the results indicated that there were not any structural or compositional differences between these particles whether they were measured under frozen or dry conditions.

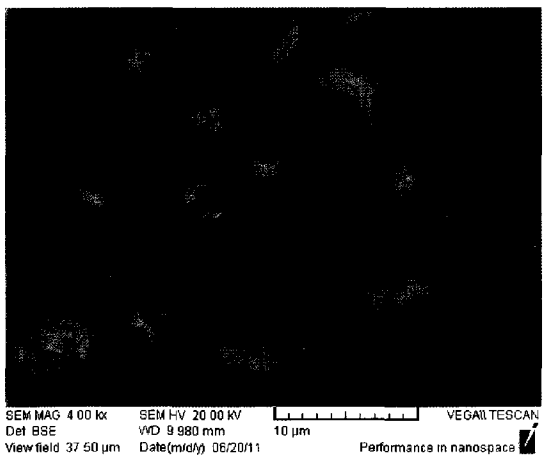

Fig.2-32 SEM image of frozen Aptamer:PSS-$CaCO_3$ particles after deposition of $(PDDA/PSS)_5$

Element	Weight%	Atomic%
C	16.44	30.46
O	16.24	22.59
Mg	1.98	1.82
Al	32.04	26.44
P	0.21	0.15
S	1.18	0.82
Ca	31.91	17.72
Totals	100.00	

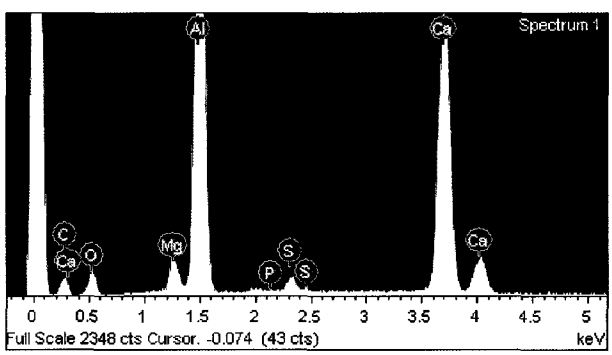

Spe.2-4 Frozen Aptamer:PSS-$CaCO_3$ particles coated with $(PDDA/PSS)_5$ EDS Spectrum and their compositions

2.3.9.2 Aptamer:PSS-$(PDDA/PSS)_5$ microcapsules under frozen conditions

Water can permeate into $(PDDA/PSS)_x$ microcapsules freely. After absorption of the water, microcapsules will swell and go back to a spherical structure.[91] In this experiment, the samples were spread on the Al stud immediately after the dissolution of $CaCO_3$ templates and stored at -80°C and measured on a cryo stage at -30°C. Compared with dried microcapsules, the semi-swollen microcapsules can be observed in this sample due to absorbed water stayed inside the microcapsules under frozen conditions. (Fig.2-

33) After absorption of water, microcapsules looked transparent because their walls are composed of nanoscale thin films.

The microcapsules, however, did not completely return to a spherical structure. Some reasons for this may be 1) Supersaturated EDTA solution was used to dissolve the $CaCO_3$ and this could have limited the permeation of water into the microcapsules. 2) The sample was prepared without an incubation step; water was just used to wash them over a few minutes. As a result, the microcapsules displayed as semi-swollen structure.

Compared with the EDS spectrum of same microcapsules obtained in dry condition, P no longer can be detected in the swollen microcapsules. After dissolution of the $CaCO_3$ template, the main component in this sample was C, as before. S which comes from PSS still can be detected. (Spe.2-5)

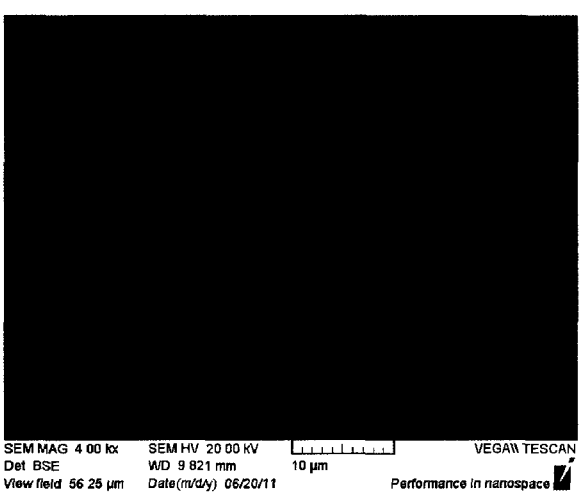

Fig.2-33 SEM image of frozen Aptamer:PSS-$(PDDA/PSS)_5$ microcapsules

Element	Weight%	Atomic%
C	55 04	70 03
O	11 76	11 23
Mg	1 87	1 17
Al	29 24	16 56
S	2 09	1 00
Totals	100 00	

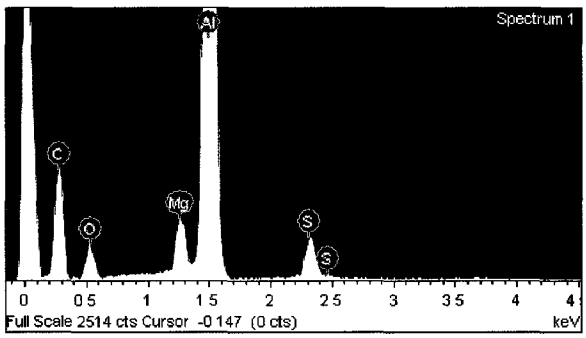

Spe.2-5 Frozen Aptamer:PSS-(PDDA/PSS)$_5$ microcapsules EDS spectrum and their compositions

2.3.9.3 Incubation in 1mM SRB dye for 16 hours

The initial thought was that microcapsules will burst after incubation in 1mM SRB dye for short time such as in 16 hours. The idea is that, assuming the aptamers are still present in the microcapsules and serving to support the microcapsule, in the presence of the target, they will fold up and allow for the collapse of the capsules. But after the measurement of the SEM image, (Fig.2-34) all microcapsules were complete and swollen in spherical structure. None of them were burst at this point. The reason may be that SRB needs some time to bind with the aptamers and drive the collapse of microcapsules. Then, the next experiment's incubation time was prolonged to 1day. The element contents of this sample were the same as pure microcapsules in frozen condition due as the incubation of SRB dye did not introduce new elements. (Spe.2-6)

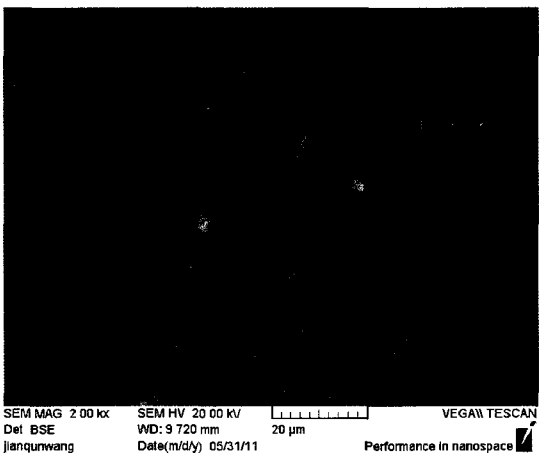

Fig.2-34 SEM image of swollen microcapsules after incubation in 1mM SRB dye for 16 hours

Element	Weight%	Atomic%
C	48.93	65.62
O	9.81	9.88
Mg	1.78	1.18
Al	36.84	21.99
S	2.64	1.32
Totals	100.00	

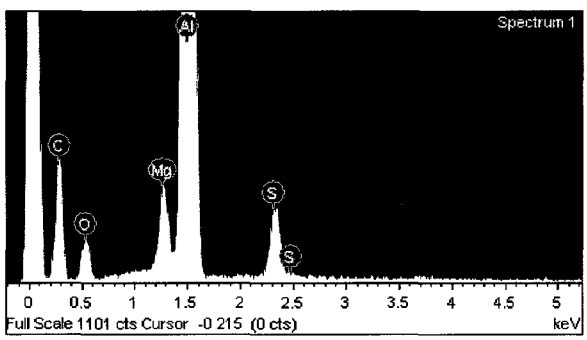

Spe.2-6 Microcapsules EDS spectrum and compositions after incubation in 1mM SRB dye for 16 hours

2.3.9.4 Incubation in 1mM SRB for 1 day

When incubation time for 1mM SRB dye was lengthened to 1 day (24 hours), some collapsed microcapsules were discovered on the surface of the cryo stage even though the sample was stored and checked in water medium. (Fig.2-35) As designed in this dye concentration, at least 50% aptamers will bind with the SRB dye and form the aptamer-dye complex. After the SRB dye bound to aptamers with high affinity, as discussed before, aptamers will no longer work as a scaffold to support the microcapsules. The conformational change may cause the formation of pores in the microcapsule walls. [27c,

[34, 38] As a result, microcapsules appeared more collapsed after incubation in 1mM SRB dye for 1 day. But, there was no detected element composition change in this sample comparing with the frozen pure microcapsules. (Spe.2-7)

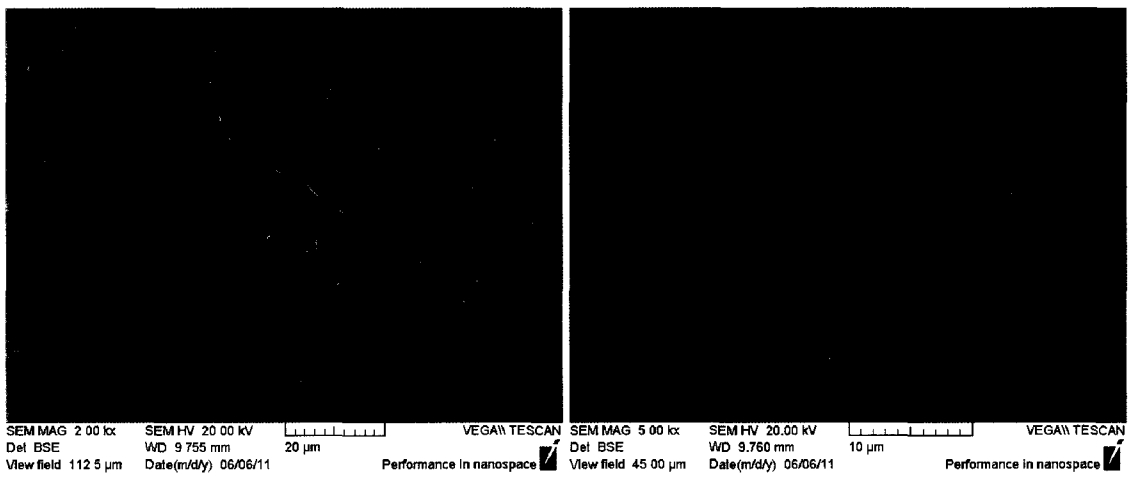

Fig.2-35 SEM images of collapsed microcapsules after incubation in 1mM SRB dye for 1day, right is a close up view

Element	Weight%	Atomic%
C	59.97	73.24
O	13.87	12 72
Mg	1.18	0.71
Al	22.01	11 97
S	2.97	1.36
Totals	100 00	

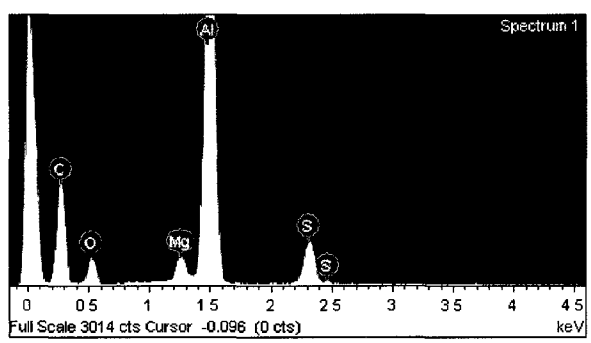

Spe.2-7 Microcapsules EDS spectrum and their compositions after incubation in 1mM SRB dye for 1day

2.3.9.5 Incubation in 10µM SRB for 1 day

The microcapsules incubated in the low concentration of SRB dye (10µM) after 1 day (24 hours) remained as swollen spherical structures. (Fig.2-36) At this dye concentration, very few aptamers will bind with the SRB dye, thus most of them will still work as the scaffold and support the completeness of microcapsules. Comparing the microcapsules

incubated in 1mM dye 0.1M KCl solution, this result suggested the collapse of microcapsules at high dye concentration may have come from the binding of aptamers with the dyes and not from other reasons such as long time incubation in water or storage under frozen conditions. The element analysis illustrated that there was no obviously element contents difference in this sample with the frozen microcapsules. (Spe.2-8)

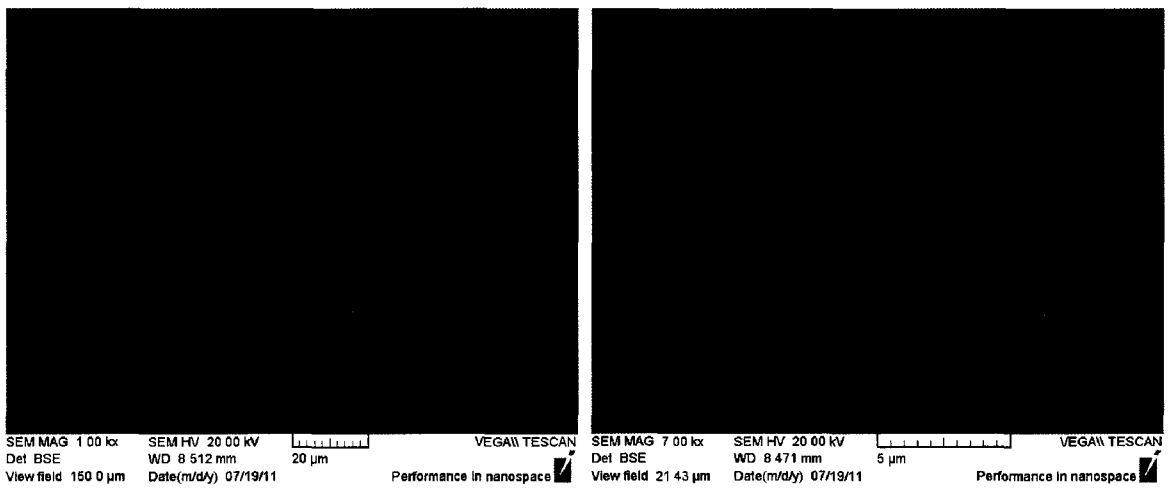

Fig.2-36 SEM images of swollen microcapsules after incubation in 10µM SRB dye for 1day, right is a close up view

Element	Weight%	Atomic%
C	50 25	66 19
O	11 73	11 60
Mg	2 00	1 30
Al	33 77	19 80
S	2 24	1 11
Totals	100 00	

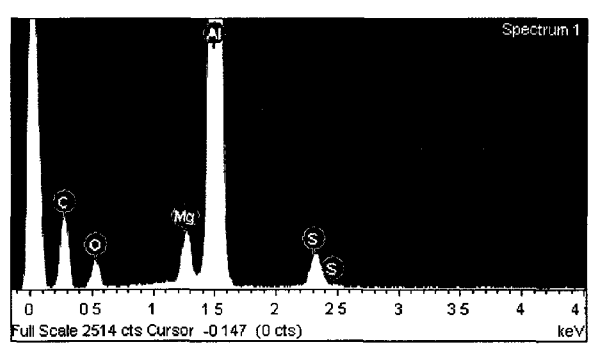

Spe.2-8 Microcapsules EDS spectrum and compositions after incubation in 10µM SRB dye for 1day

2.3.9.6 Incubation in 1mM SRB for 6 days

After incubation in 1mM SRB dye for 6 days, almost all the microcapsules appeared to be burst. Only the bottom of microcapsules were left on the surface of cryo stage and from the enlarged SEM image it can be observed that the morphology of microcapsules bottoms were uneven. (Fig. 2-37 right) The EDS spectrum of this sample contained a new element: "K". Based on the literatures, this monovalent cation K^+ will coordinate with the SRB aptamers within the plane of their G quartets plane and stabilize this active conformation. In this experiment, the concentration of K^+ was at 0.1 M while the aptamers concentration was at about 0.01M. So K^+ spectrums may be easier to be detected than the P spectrum in the burst microcapsules. Even though the P spectrums was not present in this EDS spectrum, the finding of this element which could be part of the SRB aptamer-dye complex gives some suggestion that the aptamers are still present in the microcapsules and that they have bound with the targets. (Spe.2-9) The detection of K^+ leads some credibility to the idea that the breaking of the microcapsules could have been driven by aptamer-SRB dye binding.

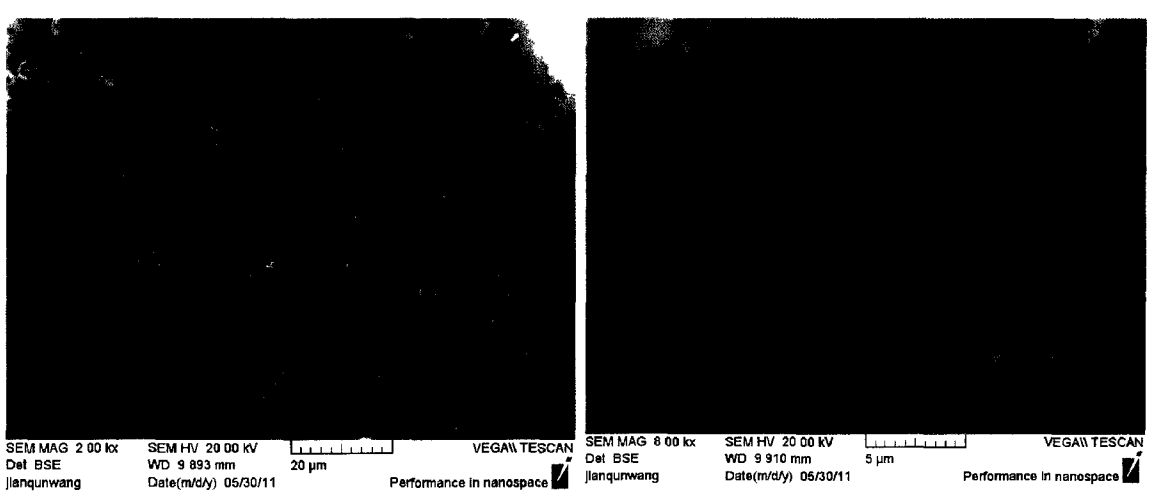

Fig.2-37 SEM images of burst microcapsules after incubation in 1mM SRB dye for 6 days; right is a close up view

Element	Weight%	Atomic%
C	51 17	68 29
O	9 95	9 97
Mg	1 24	0 82
Al	22 96	13 64
S	14 05	7 03
K	0 62	0 26
Totals	100 00	

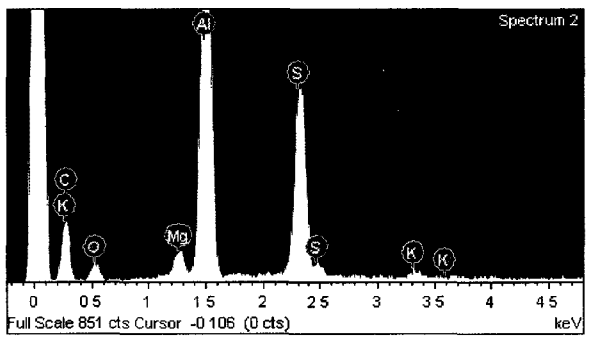

Spe.2-9 Microcapsules EDS spectrum and compositions after incubation in 1mM SRB dye for 6 days

2.3.9.7 Incubation in 10μM SRB for 6 days

After checking different areas on the cryo stages at -30°C, microcapsules incubated in 10μM SRB dye for 6 days, all remain swollen and complete spherical structures. (Fig.2-38) The completeness of the microcapsules mean that they were stable in water medium even when the incubation time was extended to 6 days. The stability of the microcapsules in water medium will be important for the future usage as smart fertilizers. Compared to the sample for microcapsules in 1mM SRB dye for 6 days, the completeness of microcapsules at lower dye concentration again suggests that the bursting of the microcapsules may have been caused due to aptamer-dye binding. The elemental analysis of this sample did not find K^+ in them, which suggested that the presence of K^+ in the burst microcapsule was not due to the absorption by the microcapsules as the counter ions during the incubation time. The EDS spectrum of this sample had the same elements as frozen microcapsules. (Spe.2-10)

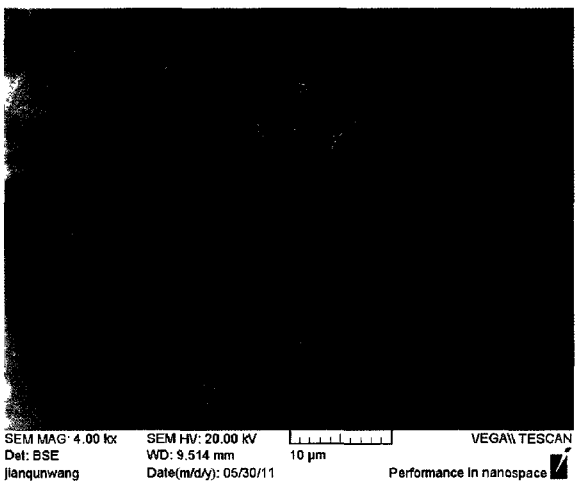

Fig.2-38 SEM image of swollen microcapsules after incubation in 10μM SRB dye for 6 days

Element	Weight%	Atomic%
C	54.54	69.36
O	13.01	12.42
Mg	1.54	0.96
Al	28.13	15.92
S	2.79	1.33
Totals	100.00	

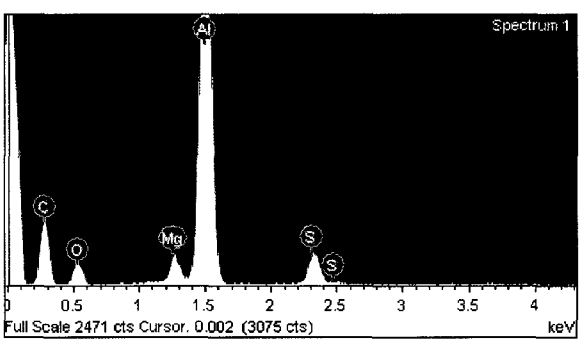

Spe.2-10 Microcapsules EDS spectrum and compositions after incubation in 10μM SRB dye for 6 days

2.3.9.8 Incubation in 1mM TMR dye for 6 days

The SRB aptamer does not bind to TMR, thus it served as a good control for our experiments. After incubation in 1mM TMR dye for 6 days, all microcapsules appeared complete and remained as spherical structure. (Fig.2-39) The elemental analysis of this samples showed that there were no new elements present compared with the frozen microcapsules. (Spe.2-11) The results revealed that the collapse and bursting of microcapsules in SRB dye solution was not simply caused by the osmotic pressure from a outside highly concentrated dye solution. The microcapsules appear to be stable with

non-target molecule at this concentration. Owing to the discriminatory nature of aptamers, they will bind with the specific target with high affinity and selectivity. As a result, in these microcapsules no aptamers bound with TMR dye and then the porosity of microcapsules did not change.

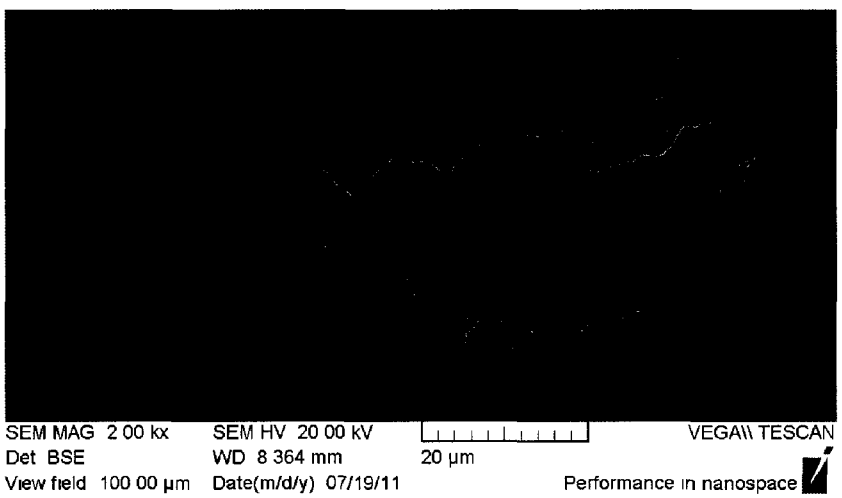

Fig.2-39 SEM image after microcapsules incubation in 1mM TMR dye for 6 days

Element	Weight%	Atomic%
C	64 48	77 50
O	10 19	9 20
Mg	1 30	0 77
Al	20 22	10 82
S	3 81	1 72
Totals	100 00	

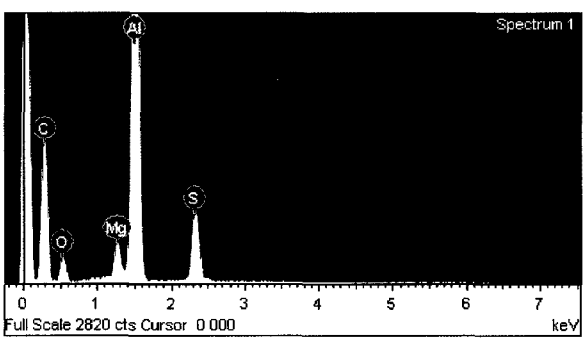

Spe.2-11 Microcapsules EDS spectrum and compositions after incubation in 1mM TMR dye for 6 days

The targeted molecule triggered release properties of aptamers encapsulated in microcapsules and their relationship with trigger concentration and time can be summarized in Fig.2-40. In lower dye concentration, no matter how long the

microcapsules are incubated, the microcapsules appear to be stable and complete and remain as swollen spherical structures. While if the microcapsules are incubated at high dye concentration when more than 50% of aptamers were bound to the target molecule, the microcapsules went through swollen, collapsed and burst forms. At short incubation time, the porosity variation of the microcapsules was not significant and then microcapsules appeared stable. With prolonged incubation time, the increased possibility of forming more pores in the microcapsule wall leads to collapse and rupture. When microcapsules were incubated in high concentration of TMR solution, which has the similar chemical structure of SRB dye, these microcapsules exhibited high selectivity. These microcapsules appear to burst only upon the binding of aptamers with the target molecule. That is to say, they will release their contents in response to the detection of their targets. However, because SEM images are not entirely clear, these results will need to be confirmed by another method, such as fluorescence microscopy.

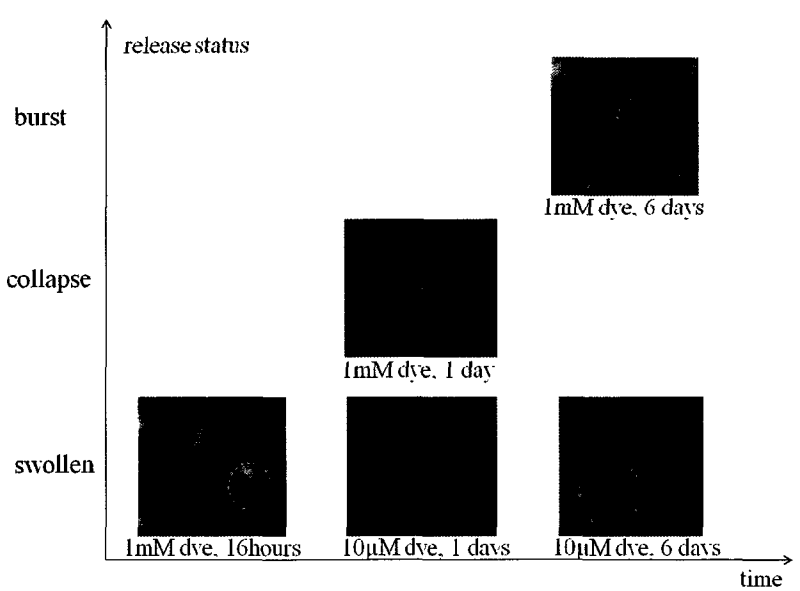

Fig.2-40 Microcapsules status of as the function of incubated dye concentration and time, single swollen, collapsed or burst microcapsule was highlight by circle.

2.4 Chapter summary

Aptamers and PSS-encapsulated porous $CaCO_3$ templates fabricated in a coprecipitation process, followed by layer-by-layer film deposition would be a suitable method for synthesis of stable aptamer-loaded microcapsules.

The refined parameters for polyelectrolyte films deposition in this work were found to be the use of 0.5M NaCl to adjust ionic strength and of supersaturated polyelectrolyte solution for deposition. When the weak polyelectrolyte PAH was chosen as the positively charged polymer, most of the aptamer-$CaCO_3$ particles aggregated during layer-by-layer films assembly process. As a result, no regular microcapsules were acquired. With loading both PSS and aptamers inside of the $CaCO_3$ particles, the percentage of synthesized porous spherical $CaCO_3$ increased. (No aptamers seem to be captured by cubic $CaCO_3$ particles.) But, the aggregation phenomenon of aptamer:PSS-$CaCO_3$ particles remain a problem in the PAH/PSS film formation process. After replacing PAH with the strong polyelectrolyte PDDA, perfect Aptamer:PSS-$(PDDA/PSS)_5$ microcapsules were attained.

SEM imaging evidence suggests that Aptamer:PSS-$(PDDA/PSS)_5$ microcapsules demonstrated target molecule triggered release properties. The bursting of the microcapsules seems to be tunable according to the target molecular concentration and related to incubation time. The conformational change of aptamers upon the binding to the target molecules may lead to pores formation on the microcapsule wall. Microcapsules went through collapse and bursting as a result of this porosity change. Owing to the discriminatory nature of aptamers, the microcapsules only seemed to burst in response to the detection of the target molecules. The microcapsules with introduced

aptamers may therefore exhibit additional "smart" functionalities than hollow microcapsules.

The release of contents in microcapsules concomitant to the detection of target molecules would be beneficial for aimed precisely targeted delivery of contents. In the future these functionalized microcapsules may be used in a "smart" fertilizer system. Ideally, the release of the fertilizer will be synchronized with the demand of crops in their growth cycle and not based on the variation of temperature, ionic strength, or environment pH value.

Chapter 3 Fabrication of a Sulforhodamine B Aptamer polymer "tape"

3.1 Introduction

In Chapter 2, collapsible microcapsules were prepared with aptamers and PSS serving as a scaffold within the capsule's core. It was found that the aptamers alone were likely too small to support the microcapsule structure. As an alternative strategy to adding PSS to help maintain the integrity of the microcapsules after dissolution of the $CaCO_3$ template, a long aptamer polymer "tape" will be prepared in this chapter with repeating sulforhodamine B aptamer units as recognition sites using a method known as rolling circle amplification (RCA). In future work, these "tapes" could be used as the collapsible scaffold for triggered release systems, or to replace the polyanion in our LbL films.

In recent years, rolling circle amplification has been widely investigated in analytical research and biotechnology due to its unique properties. [91] For example, the whole rolling circle amplification process can be conducted at room temperature and can produce long single stranded or branched repetitive DNA sequences from very small amounts of starting material at high efficiency. By using the unique polymerase phi29, this isothermal amplification process can be initiated with circular DNA as the template and then can subsequently produce long sequences of DNA. Note that since aptamers are linear, not circular, a DNA ligation to produce a circular aptamer template with a spacer will first need to be performed.

In this project, the RCA process initiates with a circular DNA template and a single primer. The nucleic acid replication will proceed in one direction in a linear fashion, resulting in a long single stranded DNA "tape". The first step is to produce a nicked circular DNA strand hybridized with a primer, followed by ligation. The second step will

proceed around this circular DNA template, starting from the free 3' hydroxyl end of the primer. The replication process will continue until the phi29 enzyme is denatured at 65°C. The schematic process is shown in Fig.3-1.

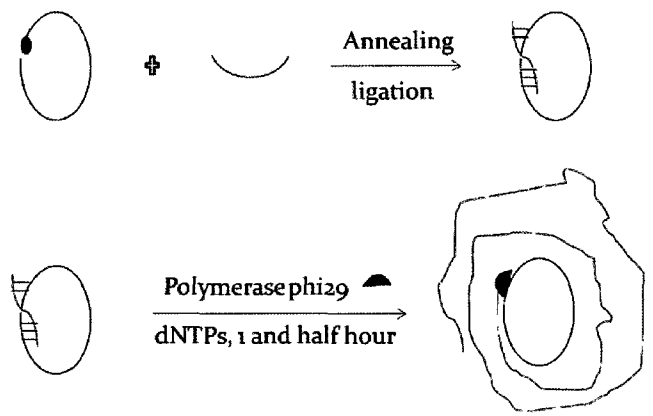

Fig.3-1 Schematic picture of RCA, the blue dot represents a 5'-phosphate group

3.2 Experimental

3.2.1 Design and synthesis of the circular DNA template

3.2.1.1 Materials

Materials for synthesizing the linear DNA and primer: The four basic phosphoramidites : dA-CE phosphoramidite, dT- CE phosphoramidite, dmf-dG-CE phosphoramidite and Ac-dC-CE phosphoramidite and chemical phosphorylation reagent used to prepare phosphorylated linear aptamer were all purchased from Glen Research (Sterling, VA) in powder condition.

Quick Ligation Kit used to make circular DNA from linear DNA template and primer was purchased from New England Biolabs. This quick ligation kit includes Quick T4 DNA ligase and 2×Quick Ligation Reaction Buffer.

Materials for purification of circular DNA: Acrylamide (DNA sequence Grade), N, N'-methylenebisacrylamide, Urea (Molecular Biology Grade), Ammonium Persulfate (Electrophoresis Grade), 99% purity N,N,N',N'-tetramethylethylenediamine (TEMED) were all purchased from Bioshop Canada Company (Burlington, ON). 99% purity Formamide was purchased from Sigma-Aldrich Company. Tris/Borate/EDTA (TBE) buffer was prepared from Biotechnology Grade Boric acid (VWR Mississauga, ON), Bioultrapure Grade Tris(hydroxymethyl) aminomethane (Bioshop Company) and Biotechnology Grade ethylenediaminetetraacetic acid (EDTA) (Bioshop Company).

3.2.1.2 Methods

The design and synthesis of circular DNA: In order to form a long SRB aptamer polymer "tape" by Rolling Circle Amplification (RCA), a circular DNA template must be prepared first. A 5'-phosphorylated linear DNA was designed as the complementary strand of the SRB aptamer with a spacer sequence. The sequence of the linear DNA was *5'-GAT CCT AAC TAA GTA ACT CTG CCG GCC CCC TCC CTC CCA CCC TAG GCC GGA AAA AAA AAA AAA AAA AAA ACC GGC CCC CTC CCT CCC ACC CTA GGC CGG AAA AAA CCA CAC-3'*. The green parts in the linear DNA were designed as the reverse complementary strands for the SRB aptamer. The black parts will work as a spacer, and the primer used to hybridize the linear DNA was designed as following *5'-TTA GGA TCG TGT GGT T-3'*. The linear DNA and primer will hybridize together in a head to tail fashion at the red and purple fragments. The phosphorylated DNA template and primer were synthesized using a MerMade 6® DNA synthesizer and then isolated with high concentrated NH_4OH and DI water as described earlier.

The Quick Ligation Kit was able to ligate either cohesive or blunt ends of DNA fragments at room temperature in a short time. According to the Plasmid Recircularization Quick Ligation protocol for DNA fragments, 30μL of 7.6 μM phosphorylated linear DNA solution, 30μL of 71 μM primer solution, 240μL deionized water, 300μL of 2×Quick Ligation Reaction Buffer (132mM Tris-HCl, 20mM $MgCl_2$, 2mM dithiothreitol, 2mM ATP, 15% Polyethylene glycol, pH=7.6) and 30 μL Quick T4 DNA ligase enzyme were mixed together thoroughly and left to sit at room temperature for 30 minutes. Then the solutions were heated at 65°C for 10 minutes to denature the ligation enzyme.

Preparation of the polyacrylamide gel to purify the circular DNA: The acrylamide stock solution was made by dissolving 190g acrylamide and 10g N,N'-methylenebisacrylamide into about 250mL DI water at 37°C with stirring condition. After filtering with a 0.22μm cellulose acetate sterilizing filter, the final volume of the solution was diluted to 500mL with the addition of DI water.

5×TBE buffer was prepared by dissolving 107.8g Tris, 55.0g Boric acid and 7.44g EDTA in 2L DI water under heating and stirring condition to dissolve all the chemicals. Then the solution was filtered with a cellulose acetate filter.

An 8% polyacrylamide gel was made to separate the circular DNA from the linear DNA and the primer. The 31.5g Urea, 16ml acrylamide stock solution, and 15ml 5×TBE buffer was mixed with 21.5ml DI water to make the 8% polyacrylamide gel. The solution was stirred and heated at 37°C to dissolve all the solids. Then after filtration with cellulose acetate filter, the solution was left to cool to room temperature. When the

solution was cooling, 450μl 10% ammonium persulfate solution and 35μl TEMED were added into solution with mild swirling, taking care not to introduce bubbles. Then the solution was quickly cast into the polyacrylamide gel electrophoresis (PAGE) system and left for 30 minutes for complete polymerization of the gel. PAGE electrophoresis experiments were conducted in a Hoefer 600X Chroma Vertical Electrophoresis system. A FB1000 Electrophoresis Power Supply (Fisher Scientific Company) was used to provide the power.

After the polyacrylamide gels were prepared, the gels were pre-run for 30 minutes in 1×TBE buffer before being loaded with DNA samples. The DNA samples were prepared by adding 10μl of DNA solution with 10μL of formamide and heated at 55°C for 10 minutes. Then, DNA samples were loaded into the PAGE gel and run at 25mA for 2 hours. After electrophoresis, an Alpha Innotech AlphaImager® EC was used to image the gels.

After imaging, only circular DNA was cut from the gels and eluted with 10mM Tris buffer pH=7.4. All the cutting gels were transferred to a 5ml syringe and squeezed into a 15ml Eppendorf tube. For each 0.5ml gel, 3ml of tris buffer was added to make sure all DNA was dissolved. After the thoroughly mixing the gel with the buffer, the tubes were frozen at -80°C for 30minutes. After that, incubation in two water baths was conducted. (One was at lower temperature at 55°C for 5 minutes; another was one at 90°C for 5 minutes). At last, the tubes were put into a mini incubator to shake at 37°C overnight. At this point, all DNA should be dissolved into the tris buffer. And then all the mixture was put into the 5ml syringe, using 0.45μm PVDF® syringe filters to separate the gel with tris buffer solution. The tris buffer solution with eluted DNA strands was dried in a

Labconco® Freezone 4.5 lyophilizer overnight. 1.5 ml of DI water was added to dissolve all DNA and salts and then the DNA was purified by ethanol precipitation.

Ethanol precipitation was used to purify the DNA from the gel impurities and salts (from buffer). For each purification reaction, 100μl DNA tris buffer solution was transferred into a 1.5 ml Eppendorf centrifugation tube and 50 μl of 3M NaCl was added along with 1ml of 100% ethanol to each tube. After cooling the tubes at -80°C for 45 minutes, the tubes were centrifuged at -9°C at 14×1000g for 30 minutes. The supernatant was gently decanted and the residue was dried the by the speed vacuum. The precipitation process was repeated two times to get rid of all the salts and impurities.

3.2.2 Fabrication of the Sulforhodamine B Aptamer polymer

3.2.2.1 Materials

A rolling circle amplification kit (Templiphi™ 100 amplification Kit, which includes sample buffer, reaction buffer and enzyme mix) was purchased from GE Healthcare Company. QIAEX II Gel Extraction kit, which was used for extraction the aptamer polymer from the agarose gel was purchased from Qiagen Company. This extraction kit includes buffer QX1, QIAEX II silica suspensions and buffer PE. Biotechnology grade Agarose was purchased from Bioshop Company in powder condition. Electrophoresis Grade Ethidium bromide (EtBr) was purchased from Fisher Biotech Company.

3.2.2.2 Methods

A Templiphi amplification kit was used to fabricate the Sulforhodamine B aptamer polymer. As recommend from the protocol, for each RCA reaction, 0.5μl of diluted pure circular DNA solution (in this work, every 0.5μl solution contains 7ng circular DNA)

was incubated with the 5μl templiphi amplification sample buffer and denatured at 95°C for 3 minutes. After cooling down to room temperature, 5μl reaction buffer and 0.2μl phi29 DNA polymerase enzyme were added into the mixture incubated at 30°C for 16-18 hours. The rolling circle amplification process was stopped by denaturing the enzyme at 65°C for 10 minutes. Each reaction was conducted separately in Thermo Scientific ABgene® 0.2ml flat cap tube (from Abgene Limited Head Office, Epsom KT19 9AP, United Kingdom). Every aptamer polymer tape contains thousands of periodic repeat complementary units of the circular template, in this case, the sulforhodamine B aptamer separated by a poly thymine nucleotide spacer ($polyT_{20}$).

0.6% agarose gel was used to purify and check the size of the aptamer polymer. The 0.6% agarose gel was made by following steps: 1.08g agarose particles mixed with 36ml 5×TBE buffer and 144 ml DI water and heated in microwave for 3 minutes. 10μl of 10mg/ml EtBr solution was added into the mixture and then they were cooled down to 60°C. Then the whole solution was poured into Owl® Horizontal Electrophoresis tray. (Owl Separation System model A1, Portsmouth, NH, USA). The DNA samples for each lane were made by mixing 5μl rolling circle amplification solution with 1μl agarose gel loading dye. The 5μl Invitrogen® (Invitrogen Canada Inc., Burlington, ON) 1kb DNA ladder mixed with 1μl loading dye was also loaded as the reference. As described by the producer, this 1kb DNA ladder was used to size linear DNA fragments from 500bp to 12kb. The ladder is composed by 12 bands from 506 bp to 12,216 bp and the biggest one will be 12kb. After loading the samples, the gel was run in 1×TBE buffer at 170~180 for 5 hours.

After the separation process, a QIAEX II kit was used to extract the DNA from the excised agarose gel. Firstly the aptamer polymer band was cut from the gel and put into the 5ml syringe and squeezed into a 15ml sterile Eppendorf tube. QX1 buffer and DI water were added to the gel fragments. The QX1 buffer was used to dissolve the gel releasing the aptamer polymer into the water. Then, the QIAEX II suspension, which contains the silica particles, was added to the gel solution and the mixture was incubated at 50°C for 10 min to let the DNA efficiently bind to the silica particles. Centrifugation at 5,000g for 1 min separated the beads from QX 1 buffer and the dissolved agarose gel. DNA bound silica particles were washed with buffer PE two times to remove all of the impurities. The particles were air dried at least 30 minutes to evaporate the ethanol (introduced with buffer PE). Then, the silica particles were incubated in 10mM tris buffer, pH=8.4 at 50°C for 5 minutes to elute the aptamer polymer. The mixture was centrifuged again, repeating the tris buffer elution step to extract all the aptamer polymer. The tris buffer-aptamer polymer solution was desalted using Millipore™ Amicon® ultra 0.5ml centrifuge filter tube (MWCO will be 3,000) at 13×1000g for 30 minutes. The aptamer polymer solution was dried in speedvac and the purified aptamer polymer was stored at -20°C.

An Ntegra NTMDT® STO505 AFM (Atomic Force Microscope) instrument was used to check the topographical image of aptamer polymer. The sample was prepared by drying 5μl of 50μg/ml aptamer polymer solution on the freshly cleaved mica surface.

3.3 Results and Discussion

3.3.1 Circulation results

After the quick ligation process, a small aliquot of sample was loaded in the 8% polyacrylamide gel to check the results. The sample after ligation reaction was loaded in lane 8. The reference 5'-phosphorylated linear DNA and primer mixture was loaded in lane 11. In Fig.3-2, it is clearly shown that the circular DNA runs more slowly than the linear DNA, suggesting that the ligation process was successful. Then all the concentrated solution from the ligation reaction was loaded into the gel to purify the circular DNA.

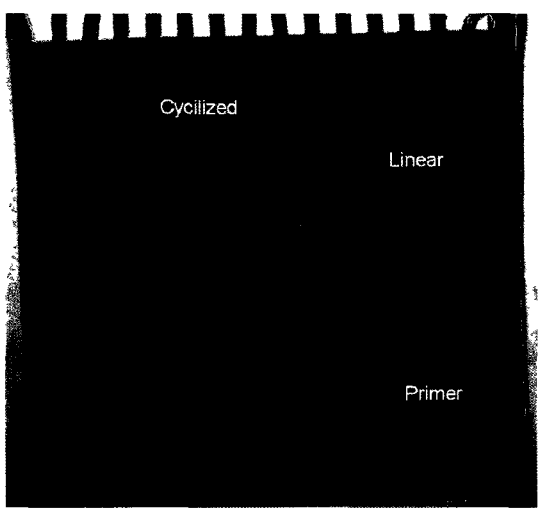

Fig. 3-2 8% PAGE image for checking the ligation reaction of circular DNA

3.3.2 RCA on a small reaction scale

Using the purified circular template, RCA was attempted on a small scale. The products after RCA were loaded onto an agarose gel to check the results of amplification reaction. The sample from 10 amplification reactions was loaded in lane 4, and the reference 1Kd DNA ladder was loaded in lane 7. As shown in Fig. 3-3, the aptamer polymer moved even slower than the biggest DNA ladder band, these high molecular weight aptamer polymers were almost not moving under this separation condition and appear to be left inside the wells. Based on the principle that the bigger the DNA strand, the slower it

moves through the gel, we cab estimate that the size of the aptamer polymer tape is at least larger than 12Kd. The agarose gel image indicated that the aptamer polymer amplification was successful. [92]

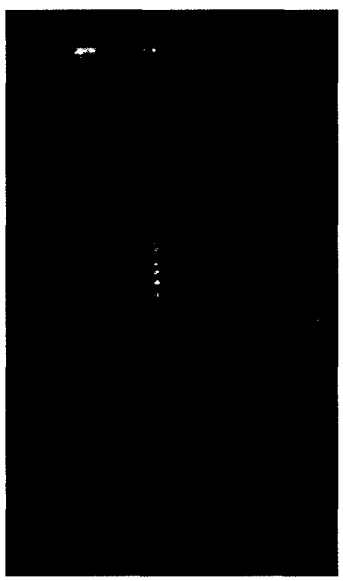

Fig.3-3 0.6 % agarose gel image for checking the results of RCA

3.3.3 AFM image of the aptamer polymer tape

After extraction of the aptamer polymer from the gel, the morphology of the aptamer polymer was checked by AFM. As shown in Fig.3-5, the single stranded polymer was folded together like a drop of water. But, the size of the aptamer polymer is on the micrometer scale and the highest height of aptamer polymer is at 4.5nm, which is comparable to other DNA polymer tapes obtained from the RCA process. [93] This long DNA polymer was composed of thousands of repeating SRB aptamers units as the active sites along the polymer chain, which should bind with the target molecules at high affinity and selectivity.

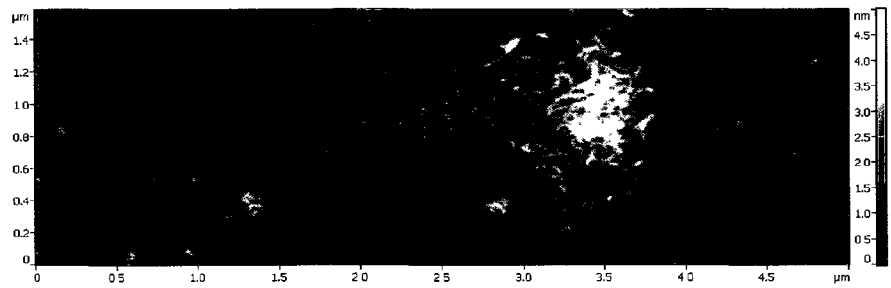

Fig.3-4 AFM image of aptamer polymer

3.3.4 Results for RCA on a large scale

As described before, for this alternative method, the aptamer polymer alone will be encapsulated into polyelectrolyte $(PDDA/PSS)_5$ microcapsules and used as the collapsible scaffold [94] to support the stability of thin-walled microcapsules after dissolution of sacrificial $CaCO_3$ template. If so, from the previous study, at least 0.7mg aptamer polymer tape will be needed for a 1ml 0.33M $CaCl_2$ and 1ml 0.33M $NaHCO_3$ reaction. As claimed in Templiphi™, each rolling circle amplification reaction after 16-18 hours incubation at 30°C, yields of DNA polymer in the 1.25μg-1.75μg range. As a result, almost 500 reactions were needed to fabricate enough amounts of aptamer polymer from the RCA reaction.

Considering the RCA reactions are conducted at constant temperature 30°C, we tested if the reactions could perhaps be run on a large scale of 50 reactions together in one 1.5ml centrifuge tube. The reaction process was as the same as recommended by the Templiphi protocol. After the large scale amplification reaction, agarose gel electrophoresis was also used to separate the aptamer polymer. For each gel separation reaction, the 1kb DNA ladder reference was loaded in lane 1, and the aptamer polymer samples were loaded from lane 2-11. As shown in Fig.3-5, there are faint broad bands in lane 2-11 in the range size lower than 12Kd DNA band. The reason for fabrication of shorter aptamer polymers

may be that in this large scale reaction, circular DNA template were not in adequate contact with the dNTP, so some shorter aptamer polymers were lower than 12kb.

The aptamer polymers with the size larger than 12kb were cut from the agarose gel and extracted by the QIAEX II kit with the same procedure as before. After the extraction process, the aptamer polymer was desalted and dried in speedvac and then stored at -20°C in freezer.

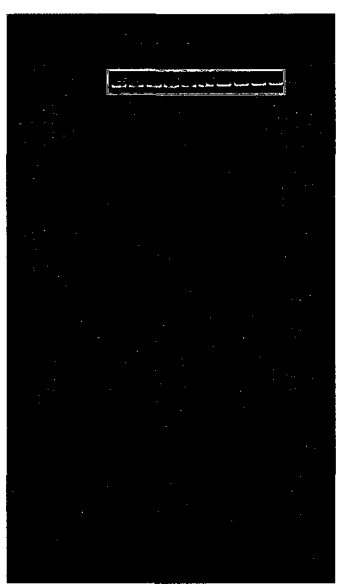

Fig.3-5 0.6 % agarose gel image for separation aptamer polymer from large scale RCA reactions, the excised aptamer polymer was highlight in the blue box (from right, lane 1, 1 Kd DNA ladder, lane 2-11, condensed DNA solution)

Until now, the 500 reactions for aptamer polymer RCA reactions were done and all of them have been separated by agarose gel and purified by QIAEX II extraction kit.

Chapter 4 Summary and future work

Based on the results in this work, aptamer encapsulated microcapsules can be fabricated by using aptamer-loaded porous $CaCO_3$ particles as templates, followed by the layer-by-layer assembly process to deposit films and template dissolution.

The introduction of aptamers in polyelectrolyte microcapsules will add functionality to them. Aptamer that can bind with their targets with high affinity and selectivity may allow for targeted delivery of microcapsule contents.

Aptamer:PSS-$(PDDA/PSS)_5$ microcapsules were the most promising system developed in this work and these microcapsules presented evidence for target-molecule-triggered release properties. While in non-target molecular solution they appeared to be stable under our experimental condition.

In the future the status of the aptamers in these microcapsules under wet conditions will be confirmed by CLSM measurements. The fluorescence experiments will be conducted to confirm the presence of aptamer after incubation with the target molecules. The samples will be prepared under the same reaction conditions as the SEM measurements for microcapsules triggered release properties.

Furthermore, the permeability to target molecule of the microcapsules loaded with aptamer will be compared with hollow microcapsules. Fluorescence Recovery after Photobleaching (FRAP) experiments will be carried out to decipher the fluorescent recovery rate when incubated both in target molecular and non-target molecular solution. The results will demonstrate the selectivity of the aptamers-encapsulated microcapsules.

Eventually, fertilizer with exudates aptamer will be encapsulated in the microcapsules; the binding of the exudate aptamer with the target will trigger the release of fertilizer from the microcapsules.

As an alternative method, the aptamer polymer alone will work as the microcapsule scaffold, as we have shown that aptamer polymer tapes were successfully fabricated.

In the future, the binding ability and specificity of the aptamer polymer tapes will need to be confirmed prior to any microcapsule experiments. Fluorescence anisotropy methods could be employed for this purpose.

Assuming these experiments are successful, in the future, the Aptamer polymer-$CaCO_3$ particles will be fabricated by the coprecipitation method. The question to be investigated is when the short aptamer strands are replaced with the aptamer polymer tape, can aptamer polymer-loaded $CaCO_3$ particles still be prepared? The status of the aptamer polymer within the particles will be checked by CLSM using fluorescent-labeled aptamer polymer.

If the aptamer polymer can be loaded inside the porous $CaCO_3$ particles, and then coated by the layer-by-layer process, a 5 bilayer PDDA/PSS film will be deposited onto the surface using the same deposition conditions which were discussed in chapter 2. After dissolution of the $CaCO_3$ template, the $(PDDA/PSS)_5$ microcapsules with aptamer polymer as the core will be obtained.

With the loading of the aptamer polymer within these microcapsules, the stability and permeability of Aptamer polymer-$(PDDA/PSS)_5$ will be studied. For Aptamer polymer-$(PDDA/PSS)_5$ microcapsules, as they only have aptamer polymer encapsulated inside of

the microcapsules, the target such as the sulforhodamine B may have a higher likelihood of binding with the aptamer. The triggered release properties of the Aptamer polymer-$(PDDA/PSS)_5$ will be investigated. In the absence of additional PSS structural support, perhaps the Aptamer polymer-$(PDDA/PSS)_5$ microcapsules will burst at lower target concentration or perhaps will need less time to collapse and burst . So, initially, the triggered release properties will be checked under the same conditions as for aptamer:PSS-$(PDDA/PSS)_5$ microcapsules. In later experiments, the triggered release properties will be checked at lower target concentration or for fewer days.

Chapter 5 References

1,a) Liu J.G, Daily G.C., Ehrlich P.R., Luck G.W., "Effects of household dynamics on resource consumption and biodiversity". ***Nature***, Vol.421, 530-533, **2003**; b) http://geography.about.com/od/obtainpopulationdata/a/worldpopulation.htm

2, http://tinyurl.com/yp8f5h

3, Bock B.R., Hergert G.W., "Fertiliser Nitrogens Management. In Managing nitrogen for ground water quality and farm profitability". ***SSSA Madison***, 139-164, **1991**.

4, Geetanjali G.N, "Symbiotic nitrogen fixation in legume nodules: process and signaling. A review". ***Agron. Sustain. Develop.***, Vol.27, 59-68, **2007**.

5, a) Huett D.O., Morris S.C., "Fertilizer use efficiency by containerized nursery plants. 3. Effect of heavy leaching and damaged fertilizer prills on plant growth, nutrient uptake, and nutrient loss". ***Aust. J. Agric. Res.***, Vol.50, 217-222. **1999**; b) http://wondergreen.com/

6, http://bioscholars2.wikispaces.com/Biogeochemical+Cycles

7, Johnson G.V.; Raun W.R., "Nitrogen response index as a guide to fertilizer management". ***J. Plant Nut.*** Vol. 26, 249-262, **2003**.

8, a) Hirel B; Le Gouis J., Ney B., Gallais A.J., "The challenge of improving nitrogen use efficiency in crop plants". ***J. Exp. Bot.***, Vol. 58, 2369-2387, **2007**. b) Newbould P., "The use of fertiliser in agriculture. Where do we go practically and ecologically?". ***Plant Soil***, Vol. 115, 297-311,**1989**.

9, Raun W.R., Johnson G.V., "Improving nitrogen use efficiency for cereal production". ***Agron. J.***, vol. 91, 357-363, **1999**.

10, Nielsen N.E., "Plant parameters controlling the efficiency of nutrients uptake from soil. In "Efficient use of fertilisers in agriculture", ***UN Econ. Comm. Europe. Dev. Plant Soil Sci***, Vol.10, 199-219,**1983**.

11, http://www.agrium.com/uploads/Environmentally_Smart_Nitrogen.pdf

12, Shaviv A., "Advances in Controlled Release of Fertilizers". ***Adv. Agron.***, Vol. 71, 1-49, **2000**.

13, a) Shaviv A. "Preparation methods and release mechanisms of controlled release fertilizers: Agronomic efficiency and environmental significance". ***Proceedings***, No.431, 1-35, **1999**. b) Trenkel M.E., "Controlled release and Stabilized Fertilisers in Agriculture". ***IFA***, Paris.**1997**.

14, Hauck R.D., "Slow release and bio-inhibitor-amended nitrogen fertilizers". ***Fertiliser Technology and Use***, 3rd ed. 293-322, **1985**.

15, a) Landels S.P., "Markets for controlled-release fertilisers: Present size and value, projected demand, trends, and opportunities for new CRF products". ***TVA 1991 Controlled release fertiliser workshop***, 87-101, **1991**; b) Zhang J.Z., Wang W., Sun G.F., Liu H.Z., Li X.D., "Photosynthesis of Hosta under Light and Controlled-Release Nitrogen Fertilizer". ***Russian J. Plant Physiology***, Vol.58, 261-270, **2011**; c)Wilson P.C., Albano J.P., "Impact of Fertigation versus Controlled-release Fertilizer Formulations on Nitrate Concentrations in Nursery Drainage Water". ***Horttechnology***, Vol.21, 176-180, **2011**; d) Xie L.H., Liu M.Z., Ni B.L., Zhang X., Wang Y.F., "Slow-release nitrogen and boron fertilizer from a functional superabsorbent formulation based on wheat straw and attapulgite". ***Chem. Engin. J.***, Vol.167, 342-348, **2011**; e) Tao S.M., Liu J., Jin K.M., Qiu X.Y., Zhang Y., Ren X.Q., Hu S.W., "Preparation and Characterization of Triple Polymer-Coated Controlled-Release Urea With Water-Retention Property and Enhanced Durability". ***J. Applied Polymer Sci.***, Vol.120, 2103-2111, **2011**; f) Wu S., Li Q.S., Ru T.J., Wang L.M., Xing G.Z., Wang J.M., "FTIR Spectra Study on the Him of Polyurethane Coated Urea Controlled-Release Fertilizer". ***Spectro. Spec. Anal.***, Vol.31, 630-634, **2011**.g) Ziadi N., Grant C., Samson N., Nyiraneza J., Belanger G., Parent L., "Efficiency of Controlled-Release Urea for a Potato Production System in Quebec, Canada". ***Agronomy J.***, Vol.103, 60-66, **2011**; h)Yuan C.L., Mou C.X., Wu W.L., Guo Y.B., "Effect of different fertilization treatments on indole-3-acetic acid producing bacteria in soil". ***J. Soils and Sediments***, Vol.11, 322-329, **2011**. i)Xiong Y.S., Yuan J.F., Hu R.G., "Characteristics of nutrient release kinetics for organic polymer-coated fertilizers". ***J. Food Agriculture & Environment***, Vol.8, 733-735, **2010**.

16, a) Schrodera M., Kunza U., Stelzera R., Lehmann H., "On the evidence of a diffusion barrier in the outer cortex apoplast of cress-roots (Lepidium sativum), demonstrated by analytical electron microscopy". ***J. Plant Physiology***, Vol.159, 1197-1204, **2002**; b) Clarkson D.T., "Root structure and sites of ion uptake". ***Plant roots, The hidden half***, (2 ed), 483-503, **1996**. c) Clarkson D.T., Sanderson J., "Inhibition of the uptake and long-distance transport of calcium by aluminium and other polyvalent cations". ***J. Exp. Bot.***, Vol.23, 837-851, **1971**.

17, Bertin C., Yang X.H., Weston L.A., "The role of root exudates and allelochemicals in the rhizosphere". ***Plant and Soil***, Vol.256, 67-83, **2003**.

18, a) Uren N, "Types, amounts, and possible functions of compounds released into the rhizosphere by soil grown plants." ***The rhizosphere: Biochemistry and Organic Substances at the Soil-Plant Interface***, 19-40, **2000**; b) Dakora F., Phillips D., "Root exudates as mediators of mineral acquisition in low-nutrient environments". ***Plant Soil***, Vol. 245, 35-47, **2002**.

19, a) Bais H., Weir T., Perry L., Gilroy S., Vivanco J., "The Role of Root Exudates in Rhizosphere Interactions with Plants and Other Organisms". ***Annu. Rev. Plant Biol.***, Vol. 57, 233-266, **2006**; b) Rovira A.D., McDougall M., Ch. 16: 417, ***Soil Biochemistry***, Marcel Dekker Inc., **1967**; c) Subbarao G.V., Nakahara K., Hurtado M.P., Ono H., Moreta D.E., Salcedo A.F., Yoshihashi A.T., Ishikawa T., Ishitani M., Ohinishi-Kameyama M., Yoshida M., Rondon M., Rao I.M., Lascano C.E., Berry W.L., Ito O., "Evidence for biological nitrification inhibition in Brachiaria pastures". ***Proc. Natl. Acad. Sci.***, Vol.106, 17302-17307, **2009**; d) Phillips R.P., Fahey T. J., "Fertilization effects on fine root biomass, rhizosphere microbes and respiratory fluxes in hardwood forest soils". ***New Phytologist***, Vol.176, 655-664, **2007**; e) Hu J.L., Lin X.G., Wang J.H, Dai J., Chen R.R., Zhang J.B., Wong M.H., " Microbial functional diversity, metabolic quotient, and invertase activity of a sandy loam soil as affected by long-term application of organic amendment and mineral fertilizer". ***J. Soils and Sediments***, Vol.11, 271-280, **2011**; f)Yang L.F., Cai Z.C., "Effects of shading soybean plants on N_2O emission from soil". ***Plant and Soil***, Vol.283, 265-274, **2006**; g)Landi L., Valori F., Ascher J., Renella G., Falchini L., Nannipieri P., "Root exudate effects on the bacterial communities, CO_2 evolution, nitrogen transformations and ATP content of rhizosphere and bulk soils". ***Soil Biology & Biochem.***, Vol.38, 509-516, **2006**; h) Bertin C., Harmon R., Akaogi M., Weidenhamer J.D., Weston L.A., "Assessment of the Phytotoxic Potential of m-Tyrosine in Laboratory Soil Bioassays". ***J. Chem. Ecology***, Vol.35, 1288-1294, **2009**; i)Aira M., Gomez-Brandon M., Lazcano C., Baath E., Dominguez J., "Plant genotype strongly modifies the structure and growth of maize rhizosphere microbial communities". ***Soil Biology & Biochem.***, Vol.42, 2276-2281, **2010**.

20, a) Neumann G., Romheld V., "The release of root exudates as affected by the plant physiological status". ***The Rhizosphere: Biochemistry and organic substances at the soil-plant interface***. Marcel Dekker, **2000**;. b) Neumann G., Römheld V., "Root excretion of carboxylic acids and protons in phosphorus-deficient plants". ***Plant and Soil***, Vol.211, 121-130, **1999**; c) Guern J., Renaudin J.P., Brown S.C., "The compartimentation of secondary metabolites in plant cell cultures". ***Cell Culture and Somatic Cell Genetics of Plants***, 43-46, **1987**.

21, Rovira A.D., "Plant root excretions in relation to the rhizosphere effect. I. Nature of root exudate from oats and peas". ***Plant Soil***, Vol. 7, 178-194, **1956**.

22, Darwent M.J., Paterson E., McDonald A.J., Tomos A.D., "Biosensor reporting of root exudation from Hordeum vulgare in relation to shoot nitrate concentration". ***J. Exp. Botany***, Vol.54, 325-334, **2003**.

23, a) Carpita N., Sabulase D., Montezinos D., Delmer D., " Determination of the pore size of cell walls of living plant cells". ***Science***, Vol.205, 144-147,**1979**; b) Dolan L., "How and where to build a root hair". ***Curr. Opin. Plant Biol.*** Vol.4, 550-554, **2001**; c)

DeRosa M., Monreal C., Schnitzer M., Walsh R., Sultan Y., "Nanotechnology in fertilizers". ***Nature Nanotech.***, Vol.5, 91, **2010**.

24, Lima J.E., Kojima S., Takahashi H., Wiren N.V., " Ammonium triggers lateral root branching in Arabidopsis in an AMT1;3-dependent manner". ***The Plant Cell***, Vol. 22, 3621-3633, **2010**.

25, a) Desnos T., "Root branching responses to phosphate and nitrate". ***Curr. Opin. Plant Biol.***, Vol.11, 82-87, **2008**; b) Svistoonoff S., Creff A., Reymond M., Sigoillot-Claude C., Ricaud L., Blanchet A., Nussaume L., Desnos T., "Root tip contact with low-phosphate media reprograms plant root architecture". ***Nat. Genet.***, Vol.39, 792-796, **2007**; c) Zhang H., Jennings A., Barlow P. W., Forde B. G., "Dual pathways for regulation of root branching by nitrate". ***Proc. Natl. Acad. Sci.***, Vol.96, 6529-6534, **1999**; d) Paynel F., Murray P. J., Cliquet J. B., "Root exudates: a pathway for short-term N transfer from clover and ryegrass". ***Plant Soil***, Vol.229, 235-243, **2001**.

26, Caffaro M.M., Vivanco J.M., Gutierrez B.F.H., "The effect of root exudates on root architecture in Arabidopsis thaliana" ***Plant Growth Regulation***, Vol.64, 241-249, **2011**.

27, a) Chandrasekaran S., "Production of organic acids by soil micro organisms". ***Plant and Soil***, Vol.30, 299-304, **1969**; b) Szajdak L., Osterberg R., "Amino acids present in humic acids from soils under different cultivations". ***Environment International***, Vol.22, 331-334, **1996**; c) Sultan Y., DeRosa M.C., "Target Binding Influences Permeability in Aptamer-Polyelectrolyte Microcapsules". ***Small***, Vol.7, 1219-1226, **2011**.

28, Iler R.K., "Multilayers of Colloidal Particles". ***J. Colloid and Interface Science***, Vol.21, 569-594, **1966**.

29, a) Decher G., Hong J.D., Schmitt J., "Buildup of ultrathin multilayer films by a self-assembly process. III. Consecutively alternating adsorption of anionic and cationic polyelectrolytes on charged surfaces". ***Thin Solid Films***, Vol. 210, 831-835, **1992**; b) Sukhishvili S.A., "Responsive polymer films and capsules via layer-by-layer Assembly". ***Curr. Opin. Colloid Interf. Sci***. Vol.10, 37-44, **2005**.

30, a) Tang Z.; Wang Y., Podsiadlo P., Kotov N.A. "Biomedical Applications of Layer-by-Layer Assembly: From Biomimetics to Tissue Engineering". ***Adv. Mater.***, Vol. 18, 3203-3224, **2006**; b) Decher G., "Fuzzy nanoassemblies: toward layered polymeric multicomposites". ***Science***, Vol.277, 1232-1237, **1997**.

31,a) Decher G., Eckle M., Schmitt J., Struth B., "Layer-by-layer assembled multicomposite films". ***Curr Opin Coll Interface Sci***, Vol. 3, 32-39, **1998**; b) Anzai J., Kobayashi Y., Nakamura N., Nishimura M., Hoshi T., "Layer-by-layer construction of

multilayer thin films composed of avidin and biotin-labeled poly(amine)s". ***Langmuir***, Vol.15, 221-226, **1999**; c) Serizawa T., Yamaguchi M., Akashi M., "Enzymatic hydrolysis of a layer-by-layer assembly prepared from chitosan and dextran sulfate". ***Macromol.***, Vol. 35, 8656-8658, **2002**; d) Caruso F., Niikura K., Furlong D.N., Okahata Y., "Assembly of alternating polyelectrolyte and protein multilayer films for immunosensing 2". ***Langmuir***, Vol.13, 3427-3433, **1997**; e) Caruso F., Niikura K., Furlong D.N., Okahata Y., "Ultrathin multilayer polyelectrolyte films on gold: Construction and thickness determination 1". ***Langmuir***, Vol.13, 3422-3426, **1997**; f) Jin W., Shi X.Y., Caruso F., "High activity enzyme microcrystal multilayer films". ***J. Am. Chem. Soc.***, Vol.123, 8121-8122, **2001**; g) Ichinose I., Fujiyoshi K., Mizuki S., Lvov Y., Kunitake T., "Layer-by-layer assembly of aqueous bilayer membranes on charged surfaces". ***Chem. Lett.***, Vol.4, 257-258, **1996**; h) Katagiri K., Hamasaki R., Ariga K., Kikuchi J., "Layered paving of vesicular nanoparticles formed with cerasome as a bioinspired organic-inorganic hybrid". ***J. Am. Chem. Soc.***, Vol.124, 7892-7893, **2002**; i) Katagiri K., Hamasaki R., Ariga K., Kikuchi J., "Layer-by-layer self-assembling of liposomal nanohybrid "cerasome" on substrates". ***Langmuir***, Vol.18, 6709-6711, **2002**; j) Michel M., Arntz Y., Fleith G., Toquant J., Haikel Y., Voegel J.C., Schaaf P., Ball V., "Layer-by-layer self-assembled polyelectrolyte multilayers with embedded liposomes: Immobilized submicronic reactors for mineralization". ***Langmuir***, Vol.22, 2358-2364, **2006**; k) Mamedov A., Ostrander J., Aliev F., Kotov N.A., "Stratified assemblies of magnetite nanoparticles and montmorillonite prepared by the layer-by-layer assembly". ***Langmuir***, Vol.16, 3941-3949, **2000**; l) Ichinose I., Tagawa H., Mizuki S., Lvov Y., Kunitake T., "Formation process of ultrathin multilayer films of molybdenum oxide by alternate adsorption of octamolybdate and linear polycations". ***Langmuir***, Vol.14, 187-192, **1998**; m) Ariga K., Lvov Y., Kunitake T., "Assembling alternate dye-polyion molecular films by electrostatic layer-by-layer adsorption". ***J. Am. Chem. Soc.***, Vol.119, 2224-2231, **1997**; n) Locklin J., Shinbo K., Onishi K., Kaneko F., Bao Z. N., Advincula R.C., "Ambipolar organic thin film transistor-like behavior of cationic and anionic phthalocyanines fabricated using layer-by-layer deposition from aqueous solution". ***Chem. Mater.***, Vol.15, 1404-1412, **2003**; o) Hammond P.T., "Recent explorations in electrostatic multilayer thin film assembly". ***Curr. Opin. Coll. Interface Sci.***, Vol.4, 430-442, **1999**; p) Bertrand P., Jonas A., Laschewsky A., Legras R., "Ultrathin polymer coatings by complexation of polyelectrolytes at interfaces: suitable materials, structure and properties". ***Macromol. Rap. Commun.***, Vol.21, 319-348, **2000**.

32, a) Ding B., Du J., Hsieh Y., "Tubular Multi-Bilayer Polysaccharide Biofilms on Ultra-Thin Cellulose Fibers", ***J. Appl. Poly. Sci.***, Vol.121, 2526-2534, **2011**; b) Schonhoff M., "Layered polyelectrolyte complexes: physics of formation and molecular properties". ***J. Phys.: Condens. Matter***, Vol.15, R1781-R1808. **2003**; c) Sukhorukov G.B., Donath E., Lichtenfeld H., "Layer-by-layer self assembly of polyelectrolytes on colloidal particles". ***Coll. Surf. A***, Vol.137, 253-266, **1998**; d) Donath E., Sukhorukov

G.B., Caruso F., Davis S.A., Mohwald H., "Novel hollow polymer shells by colloid-templated assembly of polyelectrolytes". ***Angew Chem-Int Ed***, Vol.37, 2201-2205, **1998**; e) Losche M., Schmitt J., Decher G., Bouwman W.G., Kjaer K., "Detailed Structure of Molecularly Thin Polyelectrolyte Multilayer Films on Solid Substrates as Revealed by Neutron Reflectometry". ***Macromol.***, Vol.31, 8893-8906, **1998**.

33, a) Caruso F., Caruso R. A., Mohwald H., "Nanoengineering of inorganic and hybrid hollow spheres by colloidal templating". ***Science***, Vol.282, 1111-1114, **1998**; b) Johnston A.P.R., Read E.S., Caruso F., "DNA multilayer films on planar and colloidal supports: Sequential assembly of like-charged polyelectrolytes". ***Nano Lett.***, Vol.5, 953-956, **2005**; c) Caruso F., "Hollow Capsule Processing through Colloidal Templating and Self-Assembly". ***Chem. Eur. J.***, Vol.6, 413-419, **2000**; d) Shi X.Y., Caruso F., "Release behavior of thin-walled microcapsules composed of polyelectrolyte multilayers". ***Langmuir***, Vol.17, 2036-2042, **2001**; e), Ai H., Fang M., Jones S. A., Lvov Y. M., "Electrostatic layer-by-layer nanoassembly on biological microtemplates: Platelets". ***Biomacromol.***, Vol.3, 560-564, **2002**.

34, a) Volodkin D.V., Petrov A. I., Prevot M., Sukhorukov G.B., "Matrix Polyelectrolyte Microcapsules: New System for Macromolecule Encapsulation". ***Langmuir***, Vol.20, 3398-3406, **2004**; b)Buscher K., Graf K., Ahrens H., Helm C.A., "Influence of adsorption conditions on the structure of polyelectrolyte multilayers". ***Langmuir***, Vol.18, 3585-3591, **2002**; c) Schwarz B., Schonhoff M., "Surface potential driven swelling of polyelectrolyte multilayers". ***Langmuir***, Vol.18, 2964-2966, **2002**.

35, a) Caruso F., Lichtenfeld H., Donath E., Mohwald H., "Investigation of electrostatic interactions in polyelectrolyte multilayer films: binding of anionic fluorescent probes to layers assembled onto colloids". ***Macromol.***, Vol.32, 2317-2328, **1999**; b) Tedeschi C., Caruso F., Mohwald H., Kirstein S., "Adsorption and desorption behavior of an anionic pyrene chromophore in sequentially deposited polyelectrolyte-dye thin films". ***J. Am. Chem. Soc.***, Vol.122, 5841-5848, **2000**; c) Schlenoff J.B., Ly H., Li M., "Charge and mass balance in polyelectrolyte multilayers". ***J. Am. Chem. Soc.***, Vol.120, 7626-7634, **1998**; d) Finkenstadt D., Johnson D.D., "Model of ionization response of weak polyacids in a layered polyelectrolyte self-assembly". ***Langmuir***, Vol.18, 1433-1436, **2002**; e) Xie A.F., Granick S., "Local electrostatics within a polyelectrolyte multilayer with embedded weak polyelectrolyte". ***Macromol.***, Vol.35, 1805-1813, **2002**.

36, a) Schwarz B., Schonhoff M., "A H-1 NMR relaxation study of hydration water in polyelectrolyte mono and multilayers adsorbed to colloidal particles". ***Colloid Surf. A***, Vol.198, 293-304, **2002**; b) Lowack K., Helm C. A., "Molecular Mechanisms Controlling the self-Assembly Process of Polyelectrolyte Multilayers". ***Macro.***, Vol.31, 823-833, **1998**.

37, Yoo D., Shiratori S.S., Rubner M.F., "Controlling bilayer composition and surface wettability of sequentially adsorbed multilayers of weak polyelectrolytes". ***Macromol.***, Vol.31, 4309-4318, **1998**.

38, Glinel K., Dejugnat C., Prevot M., Scholer B., Schonhoff M., Klitzing R.V., "Responsive polyelectrolyte multilayers". ***Colloid Surf. A***, Vol.303, 3-13, **2007**.

39, a) Rossier-Miranda F.J., Schroen K., Boom R., "Mechanical Characterization and pH Response of Fibril-Reinforced Microcapsules Prepared by Layer-by-Layer Adsorption". ***Langmuir***, Vol.26, 19106-19113, **2010**; b) Bird R., Freemont T.J., Saunders B.R., "Hollow polymer particles that are pH-responsive and redox sensitive: two simple steps to triggered particle swelling, gelation and disassembly". ***Chem. comm.***, Vol.47, 1443-1445, **2011**; c) Takayuki I., Toshiyuki K., Michiya M., Mitsuru A., "Preparation and Unique pH-Responsive Properties of Novel Biodegradable Nanocapsules Composed of Poly (glutamic acid) and Chitosan as Weak Polyelectrolytes". ***Macromol.***, Vol.10, 271-277, **2010**; d) Arys X., Laschewsky A., Jonas A.M., "Ordered polyelectrolyte 'multilayers'.1. Mechanisms of growth and structure formation: a comparison with classical fuzzy "multilayers". ***Macromol.***, Vol.34, 3318-3330, **2001**; e) Zhai L., Cebeci F.C., Cohen R.E., Rubner M.F., "Stable superhydrophobic coatings from polyelectrolyte multilayers". ***Nano Lett.***, Vol.4, 1349-1353, **2004**.

40, a) Dingenouts N., Norhausen C., Ballauff M., "Observation of the volume transition in thermosensitive core-shell latex particles by small-angle X-ray scattering". ***Macromol.***, Vol.31, 8912-8917, **1998**; b) Wong J.E., Richtering W., "Surface modification of thermoresponsive microgels via layer-by-layer assembly of polyelectrolyte multilayers". ***Prog. Coll. Poly. Sci.***, Vol.133, 45-51, **2006**; c) Ibarz G., Dahne L., Donath E., Mohwald H., "Controlled permeability of polyelectrolyte capsules via defined annealing". ***Chem. Mater.***, Vol.14, 4059-4062, **2002**; d)Li Z.G., Mi W.J., Huang H.J., Hu J.W., "The Preparation of Normal Temperature Microcapsule Phase Change Material and Study of Its Thermodynamic Property". ***Proceedings of the 7th National Conference on Chinese Functional Materials and Applications***, Vol.1-3, 216-218, **2010**.

41, a) Bedard M.F., De Geest Bruno G., Skirtach A.G., Moehwald H., Sukhorukov G.B., "Polymeric microcapsules with light responsive properties for encapsulation and release". ***Advan. Coll. Interf. Sci.***, Vol.158, 2-14, **2010**; b) Kiyofumi K., Atsunori M., Frank C., "Effect of UV-Irradiation on Polyelectrolyte Multilayered Films and Hollow Capsules Prepared by Layer-by-Layer Assembly". ***Macromol.***, Vol.39, 8067-8074, **2006**.

42, a) De Smedt S, "Release on demand: Artificial insemination by ovulation-triggered release of implanted sperms". ***J. Control. Release***, Vol.150, 1-1, **2011**; b) Kemmer C., Fluri D.A., Witschi U., Passeraub A., Gutzwiller A., Fussenegger M., "A designer

network coordinating bovine artificial insemination by ovulation triggered release of implanted sperms". ***J. Control. Release***, Vol.150, 23-29, **2011**.

43, a) Petrov A.I., Volodkin D.V., Sukhorukov G.B., "Protein-calcium carbonate coprecipitation: A tool for protein encapsulation". ***Biotechnol. Prog.*** Vol.21, 918-925, **2005**; b) Borodina T., Markvicheva E., Kunizhev S., Mohwald H., Sukhorukov G.B., Kreft O., "Controlled Release of DNA from Self-Degrading Microcapsules". ***Macromol. Rap. Comm.***, Vol.28, 1894-1899, **2007**; c) Tikhonenko S.A., Saburove E.A, Dubrovskii A.V, Shabarchina L.I, Dybovskaya Y.N., Sukhorukov B.I, "A Technique for Incorporating Enzymes into Polyelectrolyte Microcapsules". ***Glass Phys. Chem.***, Vol.33, 287-293, **2007**; d) Liu X.R., Zhu B.Q., Shao Y.Y., Yang X.L., "$CaCO_3$-Templated Microcapsules to Carry Heparin via Layer-by-layer Self-assembly". ***2009 3RD INTERNATIONAL CONFERENCE ON BIOINFORMATICS AND BIOMEDICAL ENGINEERING***, Vol.1-11, 1046-1050, **2009**. e) Volodkin D.V., Larionova N.I., Sukhorukov G.B., "Protein encapsulation via porous $CaCO_3$ microparticles templating". ***Biomacromol.***, Vol.5, 1962-1972, **2004**.

44, a) Li Y., Han W.W, Liao M., Wang J., Zhao X.D., "Preparation of Hollow Polyelectrolyte Microcapsules and Their Fluorescent Proteins Loading". ***Acta Polymerica Sinica***, Vol.4, 456-461, **2010**; b) Masahiro Y., Tsutomu M., Yasuo H., Takayuki T., Koichiro S., Shiro K., "Permeability control in electro-sensitive microcapsules with immobilized ferroelectric liquid crystalline segments". ***J. Polymer science part A- polymer chemistry***, Vol.46, 1749-1757, **2008**.

45, a) Robertson D., Joyce G., "Selection in vitro of an RNA enzyme that specifically cleaves single-stranded-DNA". ***Nature***, Vol.344, 467-468, **1990**; b) Tuerk C., Gold L., "Systematic evolution of ligands by exponential enrichment: RNA ligands to bacteriophage T4 Aptamer polymerase". ***Science***, Vol.249, 505-510, **1990**; c) Ellington A., Szostak J., "In vitro selection of RNA molecules that bind specific ligands". ***Nature***, Vol.346, 818-822, **1990**.

46, a) Wilson C., Szostak J.W., "In vitro evolution of a self-alkylating ribozyme". ***Nature***, Vol.374, 777-782, **1995**; b) Mendonsa S.D., Bowser M.T., "In vitro selection of high-affinity DNA ligands for human IgE using capillary electrophoresis". ***Anal. Chem.***, Vol.76, 5387-5392, **2004**; c) Stoltenburg R., Reinemann C., Strehlitz B., "FluMag-SELEX as an advantageous method for DNA aptamer selection". ***Anal. Bioanal. Chem.***, Vol.383, 83-91, **2005**; d) Bianchini M., Radrizzani M., Brocardo M.G., Reyes G.B., Gonzalez S.C., Santa-Coloma T.A., Specific oligobodies against ERK-2 that recognize both the native and the denatured state of the protein". ***J. Immunol. Methods***, Vol.252, 191-197, **2001**; e) Yang X.B., Li X., Prow T.W., Reece L.M., Bassett S.E., Luxon B.A., Herzog, N.K., Aronson J., Shope R.E., Leary J.F., Gorenstein D.G., "Immunofluorescence assay and flow-cytometry selection of bead-bound aptamers".

Nucleic Acids Res. Vol.31, e54, **2003**; f) Stoltenburg R., Reinemann C., Strehlitz B., "SELEX—A (r)evolutionary method to generate high-affinity nucleic acid ligands". ***Biomolecular Engineering***, Vol.24, 381-403, **2007**.

47, a) Jones L.A., Clancy L.E., Rawlinson W.D., White P.A., "High-Affinity Aptamers to Subtype 3a Hepatitis C Virus Polymerase Display Genotypic Specificity". ***Antimicrobial Agents and Chemotherapy***, Vol.50, 3019-3027, **2006**; b) Win M.N., Klein J.S., Smolke C.D., "Codeine-binding RNA aptamers and rapid determination of their binding constants using a direct coupling surface plasmon resonance assay". ***Nucleic Acids Research***, Vol.34, 5670-5682, **2006**; c) Ulrich H., Ippolito J.E., Pagan R., Eterovic V.A., Hann R. M., Shi H., Lis J.T., Eldefrawi M.E., Hess G.P., "In vitro selection of RNA molecules that displace cocaine from the membrane-bound nicotinic acetylcholine receptor". ***Proc. Natl. Acad. Sci.***, Vol.95, 14051-14056, **1998**.

48, a) Hermann T., Patel D.J., "Adaptive recognition by nucleic acid aptamers". ***Science***, Vol.287, 820-825, **2000**; b) Mann D., Reinemann C., Stoltenburg R., Strehlitz B., "In vitro selection of DNA aptamers binding ethanolamine". ***Biochem. Biophys. Res. Commun.***, Vol.338, 1928-1934, **2005**; c) Bruno J. G., Carrillo M.P., Phillips T., King B., "Development of DNA aptamers for cytochemical detection of acetylcholine In Vitro Cell". ***Dev. Biol. Anim.***, Vol.44, 63-72, **2008**; d) Blank M., Weinschenk T., Priemer M., Schluesener H., "Systematic evolution of a DNA aptamer binding to rat brain tumor microvessels - Selective targeting of endothelial regulatory protein pigpen". ***J. Biol. Chem.***, Vol.276, 16464-16468, **2001**; e) Daniels D. A., Chen H., Hicke B. J., Swiderek K. M., Gold L. A., "A tenascin-C aptamer identified by tumor cell SELEX: Systematic evolution of ligands by exponential enrichment". ***Proc. Natl. Acad. Sci.***, Vol.100, 15416-15421, **2003**; f) Shangguan D., Li Y., Tang Z., Cao Z., Chen H., Mallikaratchy P., Sefah K., Yang C., Tan W., "Aptamers evolved from live cells as effective molecular probes for cancer study". ***Proc. Natl. Acad. Sci.***, Vol.103, 11838-11843, **2006**; g) Cao X.X., Li S.H., Chen L.C., Ding H.M., Xu H., Huang Y.P., Li J., Liu N.L., Cao W.H., Zhu Y.J., "Combining use of a panel of ssDNA aptamers in the detection of Staphylococcus aureus". ***Nucleic Acids Res.***, Vol.37, 4621-4628, **2009**; h) Tang Z.W., Shangguan D., Wang K.M., Shi H., Sefah K., Mallikratchy P., Chen H.W., Li Y., Tan W.H., "Selection of aptamers for molecular recognition and characterization of cancer cells". ***Anal. Chem.***, Vol.79, 4900-4907, **2007**.

49, Kleinjung F., Klussmann S., Erdmann V.A., Scheller F.W., Furste J.P., Bier F.F., "High-affinity RNA as a recognition element in a biosensor". ***Anal. Chem.***, Vol.70, 328-331, **1998**; b) Buff M.C.R., Schafer F., Wulffen B., Muller J., Potzsch B., Heckel A., Mayer G., "Dependence of aptamer activity on opposed terminal extensions: improvement of light-regulation efficiency". ***Nucleic Acids Res.***, Vol.6, 2111-2118, **2010**.

50, a) Huang J., "Erros in estimating the un-bound fraction of drugs due to the volume shift in equilibrium dialysis". ***J. Pharma. Sci.***, Vol.72, 1368-1369, **1983**; b) Oehler S., Alex R., Barker A., "Is nitrocellulose filter binding really a universal assay for protein-DNA interactions?". ***Anal. Biochem.***, Vol.268, 330-336, **1999**; c) Shcherbakov D., Piendl W., "A novel view of gel-shifts: Analysis of RNA-protein complexes using a two-color fluorescence dye procedure". ***Electrophoresis***, Vol.28, 749-755, **2007**; d) Chen Z., Weber S.G., "Determination of binding constants by affinity capillary electrophoresis, electrospray ionization mass spectrometry and phase-distribution methods". ***Trac-Trends Anal. Chem.***, Vol.27, 738-748, **2008**; e) del Toro M., Gargallo R., Eritja R., Jaumot J., "Study of the interaction between the G-quadruplex-forming thrombin-binding aptamer and the porphyrin 5,10,15,20-tetrakis-(N-methyl-4-pyridyl)-21, 23H-porphyrin tetratosylate". ***Anal. Biochem.***, Vol.379, 8-15, **2008**; f) Turgeon R.T., Fonslow B.R., Jing M., Bowser M.T., "Measuring Aptamer Equilibria Using Gradient Micro Free Flow Electrophoresis". ***Anal. Chem.***, Vol.82, 3636-3641, **2010**; g) Fagerstam L.G., Frostell-Karlsson A., Karlsson R., Persson B., Ronnberg I., "Biospecific interation analysis using surface-plasmon resonance detection applied to kinetic, binding-site and concentration analysis". ***J. Chromatography***, Vol.597, 397-410, **1992**; h) Lakowicz J.R., Gryczynski I., Gryczynski Z., Dattelbaum J.D., "Anisotropy-based sensing with reference fluorophores". ***Anal. Biochem.***, Vol.267, 397-405, **1999**; i) Jing M., Bowser M. T., "Methods for measuring aptamer-protein equilibria: a review". ***Anal. Chim. Acta.***, Vol.686, 9-18, **2011**.

51, Ellington A., "RNA Selection-Aptamers Achieve the Desired Recognition". ***Curr. Biol.***, Vol.4, 427-428, **1994**.

52, a) Ruigrok V.J.B., Levisson M., Eppink M.H.M., Smidt H., van der Oost J., "Alternative affinity tools: more attractive than antibodies?". ***Biochemical J.***, Vol.436, 1-13, **2011**; b) Nimjee S.M., Rusconi C.P., Sullenger B.A., "Aptamers: an emerging class of therapeutics". ***Annu. Rev. Med.*** Vol.56, 555-583, **2005**; c) Rusconi C.P., Roberts J.D., Pitoc G.A., Nimjee S.M., White R.R., Quick G., Scardino E., Fay W.P., Sullenger B.A., "Antidote-mediated control of an anticoagulant aptamer in vivo". ***Nat. Biotechnol.*** Vol.22, 1423-1428, **2004**; d) Rimmele M., "Nucleic acid aptamers as tools and drugs: recent developments". ***Chembiochem.***, Vol.4, 963-971, **2003**.

53, a) Bunka D., Stockley P., "Aptamers come of age - at last". ***Nature Rev.***, Vol.4, 588-596, **2006**; b) Cox J. C., Rudolph P., Ellington A.D., "Automated RNA selection". ***Biotechnol. Prog***. Vol.14, 845-850, **1998**; c) Berezovski M., "Nonequilibrium capillary electrophoresis of equilibrium mixtures: a universal tool for development of aptamers". ***J. Am. Chem. Soc.***, Vol.127, 3165-3171, **2005**; d) Misono T.S., Kumar P.K.R., "Selection of RNA aptamers against human influenza virus hemagglutinin using surface plasmon resonance". ***Anal. Biochem.***, Vol.342, 312-317, **2005**.

54, a) Nimjee S.M., Rusconi C.P., Harrington R.A., Sullenger B.A., "The potential of aptamers as anticoagulants". ***Trends Cardiovasc. Med.***, Vol.15, 41-45, **2005**; b) Keefe A. D., Cload S. T., "SELEX with modified nucleotides". ***Curr. Opin. Chem. Biol.***, Vol.12, 448-456, **2008**; c) Boomer R.M., Lewis S.D., Healy J.M., Kurz M., Wilson C., McCauley T.G., "Conjugation to polyethylene glycol polymer promotes aptamer biodistribution to healthy and inflamed tissues". ***Oligonucleotides***, Vol.15, 183-195, **2005**; d) Cao Z., Tong R., Mishra A., Xu W., Wong G.C., Cheng J., Lu Y., "Reversible Cell-Specific Drug Delivery with Aptamer-Functionalized Liposomes". ***Angew. Chem., Int. Ed.***, Vol.48, 6494-6498, **2009**.

55, a) Kaur H., Babu B. R., Maiti S., "Perspectives on chemistry and therapeutic applications of Locked Nucleic Acid (LNA)". ***Chem. Rev.***, Vol.107, 4672-4697, **2007**; b) Kaur H., Wengel J., Maiti S., "LNA-modified oligonucleotides effectively drive intramolecular-stable hairpin to intermolecular-duplex state". ***Biochem. Biophys. Res. Comm.***, Vol.352, 118-122, **2007**.

56, a) Marro M.L., Daniels D.A., McNamee A., Andrew D.P., Chapman T.D., Jiang M.S., Wu Z.N., Smith J.L., Patel K.K., Gearing K.L., "Identification of potent and selective RNA antagonists of the IFNgamma- inducible CXCL10 chemokine". ***Biochem.***, Vol.44, 8449-8460, **2005**; b) Rhodes A., Deakin A., Spaull J., Coomber B., Aitken A., Life P., Rees S., "The generation and characterization of antagonist RNA aptamers to human oncostatin". ***M. J. Biol. Chem.*** Vol.275, 28555-28561, **2000**; c) Wang L., Yang C. J., Medley C. D., Benner S. A., Tan W., "Locked nucleic acid molecular beacons". ***J. Am.Chem. Soc.***, Vol.127, 15664-15665, **2005**.

57, OSullivan C.K., "Aptasensors-the future of biosensing?". ***Anal. Bioanal. Chem.*** Vol.372, 44-48, **2002**.

58, a) Dua P., Kim S., Lee D.K., "Nucleic acid aptamers targeting cell-surface proteins". ***Methods***, Vol.54, 215-225, **2011**; b) You M., Chen Y., Peng L., Han D., Yin B., Ye B., Tan W., "Engineering DNA aptamers for novel analytical and biomedical applications". ***Chem. Sci.***, Vol.2, 1003-1010, **2011**.

59, a) Wu Z.S., Zhang S.B., Zhou H., Shen G.L., Yu R.Q., "Universal Aptameric System for Highly Sensitive Detection of Protein Based on Structure-Switching-Triggered Rolling Circle Amplification". ***Anal. Chem.***, Vol.82, 2221-2227, **2010**; b) Zhou J., Battig M.R., Wang Y., "Aptamer-based molecular recognition for biosensor development". ***Anal. Bioanal. Chem***. Vol.398, 2471-2480, **2010**.

60, a) Stojanovic M.N., de Prada P., Landry D.W., "Aptamer-based folding fluorescent sensor for cocaine". ***J. Am. Chem. Soc.***, Vol.123, 4928-4931, **2001**; b) Brockstedt U., Uzaroeska A., Montpetit A., Pfau W., Labuda D., "In vitro evolution of RNA aptamers

recognizing carcinogenic aromatic amines". ***Biochem. Biophys. Res. Commun.***, Vol.313, 1004-1008, **2003**.

61, a) Hartmuth K., Vornlocher H.P., Luhrmann R., "Tobramycin affinity tag purification of spliceosomes". ***Meth. Mol. Biol.***, Vol.257, 47-64, **2004**; b) Koita R.B., Li L., McGown L.B., "Separation of nontarget compounds by DNA aptamers". ***Anal. Chem.***, Vol.72, 827-831, **2000**; c) Nguyen T.H., Pei R.J., Stojanovic M., Lin Q., "Demonstration and characterization of biomolecular enrichment on microfluidic aptamer-functionalized surfaces". ***Sensors and actuators B-Chem.***, Vol.155, 58-66, **2011**.

62, Gragoudas E.S., Adamis A.P., Cunningham E.T., Feinsod M., Guyer D.R., "Pegaptanib for neovascular age-related macular degeneration". ***New England J. Medicine***, Vol.351, 2805-2816, **2004**.

63, a) Suess B., Fink B., Berens C., Stentz R., Hillen W., "A theophylline responsive riboswitch based on helix slipping controls gene expression in vivo". ***Nucleic Acids Res.***, Vol.32, 1610-1614, **2004**; b) Davidson E.A., Ellington A.D., "Engineering regulatory RNAs". ***Trends Biotechnol.***, Vol.23, 109-112, **2005**.

64, a) McNamara J.O., Andrechek E.R., Wang Y., Viles K.D., Rempel R.E., Gilboa E., Sullenger B.A., Giangrande P.H., "Cell type-specific delivery of siRNAs with aptamer-siRNA chimeras". ***Nat. Biotechnol.***, Vol.24, 1005-1015, **2006**; b) Yang H., Liu H., Kang H., Tan W., "Engineering target-responsive hydrogels based on aptamer -Target interactions". ***J. Am. Chem. Soc.***, Vol.130, 6320-6321, **2008**; c) Wei B., Cheng I., Luo K.Q., Mi Y., "Capture and release of protein by a reversible DNA-induced sol-gel transition system". ***Angew. Chem., Int. Ed.***, Vol.47, 331-333, **2008**; d) Wu Y., Sefah K., Liu H., Wang R., Tan W., "DNA aptamer-micelle as an efficient detection/delivery vehicle toward cancer cells". ***Proc. Natl. Acad. Sci.***, Vol.107, 5-10, **2010**.

65, Sultan Y., Walsh R., Monreal C., DeRosa M.C., "Preparation of functional aptamer films using layer-by-layer self assembly". ***Biomacromol.***, Vol.10, 1149-1154, **2009**.

66, a) Koga N., Nakagoe Y.Z, Tanaka H., "Crystallization of amorphous calcium carbonate". ***Thermo. Acta***, Vol. 318, 239-244, **1998**; b) Kitamura M., Konno H., Yasui A., Masuoka H., "Controlling factors and mechanism of reactive crystallization of calcium carbonate polymorphs from calcium hydroxide suspensions". ***J. Cryst. Grow.***, Vol. 236, 323-332, **2002**; c) Guo X.H., Liu L., Wang W.N., Zhang J., Wang Y.Y., Yua S.H., "Controlled crystallization of hierarchical and porous calcium carbonate crystals using polypeptide type block copolymer as crystal growth modifier in a mixed solution". ***CrystEngComm***, Vol. 13, 2054-2061, **2011**.

67, Suzuki M., Saruwatari K., Kogure T., Yamamoto Y., Nishimura T., Kato T., Nagasawa H., " An acidic Matrix Protein, Pif, Is a Key Macromolecule for Nacre Formation". ***Science***, Vol. 325, 1388-1390, **2009**.

68, Li L., Zhu Y.J., Cao S.W., Ma M., "Preparation and Drug Release Properties of Nanostructured $CaCO_3$ Porous Hollow Microspheres". ***J. Inorg. Mater.***, Vol. 24, 166-170, **2009**.

69, a)Wang Z.J., Qian L., Wang X.L., Zhu H., Yang F., Yang X.R., "Hollow DNA/PLL microcapsules with tunable degradation property as efficient dual drug delivery vehicles by alpha-chymotrypsin degradation". ***Coll. Surf. A***, Vol.332, 164-171, **2009**; b)Wang C.Y., Ye S.Q., Sun Q.L., He C.Y., Ye W.H., Liu X.X., Tong Z., "Microcapsules for controlled release fabricated via layer-by-layer self-assembly of polyelectrolytes". ***J. Exper. Nanosci.***, Vol 3, 133-145, **2008**.

70, a) Xu G.F, Yao N., Aksay I.A., Groves J.T, "Biomimetic synthesis of macroscopic-scale calcium carbonate thin films. Evidence for a multistep assembly process". ***J. Am. Chem. Soc.***, Vol. 120, 11977-11985, **1998**; b) Liang X.H., Xiang J.H., Zhang F.S., Xing L., Song B., Chen S.W., "Fabrication of Hierarchical $CaCO_3$ Mesoporous Spheres: Particle-Mediated Self-Organization Induced by Biphase Interfaces and SAMs". ***Langmuir***, Vol.26, 5882-5888, **2010**; c) Sugih A. K., Shukla D., Heeres H.J., Mehra A., "$CaCO_3$ nanoparticle synthesis by carbonation of lime solution in microemulsion systems". ***Nanotech.***, Vol.18, Article No. 035607, **2007**; d) Nudelman F., Sonmezler E., Bomans P.H.H., de Gijsbertus W., Sommerdijk N.A.J.M., "Stabilization of amorphous calcium carbonate by controlling its particle size". ***Nanoscale***, Vol.2, 2436-2439, **2010**.

71, Huang S.C., Naka K., Chujo Y., "A Carbonate Controlled-Addition Method for Amorphous Calcium Carbonate Spheres Stabilized by Poly (acrylic acid)s". ***Langmuir***, Vol. 23, 12086-12095, **2007**.

72, Volodkin D.V., Larionova N.I., Sukhorukov G.B., "Protein encapsulation via porous $CaCO_3$ microparticles templating". ***Biomacromol.***, Vol.5, 1962-1972, **2004**.

73, Bobreshova M.E, Sukhorukov G.B, Saburova E.A, Elfimova L.I, Shabarchina L.I, Sukhorukov B.I, "Lactate dehydrogenase in interpolyelectrolyte complex. Function and stability". ***Biofizika***, Vol.44, 813-820, **1999**.

74, Wilson C., Szostak J. W., "Isolation of a fluorophore-specific DNA aptamer with weak redox activity". ***Chem. Bio.***, Vol.5, 609-617, **1998**.

75, http://www.malvern.com/LabEng/technology/zeta_potential

76, Volodkin D.V., Petrov A. I., Prevot M., Sukhorukov G.B., "Matrix Polyelectrolyte Microcapsules: New System for Macromolecule Encapsulation". ***Langmuir***, Vol.20, 3398-3406, **2004**

77, http://www.basic.northwestern.edu/biotools/oligocalc.html

78, a) Choi J.Y., Rubner M.F., "Influence of the degree of ionization on weak polyelectrolyte multilayer assembly". ***Macromol.*** Vol.38, 116-124, **2005**; b) Dubas S.T., Schlenoff J.B., "Factors controlling the growth of polyelectrolyte multilayers". ***Macromol.***, Vol.32, 8153-8160, **1999**; c) Riegler H., Essler F., "Polyelectrolytes, 2. Intrinsic or Extrinsic charge compensation? Quantitative charge analysis of PAH/PSS multilayers". ***Langmuir***, Vol. 18, 6694-6698, **2002**.

79, Donath E., Walther D., Shilov V.N., Knippel E., Budde A., Lowack K., Helm C.A., Mohwald H., "Nonlinear Hairy Layer Theory of Electrophoretic Fingerprinting Applied to Consecutive Layer by Layer Polyelectrolyte Adsorption onto Charged Polystyrene Latex Particles". ***Langmuir***, Vol.13, 5294-5305, **1997**.

80, Irigoyen J., Moya S.E., Iturri J.J, Llarena I., Azzaroni O., Donath E., "Specific ζ-potential Response of Layer-by-Layer Coated Colloidal Particles Triggered By Polyelectrolyte Ion Interactions". ***Langmuir***, Vol.25, 3374-3380, **2009**.

81, a) Bhatia S.R., Khattak S.F., Roberts S.C., "Polyelectrolytes for cell encapsulation". ***Curr. Opin. Coll. Inter. Sci.***, Vol.10, 45 -51, **2005**; b) Itano K., Choi J.Y., Rubner M.F., "Mechanism of the pH-Induced Discontinuous Swelling/Deswelling Transitions of Poly(allylaminutese hydrochloride)-Containing Polyelectrolyte Multilayer Films". ***Macromol.***, Vol.38, 3450-3460, **2005**. c) http://en.wikipedia.org/wiki/Bis-tris_methane

82, Wang F., Feng J., Tong W.J., Gao C.Y., "A facile pathway to fabricate microcapsules by in situ polyelectrolyte coacervation on poly (styrene sulfonate)-doped $CaCO_3$ particles". ***J. Mater. Chem.***,Vol.17, 670-676, **2007.**

83, a)Kohler K., Shchukin D.G, Sukhorukov G.B, Mohwald H, "Drastic morphological modification of polyelectrolyte microcapsules induced by high temperature". ***Macromol.***, Vol.37, 9546-9550, **2004**; b) Dejugnat C., Kohler K., Dubois M., Sukhorukov G.B, Mohwald H., Zemb T., Guttmann P., "Membrane densification of heated polyelectrolyte multilayer capsules characterized by soft X-ray microscopy". ***Adv. Mat.***, Vol.19, 1331-1336, **2007**.

84, Li J., Jiang Z.Y., Wu H., Zhang L., Long L.H., Jiang Y.J., "Constructing inorganic shell onto LBL microcapsule through biomimetic minuteseralization: A novel and facile method for fabrication of microbioreactors", ***Soft Matter***, vol.6, 542-550, **2010**.

85, a) Tong W.J., Dong W.F., Gao C.Y., Mohwald H., "Charge-controlled permeability of polyelectrolyte microcapsules". ***J. Phys. Chem. B***, Vol.109, 13159-13165, **2005**; b) Tong W.J., Song H.Q., Gao C.Y., Mohwald H., "Equilibrium distribution of permeants in polyelectrolyte microcapsules filled with negatively charged polyelectrolyte: The influence of ionic strength and solvent polarity". ***J. Phys. Chem. B***, Vol.110, 12905-12909, **2006**.

86, Mauser T., Dejugnat C., Sukhorukov G.B.,"Reversible pH-Dependent Properties of Multilayer Microcapsules Made of Weak Polyelectrolytes". ***Macromol. Rapid Commun.***, Vol.25, 1781-1785, **2004**.

87, Hata H., Kobayashi Y., Mallouk T.E., "Encapsulation of anionic dye molecules by a swelling fluoromica through intercalation of cationic polyelectrolytes". ***Chem. Mater.***, Vol.9, 79-87, **2007**.

88, Jiang X.M, Chen Z.C., Lv D.S., Wu Q., Lin X.F., "Basic law controlling the growth regime of layer-by-layer assembled polyelectrolyte multilayers". ***Macromol. Chem. Phys.***, Vol.209, 175-183, **2008**.

89, Pargaonkar N., Lvov Y.M., Li N., Steenekamp J.H., de Villiers M.M., "Controlled release of dexamethasone from microcapsules produced by polyelectrolyte layer-by-layer nanoassembly". ***Pharma. Res.***, Vol.22, 826-835, **2005**.

90, Kolhler K., Molhwald H., Sukhorukov G.B., "Thermal Behavior of Polyelectrolyte Multilayer Microcapsules: 2. Insight into Molecular Mechanisms for the PDADMAC/PSS System". ***J. Phys. Chem. B.***, Vol.110, 24002-24010, **2006**.

91, a) Bi S., Li L., Zhang S.S., "Amplification and DNAzyme Amplification". ***Anal. Chem.***, Vol.82, 9447-9454, **2010**; b) Li J.S., Deng T., Chu X., Yang R.H, Jiang J.H., Shen G.L., Yu R.Q., "Rolling Circle Amplification Combined with Gold Nanoparticle Aggregates for Highly Sensitive Identification of Single-Nucleotide Polymorphisms". ***Anal. Chem.***, Vol.82, 2811-2816, **2010**; c) Wu Z.S., Zhang S.B., Zhou H., Shen G.L., Yu R.Q., "Universal Aptameric System for Highly Sensitive Detection of Protein Based on Structure-Switching-Triggered Rolling Circle Amplification". ***Anal. Chem.***, Vol.82, 2221-2227, **2010**; d) Wu Z.S., Zhou H., Zhang S.B., Shen G.L., Yu R.Q., "Electrochemical Aptameric Recognition System for a Sensitive Protein Assay Based on Specific Target Binding-Induced Rolling Circle Amplification". ***Anal. Chem.***, Vol.82, 2282-2289, **2010**; e) He J.L., Wu Z.S., Zhou H., Wang H.Q., Jiang J.H., Shen G.L., Yu R.Q., "Fluorescence Aptameric Sensor for Strand Displacement Amplification Detection of Cocaine". ***Anal. Chem.***, Vol.82, 1358-1364, **2010**; f) Bi S., Zhang J.L., Hao S.Y., Ding C.F., Zhang S.S., "Exponential Amplification for Chemiluminescence Resonance Energy Transfer Detection of MicroRNA in Real Samples Based on a Cross-Catalyst Strand-Displacement Network". ***Anal. Chem.***, Vol.83, 3696-3702. **2011**.

92, a) Cheglakov Z., Weizmann Y., Braunschweig A.B., Wilner O.I., Willner I., "Increasing the complexity of periodic protein nanostructures by the rolling circle amplified synthesis of aptamers". ***Angew. Chem. Int. Ed.***, Vol. 47, 126-130, **2008**; b) Mizuta R., Mizuta M., Kitamura D., "Atomic force microscopy analysis of rolling circle amplification of plasmid DNA". ***Achives of Histology and Cytology***, Vol.66, 175-181, **2003**; c) Beals T.P., Smith J.H., Nietupski R.M., Lane D.J., "A mechanism for ramified rolling circle amplification". ***BMC Molecular Biology***, Vol.11, Article No.94, **2010**.

93, a) Barbee D.K., Chandrangsu M., Huang X.H., "Fabrication of DNA Polymer Brush Arrays by Destructive Micropatterning and Rolling-Circle Amplification". ***Macromol. Biosci.***, Vol.11, 607-617, **2011**; b) Li Z., Wei B., Nangreave J., Lin C.X., Liu Y., Mi Y.L., Yan H., "A Replicable Tetrahedral Nanostructure Self-Assembled from a Single DNA Strand". ***J. Am. Chem. Soc.***, Vol.131, 13093-13098, **2009**.

94, a) Demidov V.V., Kuhn H., Lavrentieva-Smolina I.V., Frank-Kameneteskii M. D., "Peptide nucleic acid-assisted topological labeling of duplex DNA". ***Methods***, Vol.23, 123-131, **2001**; b) Zhao Z., Liu Y., Yan H., "Organizing DNA Origami Tiles into Larger Structures Using Preformed Scaffold Frames". ***Nano Lett.***, Vol.11, 2997-3002, **2011**; c) Gnanaprakasa T.J., Oyarzabal O.A., Olsen E.V., Pedrosa V.A., Simonian A.L., "Tethered DNA scaffolds on optical sensor platforms for detection of hipO gene from Campylobacter jejuni". ***Sensors Actuators B***, Vol.156, 304-311, **2011**.